Force Propagation in Mammalian Cell Systems and the Relevance of the Mechanically Integrated Cell

Submitted in partial fulfillment of the requirements for

the degree of

Doctor of Philosophy

in

Chemical Engineering

Travis J. Armiger

B.S., Chemical Engineering, Rensselaer Polytechnic Institute

Carnegie Mellon University
Pittsburgh, PA

May, 2018

Acknowledgements

I would like to begin by thanking my Ph.D. advisor, Dr. Kris Noel Dahl, without whom I would not be the researcher that I am today. With her guidance I have grown to become a more critical and thorough investigator. She has a passion for scientific research which motivates and guides all students within her group. During my time in the Dahl group, she has always been available to discuss research successes and setbacks, and to share her insight on all aspects of obtaining a Ph.D.

When I first entered the Dahl lab, the senior lab members were Brian Holt (Ph.D. Biomedical Engineering, Carnegie Mellon University), Patrick Boyer (Ph.D. Chemical Engineering, Carnegie Mellon University), and Stephen Spagnol (Ph.D. Chemical Engineering, Carnegie Mellon University). The three of them were invaluable to my success at Carnegie Mellon. They made the extra effort by taking the time to train me on technical aspects of lab-based research, deliver critical insight on my results, and provide encouragement when experiments were unsuccessful. Upon arriving in the group, my project was most closely related to the work being done by Steve, and because of this he made a personal and often time-consuming, effort to train me. Even when he was undoubtedly overwhelmed with the vast amount of work required to complete a thesis, he would continually check-in on my work and was open to discussing my current research or the latest paper that I was reading. In addition to Steve, Pat and Brian teaching me the technical skills for success in this lab, they were also great friends who constantly kept the lab morale high. I hope that I have been able to provide similar encouragement and technical training to the new members of the Dahl lab.

I would like to thank the current Ph.D. students in the Dahl lab - Daniel Whitefield, Sumin Jin, and Kirill Lavernyuk - all of whom I have had the pleasure to work alongside. I am

confident that they will continue to do great research and move on to great things upon graduating from this lab. Additionally, I would like to thank Sarah Robb, Stefanie Baker, Piyumi Wijesekara, Pragna Vellala, Alexandra Eggleston, Maya Holay, and Casey Salandra, all of whom were involved in research in the Dahl lab that I had the pleasure to work with.

I would like to thank all of the people who make the Chemical Engineering Department at Carnegie Mellon a high functioning and enjoyable department to be a part of. I would like to thank the staff (including, Julie Tilton, Janet Latini, Allyson Danley, Justin Dawber, Cindy Vicker), faculty, and students of this department. In addition to their teaching and research roles, the professors within this department do a fantastic job of making new students feel welcome within the department. I would like to specifically thank Professor Katie Whitehead, whom I took a class from, was on my qualifier committee, and is a member of my thesis committee. She was particularly supportive during my time at Carnegie Mellon, for which I am very grateful.

At Carnegie Mellon I have made some of the best friends in my life who have made my time here more enjoyable than I would have ever expected. There are too many friends that I've met during my time in Pittsburgh to highlight everyone individually, but it is because of these friends and colleagues that the classes, seminars, and social events that we collectively took part in will remain highlights of my time at Carnegie Mellon. I would like to specifically mention three of my friends Blake Bleier, Alex Bertuccio and Yuan Chen. Blake Bleier and Alex Bertuccio were two of the first students I became friends with here, and they have remained my best friends within the department. Specifically, Blake's intellectual rigor, sense of humor, and unmatched enthusiasm for singing karaoke versions of Blink 182 and Zac Brown Band have helped me through the highs and lows of my time at Carnegie Mellon. Alex is one of the most sincerely happy and encouraging people that I have ever met, who, regardless of the hour of the

day, was always willing to pop his head over someone's cubical wall to put a smile on their face. Alex's desire to make others happy is manifested by providing birthday cards for everyone in the office and somehow remembering everyone's birthdays without the use of Facebook. Blake's first year roommate, Yuan Chen (who is apparently in Electrical and Computer Engineering and not Chemical Engineering at Carnegie Mellon) also quickly became one of my closest friends, who is always up to discuss the latest news and highlights in the NFL.

I cannot say enough kind words to do justice to the support provided by my fiancé, Sarah Guyer. Together, we moved to Pittsburgh, and she has always been a friend to enjoy the good times and a companion to get through the rough times. She exemplifies kindness in her professional and personal life, and I hope that I am able to show her at least some of the unending encouragement that she has given me throughout our time in Pittsburgh.

I would like to thank my family for their contestant support throughout my life as well as the encouragement to be creative and pursue whatever goals I had. In particular I would like to thank my mother, Linda, father, Bill, and brother Jacob. I could not ask for a better family to learn from and to help me through all aspects of life. Additionally, I would like to thank Mary and Dave Guyer for their constant support during my studies.

Last, and certainly least, I would like to thank the Super Bowl LII Champions - the Philadelphia Eagles - from whom I learned about overcoming adversity and, more importantly, that greatness is never achieved by an induvial. Thus, I hope that I have highlighted some of the many people that without whom, I could not have been successful as an individual.

Funding

I would like to acknowledge the following funding sources for supporting this research. The National Institutes of Health (NIH-EB003392 awarded to Travis J. Armiger). I would also like to acknowledge the National Science Foundation (NSF-CMMI-1634888 awarded to Kris N. Dahl, as well as NSF-CMMI-1300476 awarded to Kris N. Dahl).

Doctorate Committee

I would like to thank my Ph.D. thesis committee for their assistance in developing this research project. Their intellectual insight as well as their diverse expertise related to various aspects of this work has helped to guide my Ph.D. studies at Carnegie Mellon University.

Kris Noel Dahl, Ph.D.
Committee Chair, Professor, Chemical Engineering, Carnegie Mellon University

Aditya Khair, Ph.D.
Associate Professor, Chemical Engineering, Carnegie Mellon University

Kathryn A. Whitehead, Ph.D.
Assistant Professor, Chemical Engineering and Biomedical Engineering (courtesy), Carnegie Mellon University

Adam W. Feinberg, Ph.D.
Associate Professor, Biomedical Engineering and Materials Science & Engineering, Carnegie Mellon University

Abstract

Mammalian cells are known to respond to both extra- and intra- cellular forces as well as the physical properties of the surrounding tissue. There is increasing evidence to support the fundamental role of force, applied to or generated within cells, in maintaining proper tissue function. The mechanical integration from the exterior of a cell to the interior of the nucleus is crucial for cellular sensing of, and response to, the physical environment. Further, misregulation of this mechanosensitive ability can lead to the development or propagation of many diseases such as cancers, cardiovascular diseases, and tissue fibrosis. In this thesis, we investigate the role of various proteins in regulating the mechanical properties of mammalian cells. We also develop techniques to examine the propagation of forces through cells and multicell systems with the aim of elucidating critical biophysical factors involved in regulating cell function. The idea that the genome can be regulated through changes in forces applied to cells or changes in the propagation of forces through a cell, (i.e. mechanotransduction) is becoming widely accepted. The complex interplay between biochemical and biophysical mechanisms that ultimately control mechanotransduction are beginning to be uncovered; however, a true understanding of this remarkable cellular process has not yet been achieved. By investigating multiple factors which impact mechanosensitivity (such as protein expression, cell-cell and cell-environment connections, cell generated contractions, and physical connections through the cellular interior), we aim to further the understanding of potential pathways of mechanotransduction. Through novel studies and technological advances, the field of cellular biomechanics will continue to grow as we hope to uncover the physical mechanisms that regulate cell function or lead to disease.

Table of Contents

List of Tables

Chapter IV

Appendix C

List of Figures

Chapter I

Chapter II

Chapter III

Chapter IV

Chapter V

Appendix A

Appendix B

Appendix C

Chapter I: Introduction

Introduction to Cellular Biomechanics

The mechanical properties of cells within the body are paramount to the proper function and maintenance of tissues and organs[1,2]. Additionally, cells necessarily expend energy to generate forces in order to physically probe their extracellular environment and, in turn, regulate their function[3–6]. These properties of cells, broadly referred to here as cell mechanics (or biomechanics), are key factors in dictating their fate from cells in culture flasks to whole organisms. The field of cellular and molecular biophysics is based upon idea that a thorough understanding of the physical interactions of proteins and cellular components will lead to a better understanding of cell and tissue function to ultimately cure or mitigate diseases and improve human health. It is important to note that while the bulk of this thesis is dedicated to cellular biomechanics, chemical and biochemical factors are of equal importance to (and often intimately coupled with) the biophysical regulators of cell function. Furthermore, the vast majority of biological studies are plagued by the fact that perturbing one variable within a biological system often leads to a cascade of multiple downstream effects, and thus determination of true cause and effect relationships remains difficult. For this reason, there is often a give and take when designing experiments in which the closer an experiment mimics an *in vivo* system, the more difficult a detailed understanding becomes. These difficulties were noted in some of the early biomechanical studies of the eukaryotic cell protoplasm (cytoplasm) performed by Heilbrunn in the 1920s, in which he states:

> The physical and chemical study of protoplasm is never easy. The intrinsic difficulties are obvious. The colloid chemist has large masses of material at his disposal, but the biophysicist must be content with droplets too small for ordinary

> vision. Moreover in the manipulation of these microscopic droplets he must be extremely cautious. Almost anything he does is likely to cause death, and once this occurs the protoplasm is no longer protoplasm[7]

While technological advances have vastly improved scientists' ability to study cells, the idea that measuring the properties of a biological system can cause unfavorable and confounding effects is just as relevant today. Thus, multiple unique methods of system perturbation are crucial to advancing this field. Further, many biological systems contain redundant mechanisms, such as expression of multiple proteins with similar function[8–11], likely for evolutionary advantage. However, these redundancies can also lead to difficult interpretation of results. For example, the reduction of a given protein may lead to the upregulation of a different protein with similar function[12,13] resulting in a difficult understanding of the protein of interest. Nonetheless, with all the challenges associated with studying biological systems through a biomechanical perspective, the field continues to grow as a homage to its importance to the understanding of nature and human health. Further, new techniques to better probe biological systems are continuing to improve the field. In this thesis, we focus on cellular mechanics, specifically highlighting the physical connections through cells and multicell systems and the role of cellular connectivity as it relates to cell function.

Historical Context of the Study of Cell Mechanics

Throughout this thesis we utilize techniques and knowledge based upon centuries of innovation from scientists and engineers. In this section, we aim to highlight several of the groundbreaking techniques, discoveries, and insights that are particularly relevant to topics covered in this thesis and, without which, the research landscape of cellular biomechanics would not be what it is today. The current study of biological systems - particularly when investigating

live cell systems - relies heavily on microscopy, specifically fluorescence microscopy, as is evident throughout the work presented in this thesis.

Some of the earliest experiments that gave rise to the microscope as we know it today were performed in the early parts of the 11th century by the scientist Abu Ali al-Hasan ibn al-Haytham (Latinized as Alhazen), born in what is modern-day Iraq[14]. In the context of microscopy, Alhazen wrote a work on optics, "Book of Optics," between the years 1011-1021 C.E. in which one of the first magnifying devices is described in detail. There is debate over who should be credited with the invention of the first microscope as well as the first compound microscope which we will not address here. Instead, we move ahead to the 1600s and the work of two famous scientists, the English scientist Robert Hooke (1635-1703) and the Dutch scientist Antonie van Leeuwenhoek (1632-1723). In Hooke's famous work, "Micrographia," he depicts illustrations of various biological specimens viewed under the compound microscope (perhaps most well-known for the illustration of a flea) as well as diagrams of his microscopes[15,16]. Hooke is also credited with the coining of the term "cell" based on his microscopic observations. Leeuwenhoek is highly regarded in the area of microscopy as his microscopes (some of which are of closer resemblance to miniature canoe paddles than a microscope by today's standards) were able to achieve magnification of over 250x, compared with those of Hooke which the magnification power was around 50x[17]. Although Leeuwenhoek's inventions were originally created to count threads of textiles, they were later used on biological specimens to observe bacteria and sperm for first times[15,16]. Moving forward approximately one century, Carl Zeiss (1816 – 1888, and founder of the microscopy company Carl Zeiss) in conjunction with Ernst Abbe (1840-1905) revolutionized microscopy in the mid to late 1800s through manufacturing improvements and the use of oil immersion lenses to further improve microscope resolution[17].

Later, fluorescence microscopy emerged as a method to further improve resolution. In the early 1900s, the Carl Zeiss and Carl Reichert (which would eventually become Leica) companies manufactured some of the first fluorescence microscopes[18]. While August Köhler (of the Carl Zeiss company) observed fluorescence in the UV range, it is Oskar Heimstädt (of the Carl Reichert company) who, based on Köhler's work, is credited with the creation of the first fluorescence microscope[19]. In the 1930s, the Austrian scientist Max Haitinger (1868-1946) is credited with the labeling of specimens with fluorescent chemicals to further expand the applications fluorescence microscopy[19]. In the 1940s-1960s, Albert Coons (1912-1978) took protein labeling to new heights by using fluorescent antibodies to label proteins (i.e. immunofluorescence)[20]. The American scientist Marvin Minsky (1927-2016) is credited with using pinholes in conjunction with fluorescence microscopy in the 1950-60s, eventually leading to the creation of the first confocal microscope[18]. Based on work on green fluorescent protein (GFP) from the 1960s to the 1990s (which lead to the Nobel prize in chemistry awarded to Osamu Shimomura (born 1928), Martin Chalfie (born 1947), and Roger Tsien (1952 – 2016)), fluorescence in live cells and organisms has become standard[21]. Further innovations in fluorescent labeling have made the labeling and detection of various proteins and subcellular structures possible in live cells which can be accomplished by virtually any lab interested in studying biology. Scientists continue to push the limits of fluorescence microscopy with techniques such as super-resolution microcopy, multiphoton microscopy, and total internal reflection fluorescence microscopy.

Microscopy represents and invaluable tool for the investigation of biological systems. For this reason, groundbreaking biological and biomechanical studies have historically occurred in parallel with advances in microscopy. We focus the remainder of this section on discoveries in

cell biology and biomechanics determined to be most impactful for the advancement of these fields in the context of the work presented in this thesis. Mainly we focus on early studies of the cell nucleus, cell force generation, and mechanical and rheological techniques for biophysical studies. As noted above, the term "cell" is attributed to Robert Hooke, based on his observation of the unique structure of plant tissue in the 1660s[15]. However, it was Leeuwenhoek who first described what is believed to be the cell nucleus in animal cells (described as a "little clear sort of a light") through observing the red blood cells of salmon and other fish around 1700 (unlike human red blood cells, the red blood cells of fish are nucleated)[22]. The term nucleus to describe the organelle was first used by the Scottish botanist Robert Brown (1773-1858) in the early 1800s[23]. In 1869, the Swiss scientist Friedrich Miescher (1844-1895) first described a substance within white blood cell nuclei as nuclein, which is now known to be DNA, and nearly 100 years later James Watson (born 1928) and Francis Crick (1916-2004) proposed the famous double helix structure of DNA[24]. In the context of genetic expression, some of the earliest studies of the location of genes within chromatin (the functional unit of DNA within the nucleus) and chromatin mutations as they related to phenotypic changes in *Drosophila* (i.e. the fruit fly) occurred in the early 1900s by scientists such as Thomas Morgan (1866-1945) and Hermann Muller (1890-1967)[25] These groundbreaking discoveries were monumental to the understanding of genetic regulation which is still being investigated today. For a further review of the history of the study of genetic regulation the reader is referred to a review by Felsenfeld[25]. We are beginning to understand the physical mechanisms of genetic regulation, of which recent work is described throughout this thesis, and in Chapter IV we perform studies to quantify the motion of chromatin within live cell nuclei.

Some of the earliest studies of cell mechanics in live cells were performed in the 1920s by the American biologist Lewis Heilbrunn (1892-1959) in which sea urchin eggs were centrifuged and the viscosity of the protoplasm was estimated based on the motion of granules within the cells[26]. Within the same issue of The American Naturalist journal, Samuel Mast (1871-1947) describes the Brownian motion of particles within the ameboid protoplasm in his work titled "The Structure of Protoplasm in Amoeba"[27]. In this work published in 1926, decades before the mechanical integration throughout cell systems was understood, Mast wrote:

> If then protoplasm is defined as living substance, its structure must involve the cell as a whole, not the nucleus by itself or the cytoplasm or this portion or that portion or the other portion, but all these together organized into a working coordinate system; and if this obtains, the structure of protoplasm can no more adequately be described by portraying the structure of any given part, no matter how detailed it may be, than can a Ford or a Rolls-Royce by elucidating the structure of a wheel or any other individual part.[27]

This idea that we must study cells as integrated systems is particularly relevant to the works of this thesis as the current understanding of the mechanical connections throughout mammalian cells is discussed in a later sections. Also in the early 1900s, the German botanist Heilbronn (cited by, and not to be confused with Heilbrunn) studied the protoplasm in plant cells by probing the mechanical properties with a needle, and the American scientist William Seifriz (1888-1955) studied plant and animal cells with similar methods and methods which involved inserting magnetic nickel particles into cells[28]. A work by Cowdry and Paletta in 1940 utilized centrifugation and the displacement of "chromosome clumps" within the nucleus to begin to investigate the mechanics and viscosity of the cell nucleus as it related to cancer[29]. In the 1980s

the technique of atomic force microscopy (AFM) was developed and used as a tool to probe the mechanical properties of cells and is widely relevant today[30]. For a historical review of cell mechanics with a focus on AFM (as well as an amusing commentary on the idea that the mechanical forces within cells were once attributed solely to a divine creator) the reader is referred to a review by Pelling and Horton[30]. The early studies of cell mechanics have grown into a multidisciplinary field aimed at uncovering how life functions at the cellular and subcellular level. The current state of the art techniques for studying cell mechanics are discussed briefly in the "Mechanical Properties of the Nuclear Interior" section of this introduction.

In addition to the studies of mechanical cell properties, the mechanisms behind cell force generation were also beginning to be investigated in the early to mid-1900s. The German scientist Wilhelm Kühne (1837-1900) is credited with discovering and naming "myosin" in 1864 which was originally thought to be structural rather than an element capable of force generation. In 1939 Engelhardt and Ljubimowa found that myosin uses ATP as an energy source. Then, in 1942 Albert Szent-Gyorgyi discovered actin as the binding partner of myosin responsible for cell contractions[31]. We now know that actomyosin contractions are responsible for a wide variety of cell functions, such as genome regulation (discussed later), which would have seemed highly improbable at the time of their discovery. For a historical perspective on the evolution of the idea that cellular forces can modulate gene expression (i.e. mechanotransduction) the reader is referred to a review by Iskratsch et al.[32].

All of the early discoveries mentioned above where selected as examples of innovation and discovery without which this thesis would not exist in its current form. We did not highlight other crucial advances, such as advances in mammalian cell culture, data processing, and image analysis which have proven invaluable toward expanding the field of cellular biomechanics to

what it is today. In learning about the early works of scientists who laid the foundations before us, it is fascinating to note the ideas and hypotheses which have (as of 2018) stood the test of time. It is also noteworthy to point out that many ideas, which at the time were accepted as facts, have proven incorrect based on our current knowledge. For example, in the British scientist and paleontologist Henry Nicholson's 1880 work, "Life and Its Physical Basis," he states that microscopy has revealed no structure within the protoplasm, but to his credit admits the shortcomings of the technology at the time[33]. Today imaging various structural elements of what was originally termed the protoplasm (i.e. the cytoskeleton) can now be achieved within several hours during an introductory laboratory class. It is with this notion of science as a constantly growing field in which no hypothesis or theory should be taken as absolute truth that we must bear in mind, as new innovations will continue to challenge what we currently accept to be true.

Cell Mechanics in Healthy Cell Function

Within an individual, each somatic cell nucleus (of which there are trillions[34]) contains an identical sequence of DNA; however, cells which comprise different tissues must function differently and express proteins at different levels. It is the regulation of the expression of this genetic sequence, or epigenetic (literally "above genetics") regulation which must ultimately be understood in order to uncover the mysteries of cell and tissue function. In healthy cells this epigenetic regulation, as it relates to cellular biomechanics, is particularly evident in the areas of embryonic development, differentiation, monolayer barrier and permeability regulation, and wound healing.

Upon fertilization of an egg cell, the single cell zygote must divide to become a multicell embryo. Cells begin to differentiate into the three germ layers during gastrulation, and later functional organs begin to form. Throughout this entire process chemical and physical cues are

sensed by cells for proper organogenesis. Here, we focus primarily on the mechanical cues, but chemical signaling is briefly addressed in a later section. The idea that physical forces can ultimately lead to changes in gene expression is termed mechanotransduction and is crucial for embryonic development[35]. Developing embryos generate forces to properly fold and shape organs and also respond to mechanical forces[36]. Using the model organism *Drosophila*, scientists in the late 20th century hypothesized that actomyosin contractions were involved in the drastic shape changes observed during embryogenesis[37–39]. More recent work has further demonstrated the importance of actomyosin contractions in this process as well as the roles of the transcription factors Twist and Snail, which are required for ventral furrow formation at the early stages of gastrulation[40,41]. Developing embryos appear to be mechanosensitive, as *Drosophila* oocytes have been shown to respond to osmotic and hydrostatic pressure changes, via changes in translation of the protein smaug and increased hardening of the membrane surrounding the oocyte[42]. Additionally, the applications of force to developing *Drosophila* embryos using magnetic tweezers appears to induce changes in nuclear morphology[43]. For in depth reviews on the role of forces during embryonic and tissue development, the reader is directed to the following review articles[35,36,44,45].

While model organisms such as *Drosophila* are valuable for studying mechanotransduction at the embryonic level, mammalian cell systems prove vital to an understanding of mechanotransduction at the cellular level, as it relates to human health. Campàs et al. have presented a novel method of quantifying forces in mouse embryonic mandible tissue based on the deformations of oil droplets within the tissue[46]. However, due to the time required for mammalian embryonic development as well as the difficulties in maintaining the conditions for mammalian embryonic growth, force generation studies in mammalian developing

embryonic systems remains difficult compared to those preformed in the relatively rapidly developing embryos of organisms such as *Drosophila* and X*enopus*[47]. While model organisms will continue to be a valuable tool to study the role of mechanical forces *in vivo,* the current tools available to study these extremely complex systems remains limited[48–50], but there is still a vast expanse of biomechanical knowledge to be uncovered through studies performed using *in vitro* cell culture models. At the cellular level, physical forces have been demonstrated to induce changes in differentiation and gene expression[51,52]. In the case of stem cell differentiation, which is critical for development as well as for stem cell therapy applications, there is evidence to suggest that the mechanical properties of the extracellular environment, and the cellular ability to sense this environment, can direct stem cell fate[53–56]. Recent work by Kim et al. has demonstrated that human pluripotent stem cell fate can be directed via controlling the crosslinking density of fibroblast-derived matrices in which the cells are cultured, suggesting a mechanosensitive response in this system[55]. Additionally, Hadden et al. recently demonstrate the mechanosensitivity of human adipose-derived stem cells, via quantification of mechanosensitive protein expression and cell migration on gels with a stiffness gradient[57]. Differentiated cells, such as endothelial cells which line blood vessels, have been shown to alter their gene expression upon exposure to shear stress[58–60]. The force generation of monolayer cells and their response to the physical environment also has implications in regulating permeability through monolayers. For example, in endothelial cells (which form sheets of cells around various tissues and organs within the body) the stiffness of the substrate appears to impact monolayer permeability, with stiffer substrates causing cells to generate increased forces thus increasing the gaps between cells[61–63]. In Chapters IV and V of this thesis we will focus on epithelial cell monolayer mechanics. Epithelial cells are capable of undergoing epithelial to mesenchymal transition

(EMT), which can be necessary in development or detrimental in disease. EMT is characterized by cells switching from an epithelial phenotype (intact cell-cell junctions, and apical-basal polarity) to a mesenchymal phenotype (loss of cell-cell junctions and front-rear polarity)[64]. The mechanosensitivity of cells appears critical for this drastic transition in cell morphology and gene expression, as stiffer extracellular environments (in combination with the proper chemical signaling) appear to favor the transition to a mesenchymal phenotype[65,66]. One of the most apparent examples in which cells need to properly regulate their force generation and sense their physical environment is wound healing. Cells need to detect their adjacent cells and then generate the proper forces to collectively migrate and close the wound. Recent works have calculated the forces associated with wound healing, as well as the traction forces generated by intact monolayers[67–70]. It is well established that isolated cells behave differently and generate increased traction forces on stiffer substrates[3,71,72]. Interestingly, the physical connects between cells can alter their behavior. For example, single epithelial cells migrate faster on stiff versus soft substrates, while collective migration appears less sensitive to substrate stiffness in some systems[67]. In slight contrast, epithelial monolayers have also been shown to migrate in the direction of increasing substrate stiffness and did so with greater persistence than isolated cells[68]. Monolayers clearly respond to the stiffness of their substrate, as endothelial monolayer clusters generated increased stresses on stiffer substrates[73,74]. Additionally, single endothelial cells generate less traction force than two touching cells (treated as one entity), and the increase in traction forces scale with substrate stiffness[75]. Similarly, the impact of cell-cell contacts is noted by Sim et al. in which they demonstrate that the traction forces of two cells are greater than that of a single cell of similar size and that the traction forces of two cells in contact are not the sum of the traction forces of two isolated cells[76]. The examples of development, differentiation,

monolayer function, and wound healing represent several areas in which cell mechanics and mechanotransduction are critical for maintaining cellular function. While nature is truly amazing in the ability of cells to regulate these processes, there are many instances in which dysfunctional biomechanical regulation leads to disease progression.

Misregulation of Cellular Mechanics in Disease

Several examples in which unfavorable alterations in cellular biomechanics cause, or advance diseases include cancers, cardiovascular disease, and tissue fibrosis. Additionally, the disease Hutchinson-Gilford progeria syndrome (HGPS), is presented as an example of how a defect of a single nuclear protein can lead to disease and change nuclear mechanical properties. In the context of cancers, the tumor microenvironment regulates the chemical and physical factors which are influential in the progression and severity of the disease[77]. Additionally, prior to establishment of a tumor, the physical and chemical environment can lead to conditions which favor a more metastatic phenotype. Analogous to EMT, in which cells lose apical basal polarity and cell-cell junctions, the feedback loop between cells and their physical environment may be critical for the onset or metastasis of cancer[77,78]. Tissue stiffening can be detrimental in cardiovascular diseases (such as atherosclerosis and fibrotic scar formation after infarction), chronic kidney disease, and liver fibrosis[79–82]. In these diseases, stiffening of the extracellular matrix, through increased fibrotic protein deposition, likely leads to a positive feedback loop further misregulating cellular function through mechanotransduction[83,84]. Finally, many diseases are the result of a single protein defect. One example is HGPS (discussed further in Chapter III), in which the mutant lamin protein, termed progerin, causes alterations to nuclear mechanics[85–87]. HGPS represents just one disease related to the nuclear lamina. However there a multiple diseases involving lamins and lamin associated proteins, collectively termed laminopathies[88].

Thus, the mechanics of nuclear proteins must be studied to truly understand tissue function and disease at the cellular level. In Chapter II, the nuclear protein spectrin is studied, in which a novel mechanical role of this protein within the nucleus is revealed. Further, many diseases are characterized by tissue stiffening and in Chapters IV and V the effects of the rigidity of the extracellular environment on cell function are studied.

Mechanical Coupling from the Extracellular Matrix to the Genome

Throughout this introduction, we have highlighted the importance of mechanotransduction in cell and tissue function. The ability of cells to regulate their genome expression based on physical inputs is likely only possible due to mechanical connections ranging from connections outside of the cell, such as integrins and cadherins, through the cell cytoskeleton, and ultimately to the nucleus and the chromatin fibers within[89–92]. The presence of these physical connections were demonstrated by Maniotis et al. in which they pulled on different regions of the cell cytoplasm and measured nuclear strain[93]. The broad range of mechanosensitive phenomena at the cellular level are likely due to a combination of direct physical strain of proteins as well as a physical strain leading to a biochemical signaling cascade through a cell[94]. For example, the straining of a protein may cause a conformational change, exposing a binding site for another protein which leads to downstream effects. This mechanism is proposed for the binding of the proteins talin and vinculin, which interact after significant force is applied to talin and further cause changes in the localization of the mechanosensitive transcriptional regulator, Yes Associated Protein (YAP)[95]. Similarly, the cadherin/catenin protein complex involved in cell-cell junctions binds to F-actin more favorably under applied tension than in solution without applied tension[96]. In this section, we provide a description of the proteins responsible for connecting the exterior of the cell to the interior of the cell nucleus and

give examples which highlight the importance of these connections. Throughout this section, it is easy to conceptualize cells as static structures with well-defined mechanical elements; however it is well established that proteins within live cells are constantly being translated, degraded, polymerized, binding, unbinding, and reorganizing which should be noted when discussing cellular mechanical properties[89,97,98].

Extracellular Connections and Adhesive Proteins

Connections on the exterior surface of the cell can be divided into two categories, linkages between cells, such as cadherins, tight junctions and gap junctions and linkages between the cell and its extracellular matrix (ECM), such as integrins and hemidesmosomes[99]. Broadly, cadherins are linkages between cells which then connect to the cytoskeleton through catenin proteins[99,100]. Tight junctions are involved in barrier function between epithelial cells, and gap junctions are involved in small molecule transfer between cells[99,100]. At the connections between the cytoskeleton and the ECM, integrin clusters, in combination with a multitude of other proteins, are collectively known as focal adhesions which can bind a variety of ECM proteins such as fibronectin and collagen[98,101].

The cell-cell or cell-ECM junctions typically represent the first segment of the mechanosensing pathway and act as sensors on the outside of the cell capable of probing the mechanical properties of the surroundings[3,4]. Intercellular adherens junctions, which connect to cytoskeletal actin, are involved in regulating cell proliferation (i.e. contact inhibition)[102], cellular force distribution in monolayers[103,104], and collective migration[68,105]. It is logical that cells are required to sense their neighbors in order to inhibit or promote proliferation. For example, in mammary epithelial cells, E-cadherin appear to regulate contact inhibition via the HIPPO signaling pathway, which is responsible for YAP localization[102]. Through magnetic twisting

cytometry, Barry et al. demonstrate that VE-cadherins are involved in regulating monolayer integrity and force transmission through monolayers using magnetic twisting cytometry[104]. In this study cell junctions (nearby and distant to applied force) were disrupted to a greater extent when the magnetic bead was coated in a non-function blocking VE-cadherin antibody or full length VE-cadherin[104]. Knock-down of various adherens junction proteins (cadherins and catenin), lead to changes in intercellular tension, traction forces, and cell migration in mammary epithelial monolayers[103]. Additionally, durotaxis (i.e. cells migrating in response to a stiffness gradient) was lost in cell monolayers in which the adherens junction protein α-catenin was knocked-down[68]. Similarly, collective migration was altered upon adherens junction disruption, and changes in cell coordination appear to correlate with myosin contractility (i.e. cell tension)[105].

The proteins which comprise focal adhesions are also mechanosensitive and assist in maintaining cell function by sensing the physical properties of the ECM[106]. For example, Wong et al. propose a mechanism by which fibroblasts extend filopodia and form a nascent focal adhesion, which can either mature or retract based upon the rigidity of the substrate through myosin-II mediated sensing[107]. As mentioned previously, there appears to be a critical threshold in which talin unfolding allows vinculin binding and further downstream mechanotransduction[95,108]. Additionally, types of integrin proteins present in a focal adhesion may alter cellular traction forces and mechonsensing[109]. Similarly, Elbediwy et al. demonstrated integrins role in mechanotransduction by showing that the integrin β_1 is required for YAP nuclear localization in keratinocyte epithelial cells[110]. A recurring theme throughout this thesis is the relevance of mechanical integration throughout cells. Focal adhesions and adherens junctions are likely not mechanically isolated. In cells which express both types of adhesions, there

appears to be coordinated regulation between adherens and focal adhesions, as VE-cadherin force loading increased focal adhesion density and size in a substrate dependent manner[73]. Both focal adhesions and adherens junctions are connected to the cytoskeleton, which is the next major mechanical feature when going from to exterior to the interior of a cell.

Structural Components of the Cytoskeleton

The major and most studied component of most cell cytoskeletons is actin[111]. Actin, in combination with myosin, is a major contributor in cellular mechanosensitivity involved in sensing extracellular stiffness[107], directing cell migration[97,105,112], and regulating mechanotransduction[52,113]. Additionally, actin polymerization and crosslinking are key mechanisms by which cells alter their mechanical properties[112,114]. Filamentous-actin (F-actin, the polymerized form of globular, G-actin) has a diameter of approximately 7 nm and persistence length of around 18 μm, which is on the order of the length of F-actin stress fibers *in situ*, and thus behaves as a semi-flexible rod in the cellular context[115,116]. In addition to actin, microtubules represent another filamentous component of the cytoskeleton. Microtubules act as stiff rods within cells, with a diameter around 25 nm and persistence length (~5,200 μm) much greater than their *in situ* length of approximately 50 μm[116,117]. Microtubules, are dynamic structures that are composed of monomer units known as tubulin, act as guiderails for the motor proteins dynein and kinesin, and are critical for mitosis[117–119]. In addition to actin and microtubules, the cytoskeleton also contains various intermediate filaments (categorized into 6 types), which are expressed in cells of different types and also regulate cell mechanical properties[120]. The dynamic regulation and mechanical properties of the cytoskeleton are too complex to cover in full within this thesis; however, one key feature of the cytoskeleton, emphasized here, is that it mechanically connects the exterior of the cell to the nucleus.

Cytoskeletal to Nucleoskeletal Connections

The nucleus is surrounded by a double lipid bilayer, as well as various structural proteins collectively known as the nucleoskeleton[121,122]. The cytoskeleton is physically connected to the nucleoskeleton through the linker of the nucleoskeleton and cytoskeleton (LINC) complex[122]. Finally, proteins within the nucleoskeleton can bind the chromatin fibers within the nuclear interior[89,121], completing the mechanical coupling from the exterior of a cell to the interior of the nucleus. The LINC complex is comprised of nuclear envelope spectrin repeat (nesprin) proteins, of which there are 4 main isoforms that bind actin, microtubules, and intermediate filaments. Nesprins are connected to Sad1p, UNC-84 (SUN) proteins, which span the gap between the inner and outer nuclear membrane, via a Klarsicht ANC-1 Syne Homology (KASH) domain. SUN proteins in turn bind nucleoskeletal proteins such as lamins and lamin associated proteins[122]. Lamin proteins are the primary structural component of the nucleoskeleton; however, many other proteins such as emerin, spectrin, and actin are present within the nucleoskeleton, with many of their distinct roles remaining to be elucidated[121,123].

The LINC complex and the nucleoskeleton are both critical regulators of force propagation to the nucleus, and mechanotransduction[90,94]. Spagnol et al. has previously demonstrated that disruption of the LINC complex as well as reduction of myosin-II activity both decrease intranuclear motion, which highlights the importance of the cytoskeleton and the LINC complex in regulating chromatin dynamics[124]. When the nucleoskeleton is stiffened through the expression of the mutant lamin protein progeria, chromatin dynamics are also impacted, with an apparent decrease in force propagation to chromatin[85]. Forster resonance energy transfer (FRET) studies performed using a mini nesprin-2G FRET sensor demonstrate that the cytoskeleton applies tension to the LINC complex via myosin[125]. Finally, for cells on rigid surfaces, the nuclear lamina appears flatter than on soft surfaces as measured via atomic force microscopy

(AFM), likely due to the increased tension generated on stiff surfaces being propagated to the nucleoskeleton[126]. In addition to transferring forces to within the nucleus, the LINC complex appears critical in force propagation from one side of the nucleus to the other, as demonstrated via traction force microscopy experiments on fibroblasts[127].

As the LINC complex is responsible for force propagation to the nucleus, it seems logical that various nucleoskeletal proteins are mechanosensitive and the LINC complex regulates mechanotransduction. For example, lamin-A expression correlates with tissue or substrate stiffness[126]. In mesenchymal stem cells, disruption of the LINC complex appears to lead to a lack of mechanotransduction (quantified by phosphorylation of the protein kinase, Akt) after application of low magnitude strain, demonstrating the role of the LINC complex in mechanotransduction[128]. One of the most convincing sets of experiments demonstrating direct mechanotransduction at the nucleoskeleton were performed by Guilluy et al. in which tension, applied directly to nesprins via magnetic tweezers, led to nuclear stiffening modulated by the nucleoskeletal protein emerin in isolated nuclei[129]. Collectively these studies suggest that the LINC complex and nucleoskeleton are important elements involved in mechanotransduction and force propagation to the nuclear interior.

Mechanical Properties of the Nuclear Interior

The forces which propagate through the nucleoskeleton and the mechanics of the nuclear interior are both major factors in governing chromatin dynamics. A major component within the nucleus is chromatin however, a multitude of other proteins - such as transcription factors, DNA repair proteins, RNA, nucleolar proteins, actin, and nuclear myosins - play key roles in nuclear function[89,130,131]. Together the components of the nuclear interior make up a densely packed system in which molecular crowding may play a key role in functional regulation[132]. The human

genome contains meters of DNA, which is ultimately packaged into a nucleus of a diameter around 10 μm[89]. DNA behaves as a flexible polymer, with a persistence length around 30-50nm, well below the length of a chromosome[133,134]. It is well established that DNA is packed into chromatin through binding with histone proteins. *In vitro* studies have indicated that DNA wraps around histones to form a "beads on a string" appearance, which further forms a 30nm diameter fiber flexible fiber and has a persistence length around 100nm[135]. However, recent studies, made possible through advanced imaging techniques, have demonstrated that in the nucleus chromatin packaging is much more complex and likely not packaged into only 30nm diameter fibers[133]. Chromatin can further be grouped into two main categories, less dense, transcriptionally active, euchromatin, or densely packaged, transcriptionally inactive heterochromatin[136]. However, as chromatin structure is becoming better understood these categories are becoming less distinct. For example, it was largely accepted that heterochromatin was transcriptionally inactive due to decreased accessibility of transcription factors in these densely packaged regions[136]. However, studies have shown that heterochromatin, while densely packed, can still allow for protein accessibility, and transcription[132,136]. Additionally, the role of RNA interference in heterochromatic silencing is beginning to be understood[137,138]. Therefore, while heterochromatin and euchromatin represent wide-spread categories to conceptualize chromatin mechanics, the reality may be much more complex with a continuum of condensation states rather than two distinct states[133,139].

One broad question which puzzles and fascinates researches of nuclear structure and function is: How does an organelle with no membrane boundaries properly regulate genetic expression? For example, the proper transcription factors must localize to a strand of DNA for gene expression or repression and maintain the plasticity to turn genes on or off based on the

needs of an individual cell. Additionally, there is evidence that repressed or expressed genes may localize to similar nuclear locations, leading to the idea of transcription factories, which are responsible for the regulation of multiple genes[140]. Like most features of live cells, these transcription factories appear to be dynamic, with proteins constantly in flux through a given factory, regulated by a combination of the local mechanical properties and binding kinetics[140–142]. The interplay between transcription factors and DNA represents one means of molecular control of gene expression. Further, the turnover rate of various DNA binding proteins can vary on time scales from seconds to hours, which may represent another means of epigenetic regulation[130]. A summary of the dynamic regulation of the nucleus is shown in Figure 1.1. Multiple studies are beginning to uncover various biochemical signaling pathways through the cell and within the nucleus[57,77,94,143,144]. One study of particular interest demonstrates that direct application of force on cells can lead to upregulation of transcription which beautifully reveals the fundamental concept of mechanotransduction[145].

As nuclear mechanical properties likely impact gene expression and almost certainly impact the nuclear response to force, we conclude this section on cell connectivity with a brief discussion of cell and nuclear mechanics. Scientists have long wondered of the mechanical properties of cells; however, their inherent complexity discussed above makes these properties difficult to accurately quantify. For example, the Young's modulus of actin stress fibers may vary by several orders of magnitude (1-100 kPa) based on the amount they are stretched within a cell[146]. Further, addressing questions such as, "What is the stiffness of a cell or a nucleus?" is deceptively difficult as cells are vastly heterogeneous, dynamical systems. Therefore, the numerical answer will depend on the method of measurement and assumptions made. For example, the stiffness of a cell can change based on the extent that the cell is spread over a

surface[147]. Additionally, as mentioned previously, there is evidence that the nucleus can stiffen after application of force through mechanotransduction-based mechanisms[129]. For this reason, proper controls or comparative studies are often required to truly understand a given experimental system. There are many techniques to measure mechanical properties of the cell (and cell nucleus) such as atomic force microscopy (AFM)[148,149], micropipette aspiration (MPA)[87,139,150], laser ablation[127,151], traction force microscopy[62,69,74–76,152], magnetic twisting cytometry[73,104,145], optical tweezers[96,153], compression and stretching devices[154–156], particle tracking microrheology[124,157,158], FRET based tension sensors[125,159], osmotic swelling[42,160], and novel techniques which are continually being evaluated[46,161–163]. MPA experiments have demonstrated that the nucleus behaves as a viscoelastic material, with a stiffness on the order of 0.5-10 kPa (several times greater than the cytoplasm), and that the stiffness appears dependent on the nuclear lamina[85,87,139,150,164]. Results from AFM studies reveal a similar range of nuclear stiffness, which can differ greatly based on cell type and experimental conditions[165]. Finally, particle tracking microrheology reveals an average mesh size within the nucleus of around 300nm; however this mesh size, as well as the mechanical properties of the intranuclear space, appear drastically heterogeneous[166]. While we cannot begin to summarize every experiment aimed at determining cellular and nuclear mechanical properties, we have demonstrated the heterogeneity within these properties as well as highlighted their importance in mechanotransduction and cellular function.

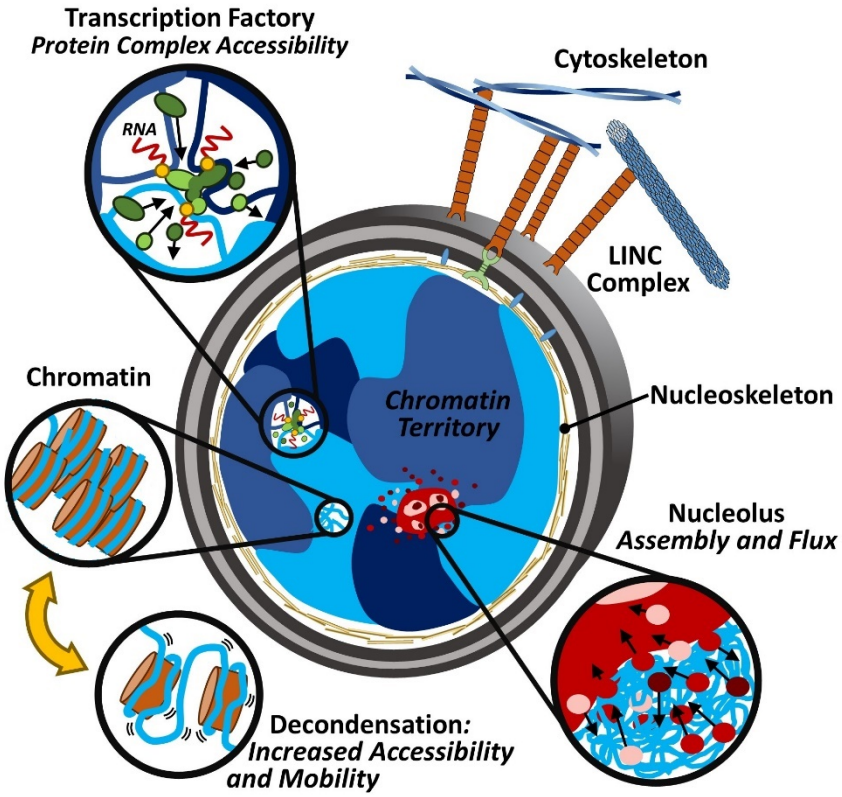

Figure 1.1: Mechanotransduction and the dynamic regulation of the nuclear interior

Forces generated from outside of the nucleus can be transmitted through the LINC complex to the chromatin fibers within the nucleus. Force induced movements within the nucleus may cause or enhance structural changes and dynamics within the nucleus. Examples of dynamic events within the nucleus include (i) altered dynamics of transcription factories and changes in local protein accessibility; (ii) decondensation of chromatin and (iii) altered stability and assembly of nuclear bodies including nucleoli. Figure from reference[89]

Interplay Between Biophysical and Biochemical Regulation

This thesis focuses on the physical properties and mechanical regulation of cell function; however, biochemical and biophysical regulation are often coupled[106,113]. For example, MDCK cells respond to transforming growth factor-β (TGF-β) in a substrate stiffness dependent manner[65]. Mechanical forces may also lead to enhanced biochemical signaling cascades, with potential mechanisms such as stretching of nuclear pores to allow more favorable transport of signaling molecules to the nucleus[108]. Additionally, while some cells are able to migrate in response to a stiffness gradient within their substrate[57,68], cells migrating in response to a chemical gradient (i.e. chemotaxis) is a well-established mechanism of directed cell migration[97]. Finally, Muhamed et al. demonstrate that cell traction forces increase upon applying a stress via magnetic twisting cytometry[113]. Interestingly this increase was dependent upon bead coating with E-cadherin coated beads leading to a larger increase in traction force than poly-L-lysin, or E-cadherin blocking anti-body coated bead. This experiment demonstrates the relationship between force and intracellular signaling cascades (in this case activated through E-cadherin activation) in mechanotransduction. If the force generated by the bead was the only requirement for changes in traction force, then bead coating would not impact results. Conversely, if the intracellular signaling were strictly biochemical than the non-E-cadherin coated beads would not increase traction force at all. The complex interplay between chemical and mechanical regulation will continue to intrigue researchers as new mechanosensitive pathways are uncovered.

Thesis Objectives

We have thus far discussed the importance of cellular biomechanics as it relates to cell and tissue function. In this thesis, we present cells as physically integrated systems, through their interactions with the extracellular matrix and adjacent cells, which are further connected through

the cytoskeleton to the nucleus and nuclear interior. We aim to highlight the importance of cellular mechanical integration through experimental techniques and perturbation of cellular systems. The overall objective of this thesis is to further investigate the various proteins and biophysical factors that are critical for regulation of cell mechanical properties and to develop novel techniques for characterization of cell systems to obtain a more comprehensive view of cellular biomechanics. We begin by focusing on two classes of nucleoskeletal proteins, spectrin and lamin proteins in Chapters II and III, respectively. We then focus on epithelial monolayer systems in which we develop a technique to investigate force propagation through these systems and characterize their mechanical integration in Chapter IV. Finally, in Chapter V we characterize the substrate dependent mechanosensitive response of epithelial monolayers to changes in cell contractility.

Determining the Mechanical Role of Nuclear Spectrin Proteins

In Chapter II we aim to determine the mechanical role of nuclear spectrin proteins (or spectrins). Spectrins are multi-domain, elastic proteins that provide elasticity to the plasma membrane of erythrocytes and select nucleated cells. Spectrins have also been found in the nucleus of non-erythrocytes, but their function within the nucleus remains to be determined. It has been hypothesized that a spring-like spectrin network exists within the lamina nucleoskeleton; however, experiments testing the mechanical impact of a spectrin network on the nucleus are lacking. In Chapter II, we knock-down levels of nuclear αII-spectrin with the goal of disrupting this nucleoskeletal spectrin network. We mechanically test live cells with intranuclear particle tracking and compression assays to probe changes in nuclear mechanics with decreases in αII-spectrin levels. We show no changes in chromatin mechanics or in the stiffness of nuclei under compression. However, we do observe a reduction in the ability of nuclei with decreased

αII-spectrin to recover after compression. These results establish spectrin as a nucleoskeletal component that specifically contributes to elastic recovery of the nucleus after compression.

Investigating the Mechanism of Irregular Nuclear Shape in Hutchinson-Gilford Progeria Syndrome

In Chapter III we investigate the mechanism by which the mutant nucleoskeletal protein progerin alters the mechanical properties of the cell nucleus in Hutchinson-Gilford progeria syndrome. The nuclear lamina is a two-dimensional structural element that lines the inner nuclear membrane and protects the DNA in the nucleus of cells. Nuclear shape changes are hallmarks of diseases including Hutchinson-Gilford progeria syndrome, but it is unclear how the expression of the lamin protein variant progerin leads to altered wrinkled structure of the nucleus. In Chapter III we utilize unique deformation modes of the nuclear lamina, particularly when nuclei are under load, to provide insight into the microstructural changes associated with the expression of the variant protein. Specifically, we observe that invaginations of a healthy nuclear lamina network have a lower lamin intensity which suggests a local dilation, whereas invaginations in progerin expressing cells are associated with localized progerin accumulation. Control cells grown on confinements of pseudo-one-dimensional lines show folds in the lamina induced by actin filaments in the direction of confinement. However, progerin expressing cells show defects unassociated with the direction of force. These data, combined with modeling of stiffened inclusions, suggest that the deformation of the lamina in progerin-expressing networks is dominated by micro-aggregates rather than by the increased global stiffness of the lamina. Based on the importance of cytoskeletal-nuclear force coupling, we suggest that the non-isotropic distribution of force through the nuclear lamina has widespread implications on force transmission through the cell and could change during cellular aging.

Studying Mechanical Features of Epithelial Monolayers Using Sensors from IntraNuclear Kinetics (SINK)

In Chapter IV we introduce a particle tracking technique to probe the mechanical features of multicell systems, specifically epithelial monolayers. Force generation within cells, mediated by motor proteins along cytoskeletal networks, maintains the function of multicellular structures during homeostasis and when generating collective forces. In Chapter IV, we describe the use of chromatin dynamics to detect cellular force propagation (a technique termed Sensors from IntraNuclear Kinetics (SINK)) and investigate the response of cells to disruption of the monolayer and changes in substrate stiffness. We find that chromatin dynamics change in a substrate stiffness dependent manner within epithelial monolayers. We also investigate point defects within monolayers to map the impact on the strain field of a heterogeneous monolayer. We find that cell monolayers behave as a colloidal assembly rather than as a continuum since the data fit an exponential decay; the lateral characteristic length of recovery from the mechanical defect is approximately 50 μm for cells with a 10 μm spacing. At distances greater than this characteristic length, cells behave similarly to those in a fully intact monolayer. This work demonstrates the power of SINK to investigate diseases that result from single cells or heterogeneities in monolayers, including cancer and atherosclerosis.

Characterizing Substrate Stiffness Dependent Responses to Increased Cellular Force Generation

The feedback loop between a cell and the physical environment is critical for development and regulation of cell function. However, when this feedback loop is improperly controlled, cellular phenotype can become altered and ultimately lead to tissue malfunction and disease. For example, in fibrosis, the extracellular environment is stiffened. Cells can physically detect this change in stiffness which may cause increased susceptibility to chemical signals such

as growth factors. In Chapter V, we study changes in epithelial monolayer phenotype due to increased cell contractility using Calyculin A. We find that monolayer response is dependent upon the rigidity of the substrate on which the cells are grown. We measure chromatin dynamics, actin distribution, and YAP nuclear localization to characterize force propagation, cell phenotype, and mechanotransduction in these systems. Our results suggest that stiff substrates may lead to monolayer disruption and the beginnings of a transition to an isolated phenotype, which has implications in the cellular response to fibrosis and the mechanical inducers necessary (but likely not sufficient) for epithelial to mesenchymal transition.

References

1. Dahl, K. N., Ribeiro, A. J. S. & Lammerding, J. Nuclear Shape, Mechanics, and Mechanotransduction. *Circ. Res.* **102,** 1307–18 (2008).
2. Fletcher, D. A. & Mullins, R. D. Cell mechanics and the cytoskeleton. *Nature* **463,** 485–492 (2010).
3. Discher, D. E., Janmey, P. & Wang, Y.-L. Tissue cells feel and respond to the stiffness of their substrate. *Science* **310,** 1139–43 (2005).
4. Hoffman, B. D. & Crocker, J. C. Cell mechanics: dissecting the physical responses of cells to force. *Annu. Rev. Biomed. Eng.* **11,** 259–88 (2009).
5. Ladoux, B. & Mège, R.-M. Mechanobiology of collective cell behaviours. *Nat. Rev. Mol. Cell Biol.* **18,** 743–757 (2017).
6. Vining, K. H. & Mooney, D. J. Mechanical forces direct stem cell behaviour in development and regeneration. *Nat. Rev. Mol. Cell Biol.* **18,** 728–742 (2017).
7. Heilbrunn, L. V. The Viscosity of Protoplasm. *Q. Rev. Biol.* **2,** 230–248 (1927).
8. Bedner, P., Steinhäuser, C. & Theis, M. Functional redundancy and compensation among members of gap junction protein families? *Biochim. Biophys. Acta* **1818,** 1971–84 (2012).

9. Avriyanti, E. *et al.* Functional redundancy of protein kinase D1 and protein kinase D2 in neuronal polarity. *Neurosci. Res.* **95,** 12–20 (2015).

10. Zhang, X. *et al.* Syne-1 and Syne-2 play crucial roles in myonuclear anchorage and motor neuron innervation. *Development* **134,** 901–908 (2007).

11. Rajgor, D. & Shanahan, C. M. Nesprins: from the nuclear envelope and beyond. *Expert Rev. Mol. Med.* **15,** e5 (2013).

12. Zhang, X. *et al.* Talin depletion reveals independence of initial cell spreading from integrin activation and traction. *Nat. Cell Biol.* **10,** 1062–1068 (2008).

13. Spellman, R., Llorian, M. & Smith, C. W. J. Crossregulation and Functional Redundancy between the Splicing Regulator PTB and Its Paralogs nPTB and ROD1. *Mol. Cell* **27,** 420–434 (2007).

14. Al-Khalili, J. In Retrospect: Book of Optics. *Nature* **518,** 164–165 (2015).

15. Kriss, T. C. & Kriss, V. M. History of the Operating Microscope: From Magnifying Glass to Microneurosurgery. *Neurosurgery* **42,** 899–907 (1998).

16. Schultheiss, D. & Denil, J. History of the microscope and development of microsurgery: A revolution for reproductive tract surgery. *Andrologia* **34,** 234–241 (2002).

17. Uluç, K., Kujoth, G. C. & Başkaya, M. K. Operating microscopes: past, present, and future. *Neurosurg. Focus* **27,** E4 (2009).

18. Renz, M. Fluorescence microscopy-A historical and technical perspective. *Cytom. Part A* **83,** 767–779 (2013).

19. Rusk, N. Milestone 4: The fluorescence microscope. *Nat. Milestones Light Microsc.* **2,** 910–919 (2005).

20. van Ooij, C. Milestone 7: Recipe for fluorescent antibodies. *Nat. Milestones Light Microsc.* (2009). doi:10.1038/ncb1932

21. Swaminathan, S. Milestone 18: GFP: the green revolution. *Nat. Milestones Light Microsc.* **11,** (2009).

22. Baker, J. R. The Cell-Theory: a Restatement, History, and Critique PART II. *Q. J. Microsc. Sci.* **90,** 87–108 (1949).

23. Mazzarello, P. A unifying concept: the history of cell theory. *Nat. Cell Biol.* **1,** E13–E15 (1999).

24. Pray, L. A. Discovery of DNA Structure and Function: Watson and Crick. *Nat. Educ.* **1,** 100 (2008).

25. Felsenfeld, G. A brief history of epigenetics. *Cold Spring Harb. Perspect. Biol.* **6,** (2014).

26. Heilbrunn, L. V. The Physical Structure of the Protoplasm of Sea-Urchin Eggs. *Am. Nat.* **60,** 143–156 (1926).

27. Mast, S. O. The Structure of Protoplasm in Amoeba. *Am. Nat.* **60,** 133–142 (1926).

28. Heilbrunn, L. V. The absolute viscosity of protoplasm. *J. Exp. Zool.* **44,** 255–278 (1926).

29. Cowdry, E. V & Palma, F. X. Alterations in Nuclear Viscosity During Experimental Carcinogenesis Determined by Ultracentrifugation. *Am. J. Pathol.* **3,** 335–358 (1940).

30. Pelling, A. E. & Horton, M. A. An historical perspective on cell mechanics. *Pflügers Arch. - Eur. J. Physiol.* **456,** 3–12 (2008).

31. Warrick, H. M. & Spudich, J. A. Myosin Structure and Function in Cell Motility. *Ann. Rev. Cell Bioi* **3,** 379–421 (1987).

32. Iskratsch, T., Wolfenson, H. & Sheetz, M. P. Appreciating force and shape — the rise of mechanotransduction in cell biology. *Nat. Rev. Mol. Cell Biol.* **15,** 825–833 (2014).

33. Nicholson, H. A. Life and its Physical Basis. *Trans. Victoria Institue* **14,** 267–291 (1880).

34. Bianconi, E. *et al.* An estimation of the number of cells in the human body. *Ann. Hum. Biol.* **40,** 463–471 (2013).

35. Petridou, N. I., Spiró, Z. & Heisenberg, C.-P. Multiscale force sensing in development. *Nat. Cell Biol.* **19,** 581–588 (2017).

36. Heisenberg, C. P. & Bellaïche, Y. Forces in Tissue Morphogenesis and Patterning. *Cell* **153,** (2013).

37. Sweeton, D., Parks, S., Costa, M. & Wieschaus, E. Gastrulation in Drosophila: the formation of the ventral furrow and posterior midgut invaginations. *Development* **112,** 775–789 (1991).

38. Young, P. E., Pesacreta, T. C. & Kiehart, D. P. Dynamic changes in the distribution of cytoplasmic myosin during Drosophila embryogenesis. *Development* **111,** 1–14 (1991).

39. Warn, R., Maleki, S. & Bullard, B. Myosin as a constituent of the Drosophila egg cortex. *Nature* **278,** 651–653 (1979).

40. Martin, A. C., Kaschube, M. & Wieschaus, E. F. Pulsed contractions of an actin–myosin network drive apical constriction. *Nature* **457,** 495–499 (2009).

41. Rauzi, M. *et al.* Embryo-scale tissue mechanics during Drosophila gastrulation movements. *Nat. Commun.* **6,** 8677 (2015).

42. Horner, V. L. & Wolfner, M. F. Mechanical stimulation by osmotic and hydrostatic pressure activates Drosophila oocytes in vitro in a calcium-dependent manner. *Dev. Biol.* **316,** 100–9 (2008).

43. Kumar, A. & Shivashankar, G. V. Mechanical Force Alters Morphogenetic Movements and Segmental Gene Expression Patterns during Drosophila Embryogenesis. *PLoS One* **7,** e33089 (2012).

44. Mammoto, T. & Ingber, D. E. Mechanical control of tissue and organ development. *Development* **137,** 1407–20 (2010).

45. Stooke-Vaughan, G. A., Davidson, L. A. & Woolner, S. Xenopus as a model for studies in mechanical stress and cell division. *genesis* **55,** e23004 (2017).

46. Campàs, O. *et al.* Quantifying cell-generated mechanical forces within living embryonic tissues. *Nat. Methods* **11,** 183–189 (2014).

47. Gilbert, S. F. *Developmental Biology. 6th Edition. Sunderland (MA): Sinauer Associates. 6th Edition. Sunderland (MA): Sinauer Associates* (2000).

48. Bressan, M. & Mikawa, T. Avians as a model system of vascular development. *Methods Mol. Biol.* **1214,** 225–42 (2015).

49. Ouyang, X. & Chen, J. K. Synthetic strategies for studying embryonic development. *Chem. Biol.* **17,** 590–606 (2010).

50. Lonergan, P. & Fair, T. The ART of studying early embryo development: progress and challenges in ruminant embryo culture. *Theriogenology* **81,** 49–55 (2014).

51. Clause, K. C., Liu, L. J. & Tobita, K. Directed stem cell differentiation: the role of physical forces. *Cell Commun. Adhes.* **17,** 48–54 (2010).

52. Vining, K. H. & Mooney, D. J. Mechanical forces direct stem cell behaviour in development and regeneration. *Nat. Rev. Mol. Cell Biol.* **18,** 728–742 (2017).

53. D'Angelo, F. *et al.* Mechanotransduction: tuning stem cells fate. *J. Funct. Biomater.* **2,** 67–87 (2011).

54. Yim, E. K. F. & Sheetz, M. P. Force-dependent cell signaling in stem cell differentiation. *Stem Cell Res. Ther.* **3,** 41 (2012).

55. Kim, I. G. *et al.* Mechanotransduction of human pluripotent stem cells cultivated on tunable cell-derived extracellular matrix. *Biomaterials* **150,** 100–111 (2018).

56. Engler, A. J., Sen, S., Sweeney, H. L. & Discher, D. E. Matrix elasticity directs stem cell lineage specification. *Cell* **126,** 677–89 (2006).

57. Hadden, W. J. *et al.* Stem cell migration and mechanotransduction on linear stiffness gradient hydrogels. *Proc. Natl. Acad. Sci. U. S. A.* **114,** 5647–5652 (2017).

58. Dekker, R. J. *et al.* Prolonged fluid shear stress induces a distinct set of endothelial cell genes, most specifically lung Krüppel-like factor (KLF2). *Blood* **100,** 1689–98 (2002).

59. Wasserman, S. M. *et al.* Gene expression profile of human endothelial cells exposed to sustained fluid shear stress.

60. Chiu, J.-J. *et al.* Shear stress regulates gene expression in vascular endothelial cells in response to tumor necrosis factor-α: a study of the transcription profile with complementary DNA microarray. *J. Biomed. Sci.* **12,** 481–502 (2005).

61. Huynh, J. *et al.* Age-Related Intimal Stiffening Enhances Endothelial Permeability and Leukocyte Transmigration. *Sci Transl Med* **3,** (2011).

62. Lampi, M. C. *et al.* Simvastatin ameliorates matrix stiffness-mediated endothelial monolayer disruption. *PLoS One* **11,** 1–20 (2016).

63. Urbano, R. L., Furia, C., Basehore, S. & Clyne, A. M. Stiff Substrates Increase Inflammation-Induced Endothelial Monolayer Tension and Permeability. *Biophys. J.* **113,** 645–655 (2017).

64. Lamouille, S., Xu, J. & Derynck, R. Molecular mechanisms of epithelial-mesenchymal transition. *Nat. Rev. Mol. Cell Biol.* **15,** 178–96 (2014).

65. Leight, J. L., Wozniak, M. A., Chen, S., Lynch, M. L. & Chen, C. S. Matrix rigidity regulates a switch between TGF- 1-induced apoptosis and epithelial-mesenchymal transition. *Mol. Biol. Cell* **23,** 781–791 (2012).

66. Wei, S. C. *et al.* Matrix stiffness drives epithelial–mesenchymal transition and tumour metastasis through a TWIST1–G3BP2 mechanotransduction pathway. *Nat. Cell Biol.* **17,** 678–688 (2015).

67. Brugués, A. *et al.* Forces driving epithelial wound healing. *Nat. Phys.* **10,** (2014).

68. Sunyer, R. *et al.* Collective cell durotaxis emerges from long-range intercellular force transmission. *Science* **353,** 1157–1161 (2016).

69. Tambe, D. T. *et al.* Collective cell guidance by cooperative intercellular forces. *Nat. Mater.* **10,** 469–475 (2011).

70. Kim, J. H. *et al.* Propulsion and navigation within the advancing monolayer sheet. *Nat. Mater.* **12,** 856–63 (2013).

71. Han, S. J., Bielawski, K. S., Ting, L. H., Rodriguez, M. L. & Sniadecki, N. J. Decoupling substrate stiffness, spread area, and micropost density: A close spatial relationship between traction forces and focal adhesions. *Biophys. J.* **103,** 640–648 (2012).

72. Ghibaudo, M. *et al.* Traction forces and rigidity sensing regulate cell functions. *Soft Matter* **4,** 1836 (2008).

73. Andresen Eguiluz, R. C., Kaylan, K. B., Underhill, G. H. & Leckband, D. E. Substrate stiffness and VE-cadherin mechano-transduction coordinate to regulate endothelial

monolayer integrity. *Biomaterials* **140,** 45–57 (2017).

74. Krishnan, R. *et al.* Substrate stiffening promotes endothelial monolayer disruption through enhanced physical forces. *Am. J. Physiol. Cell Physiol.* **300,** C146–C154 (2011).

75. Califano, J. & Reinhart-King, C. Substrate Stiffness and Cell Area Predict Cellular Traction Stresses in Single Cells and Cells in Contact. *Cell Mol Bioeng* **3,** 68–75 (2011).

76. Sim, J. Y. *et al.* Spatial distribution of cell-cell and cell-ECM adhesions regulates force balance while main taining E-cadherin molecular tension in cell pairs. *Mol. Biol. Cell* **26,** 2456–2465 (2015).

77. Broders-Bondon, F., Nguyen Ho-Bouldoires, T. H., Fernandez-Sanchez, M.-E. & Farge, E. Mechanotransduction in tumor progression: The dark side of the force. *J. Cell Biol.* jcb.201701039 (2018). doi:10.1083/jcb.201701039

78. Chin, L., Xia, Y., Discher, D. E. & Janmey, P. A. Mechanotransduction in cancer. *Curr. Opin. Chem. Eng.* **11,** 77–84 (2016).

79. Lan, T.-H., Huang, X.-Q. & Tan, H.-M. Vascular fibrosis in atherosclerosis. *Cardiovasc. Pathol.* **22,** 401–407 (2013).

80. Talman, V. & Ruskoaho, H. Cardiac fibrosis in myocardial infarction-from repair and remodeling to regeneration. *Cell Tissue Res.* **365,** 563–81 (2016).

81. Liu, L. *et al.* Mechanotransduction-modulated fibrotic microniches reveal the contribution of angiogenesis in liver fibrosis. *Nat. Mater.* **16,** 1252–1261 (2017).

82. Mutsaers, H. A. M. & Olinga, P. Editorial: Organ Fibrosis: Triggers, Pathways, and Cellular Plasticity. *Front. Med.* **3,** 55 (2016).

83. Liu, F. *et al.* Mechanosignaling through YAP and TAZ drives fibroblast activation and fibrosis. *Am. J. Physiol. - Lung Cell. Mol. Physiol.* **308,** (2015).

84. Duscher, D. *et al.* Mechanotransduction and fibrosis. *J. Biomech.* **47,** 1997–2005 (2014).

85. Booth, E. A., Spagnol, S. T., Alcoser, T. A., Dahl, K. N. & Matter, S. Nuclear stiffening and chromatin softening with progerin expression leads to an attenuated nuclear response to force. *Soft Matter* **11,** 6412–6418 (2015).

86. Booth-Gauthier, E. a *et al.* Hutchinson-Gilford progeria syndrome alters nuclear shape and reduces cell motility in three dimensional model substrates. *Integr. Biol.* **5,** 569–77 (2013).

87. Dahl, K. N. *et al.* Distinct structural and mechanical properties of the nuclear lamina in Hutchinson-Gilford progeria syndrome. *Proc. Natl. Acad. Sci. U. S. A.* **103,** 10271–6 (2006).

88. Gruenbaum, Y., Margalit, A., Goldman, R. D., Shumaker, D. K. & Wilson, K. L. The nuclear lamina comes of age. *Nat. Rev. Mol. Cell Biol.* **6,** 21–31 (2005).

89. Spagnol, S. T., Armiger, T. J. & Dahl, K. N. Mechanobiology of Chromatin and the Nuclear Interior. *Cell. Mol. Bioeng.* **9,** (2016).

90. Chang, W., Worman, H. J. & Gundersen, G. G. Accessorizing and anchoring the LINC complex for multifunctionality. *J. Cell Biol.* **208,** 11–22 (2015).

91. Hartsock, A. & Nelson, W. J. Adherens and tight junctions: structure, function and connections to the actin cytoskeleton. *Biochim. Biophys. Acta* **1778,** 660–9 (2008).

92. Vicente-Manzanares, M., Choi, C. K. & Horwitz, A. R. Integrins in cell migration – the actin connection. *J. Cell Sci. J. Cell Sci* **122,** 1473–199 (2009).

93. Maniotis, A. J., Chen, C. S. & Ingber, D. E. Demonstration of mechanical connections between integrins, cytoskeletal filaments, and nucleoplasm that stabilize nuclear structure. *Cell Biol.* **94,** 849–854 (1997).

94. Wang, N., Tytell, J. D. & Ingber, D. E. Mechanotransduction at a distance: mechanically coupling the extracellular matrix with the nucleus. *Nat. Rev. Mol. Cell Biol.* **10,** 75–82 (2009).

95. Elosegui-Artola, A. *et al.* Mechanical regulation of a molecular clutch defines force transmission and transduction in response to matrix rigidity. *Nat. Cell Biol.* **18,** 540–548 (2016).

96. Buckley, C. D. *et al.* The minimal cadherin-catenin complex binds to actin filaments under force. *Science* **346,** 1254211 (2014).

97. Wilson, A. K., Pollenz, R. S., Chisholm, R. L. & de Lanerolle, P. The role of myosin I and

II in cell motility. *Cancer Metastasis Rev.* **11,** 79–91 (1992).

98. Parsons, J. T., Horwitz, A. R. & Schwartz, M. A. Cell adhesion: integrating cytoskeletal dynamics and cellular tension. *Nat. Rev. Mol. Cell Biol.* **11,** 633–43 (2010).

99. Lodish, H. *et al. Molecular Cell Biology. 4th edition. New York: W. H. Freeman* (2000). doi:10.1017/CBO9781107415324.004

100. Cooper, G. M. Cell-Cell Interactions. in *The Cell: A Molecular Approach. 2nd edition* (Sinauer Associates, 2000).

101. Wu, C. Focal adhesion: a focal point in current cell biology and molecular medicine. *Cell Adh. Migr.* **1,** 13–8 (2007).

102. Kim, N.-G., Koh, E., Chen, X. & Gumbiner, B. M. E-cadherin mediates contact inhibition of proliferation through Hippo signaling-pathway components. *Proc. Natl. Acad. Sci.* **108,** 11930–11935 (2011).

103. Bazellières, E. *et al.* Control of cell-cell forces and collective cell dynamics by the intercellular adhesome. *Nat. Cell Biol.* **17,** 409–420 (2015).

104. Barry, A. K., Wang, N. & Leckband, D. E. Local VE-cadherin mechanotransduction triggers long-ranged remodeling of endothelial monolayers. *J. Cell Sci.* **128,** 1341–1351 (2015).

105. Ng, M. R., Besser, A., Danuser, G. & Brugge, J. S. Substrate stiffness regulates cadherin-dependent collective migration through myosin-II contractility. *J. Cell Biol.* **199,** 545–563 (2012).

106. Sun, Z., Guo, S. S. & Fässler, R. Integrin-mediated mechanotransduction. *J. Cell Biol.* **215,** 445–456 (2016).

107. Wong, S., Guo, W.-H. & Wang, Y.-L. Fibroblasts probe substrate rigidity with filopodia extensions before occupying an area. doi:10.1073/pnas.1412285111

108. Elosegui-Artola, A. *et al.* Force Triggers YAP Nuclear Entry by Regulating Transport across Nuclear Pores Molecular regulation of transport Force Triggers YAP Nuclear Entry by Regulating Transport across Nuclear Pores. *Cell* **171,** 1397–1410 (2017).

109. Elosegui-Artola, A. *et al.* Rigidity sensing and adaptation through regulation of integrin types. *Nat. Mater.* **13,** (2014).

110. Elbediwy, A. *et al.* Integrin signalling regulates YAP and TAZ to control skin homeostasis. *Development* **143,** 1674–87 (2016).

111. Cooper, G. M. Structure and Organization of Actin Filaments. in *The Cell: A Molecular Approach. 2nd edition* (2000).

112. Blanchoin, L., Boujemaa-Paterski, R., Sykes, C. & Plastino, J. Actin dynamics, architecture, and mechanics in cell motility. *Physiol. Rev.* **94,** 235–63 (2014).

113. Muhamed, I. *et al.* E-cadherin-mediated force transduction signals regulate global cell mechanics. *J. Cell Sci.* **129,** 1843–54 (2016).

114. Fletcher, D. A. & Mullins, R. D. Cell mechanics and the cytoskeleton. *Nature* **463,** 485–92 (2010).

115. Isambert, H. *et al.* Flexibility of actin filaments derived from thermal fluctuations. Effect of bound nucleotide, phalloidin, and muscle regulatory proteins. *J. Biol. Chem.* **270,** 11437–11444 (1995).

116. Gittes, F., Mickey, B., Nettleton, J. & Howard, J. Flexural rigidity of microtubules and actin filaments measured from thermal fluctuations in shape. *J. Cell Biol.* **120,** 923–34 (1993).

117. Li, J. *et al.* Estimating Microtubule Distributions from 2D Immunofluorescence Microscopy Images Reveals Differences among Human Cultured Cell Lines. *PLoS One* **7,** (2012).

118. Melbinger, A., Reese, L. & Frey, E. Microtubule Length Regulation by Molecular Motors. doi:10.1103/PhysRevLett.108.258104

119. Berg, J. M., Tymoczko, J. L. & Stryer, L. Kinesin and Dynein Move Along Microtubules. (2002).

120. Cooper, G. M. Intermediate Filaments. in *The Cell: A Molecular Approach* (Sinauer Associates, 2000).

121. Simon, D. N. & Wilson, K. L. The nucleoskeleton as a genome-associated dynamic ‘network of networks’. *Nat. Rev. Mol. Cell Biol.* **12,** 695–708 (2011).

122. Dahl, K. N. & Kalinowski, A. Nucleoskeleton mechanics at a glance. *J. Cell Sci.* **124,** 675–678 (2011).

123. Zhong, Z., Wilson, K. L. & Dahl, K. N. Beyond lamins: other structural components of the nucleoskeleton. *Methods Cell Biol* **98,** 97–119 (2010).

124. Spagnol, S. T., Dahl, K. N. & Noel Dahl, K. Active cytoskeletal force and chromatin condensation independently modulate intranuclear network fluctuations. *Integr. Biol.* **6,** 523–31 (2014).

125. Arsenovic, P. T. T. *et al.* Nesprin-2G, a Component of the Nuclear LINC Complex, Is Subject to Myosin-Dependent Tension. *Biophys. J.* **110,** 34–43 (2016).

126. Buxboim, A. *et al.* Coordinated increase of nuclear tension and lamin-A with matrix stiffness outcompetes lamin-B receptor that favors soft tissue phenotypes. *Mol. Biol. Cell* **28,** 3333–3348 (2017).

127. Alam, S. G. *et al.* The nucleus is an intracellular propagator of tensile forces in NIH 3T3 fibroblasts. *J. Cell Sci.* **128,** 1901–1911 (2015).

128. Uzer, G. *et al.* Cell Mechanosensitivity to Extremely Low-Magnitude Signals Is Enabled by a LINCed Nucleus. *Stem Cells* **33,** 2063–76 (2015).

129. Guilluy, C. *et al.* Isolated nuclei adapt to force and reveal a mechanotransduction pathway in the nucleus. *Nat. Cell Biol.* **16,** 376–381 (2014).

130. Belmont, A. Dynamics of chromatin, proteins, and bodies within the cell nucleus. *Curr. Opin. Cell Biol.* **15,** 304–310 (2003).

131. de Lanerolle, P. & Serebryannyy, L. Nuclear actin and myosins: Life without filaments. *Nat. Cell Biol.* **13,** 1282–1288 (2011).

132. Bancaud, A. *et al.* Molecular crowding affects diffusion and binding of nuclear proteins in heterochromatin and reveals the fractal organization of chromatin. *EMBO J.* **28,** 3785–98 (2009).

133. Ou, H. D. *et al.* ChromEMT: Visualizing 3D chromatin structure and compaction in interphase and mitotic cells. *Science (80-.).* **357,** (2017).

134. Manning, G. S. The persistence length of DNA is reached from the persistence length of its null isomer through an internal electrostatic stretching force. *Biophys. J.* **91,** 3607–16 (2006).

135. Bystricky, K. Chromosome dynamics and folding in eukaryotes: Insights from live cell microscopy. *FEBS Lett.* **589,** 3014–3022 (2015).

136. Saksouk, N., Simboeck, E. & Déjardin, J. Constitutive heterochromatin formation and transcription in mammals. *Epigenetics Chromatin* **8,** 3 (2015).

137. Lippman, Z. & Martienssen, R. The role of RNA interference in heterochromatic silencing. *Nature* **431,** 364–370 (2004).

138. Volpe, T. & Martienssen, R. A. RNA interference and heterochromatin assembly. *Cold Spring Harb. Perspect. Biol.* **3,** a003731 (2011).

139. Dahl, K. N., Engler, A. J., Pajerowski, J. D. & Discher, D. E. Power-law rheology of isolated nuclei with deformation mapping of nuclear substructures. *Biophys. J.* **89,** 2855–64 (2005).

140. Misteli, T. Beyond the sequence: cellular organization of genome function. *Cell* **128,** 787–800 (2007).

141. Misteli, T. Protein Dynamics: Implications for Nuclear Architecture and Gene Expression.

142. Cook, P. R. A Model for all Genomes: The Role of Transcription Factories. *J. Mol. Biol.* **395,** 1–10 (2010).

143. Dupont, S. *et al.* Role of YAP/TAZ in mechanotransduction. *Nature* **474,** 179–183 (2011).

144. Jaalouk, D. E. & Lammerding, J. Mechanotransduction gone awry. *Nat. Rev. Mol. Cell Biol.* **10,** 63–73 (2009).

145. Tajik, A. *et al.* Transcription upregulation via force-induced direct stretching of chromatin. *Nat. Mater.* **15,** 1–20 (2016).

146. Livne, A. & Geiger, B. The inner workings of stress fibers - from contractile machinery to focal adhesions and back. *J. Cell Sci.* **129,** 1293–304 (2016).

147. Pietuch, A. & Janshoff, A. Mechanics of spreading cells probed by atomic force microscopy. *Open Biol.* **3,** 130084 (2013).

148. Kim, D.-H. D.-H. *et al.* Volume regulation and shape bifurcation in the cell nucleus. *J. Cell Sci.* **128,** 457–457 (2016).

149. Lee, H. *et al.* Cytoskeletal prestress regulates nuclear shape and stiffness in cardiac myocytes. *Exp. Biol. Med. (Maywood).* **240,** 1543–54 (2015).

150. Vaziri, A. & Mofrad, M. R. K. Mechanics and deformation of the nucleus in micropipette aspiration experiment. *J. Biomech.* **40,** 2053–62 (2007).

151. Kumar, S. *et al.* Viscoelastic Retraction of Single Living Stress Fibers and Its Impact on Cell Shape, Cytoskeletal Organization, and Extracellular Matrix Mechanics. *Biophys. J.* **90,** 3762–3773 (2006).

152. Rape, A., Guo, W. & Wang, Y.-L. The Regulation of Traction Force in Relation to Cell Shape and Focal Adhesions. *Biomaterials* **32,** 2043–2051 (2011).

153. Li, J., Dao, M., Lim, C. T. & Suresh, S. Spectrin-Level Modeling of the Cytoskeleton and Optical Tweezers Stretching of the Erythrocyte. *Biophys. J.* **88,** 3707–19 (2005).

154. Armiger, T. J. & Dahl, K. N. The role of αII-spectrin in mechanics and compressive resilience of the cell nucleus. in *2015 41st Annual Northeast Biomedical Engineering Conference, NEBEC 2015* (2015). doi:10.1109/NEBEC.2015.7117147

155. Tse, J. M. *et al.* Mechanical compression drives cancer cells toward invasive phenotype. *Proc. Natl. Acad. Sci.* **109,** 911–916 (2012).

156. Steward, R. L., Cheng, C.-M., Ye, J. D., Bellin, R. M. & LeDuc, P. R. Mechanical stretch and shear flow induced reorganization and recruitment of fibronectin in fibroblasts. *Sci. Rep.* **1,** 147 (2011).

157. Guo, M. *et al.* Probing the stochastic, motor-driven properties of the cytoplasm using force spectrum microscopy. *Cell* **158,** 822–832 (2014).

158. Gal, N., Lechtman-Goldstein, D. & Weihs, D. Particle tracking in living cells: a review of the mean square displacement method and beyond. *Rheol. Acta* **52,** 425–443 (2013).

159. Cai, D. *et al.* Mechanical feedback through E-cadherin promotes direction sensing during collective cell migration. *Cell* **157,** 1146–59 (2014).

160. Dahl, K. N., Kahn, S. M., Wilson, K. L. & Discher, D. E. The nuclear envelope lamina network has elasticity and a compressibility limit suggestive of a molecular shock absorber. *J. Cell Sci.* **117,** 4779–86 (2004).

161. Khetan, S. *et al.* Degradation-mediated cellular traction directs stem cell fate in covalently crosslinked three-dimensional hydrogels. *Nat. Mater.* **12,** 458–65 (2013).

162. Hanson, L. *et al.* Vertical nanopillars for in situ probing of nuclear mechanics in adherent cells. *Nat. Nanotechnol.* 1–10 (2015). doi:10.1038/nnano.2015.88

163. Sun, Y., Duffy, R., Lee, A. & Feinberg, A. W. Optimizing the structure and contractility of engineered skeletal muscle thin films. *Acta Biomater.* **9,** 7885–7894 (2013).

164. Guilak, F., Tedrow, J. R. & Burgkart, R. Viscoelastic properties of the cell nucleus. *Biochem. Biophys. Res. Commun.* **269,** 781–6 (2000).

165. Luo, Q., Kuang, D., Zhang, B. & Song, G. Cell stiffness determined by atomic force microscopy and its correlation with cell motility. *Biochim. Biophys. Acta - Gen. Subj.* **1860,** 1953–1960 (2016).

166. Tseng, Y., Lee, J. S. H., Kole, T. P., Jiang, I. & Wirtz, D. Micro-organization and visco-elasticity of the interphase nucleus revealed by particle nanotracking. *J. Cell Sci.* **117,** 2159–67 (2004).

Chapter II: Nuclear Mechanical Resilience but Not Stiffness is Modulated by αII-Spectrin

Introduction

Spectrin proteins (spectrins) are multi-domain, elastic proteins which are known to have a dominant role in red blood cell mechanics. Despite their known association with nuclear structural proteins, their mechanical role within the nucleus remains to be determined. Spectrins are best studied in erythrocytes, where αI-spectrin and βI-spectrin form the primary membrane-bound network that provides elasticity and resilience to the red blood cell plasma membrane[1–4]. αII-spectrin (in combination with various β-spectrin isoforms) is found associated with the membrane and in the cytoskeleton of nucleated cells. In nucleated cells, spectrins help regulate membrane stability[5–7] and have been identified in various organelles such as the Golgi apparatus[8,9] and the nucleus[10,11].

Nuclear αII-spectrin (αII-Sp) is associated with DNA damage repair. While there are no known human mutations of the αII-Sp gene *SPTAN1*, lymphoblastoid cells from patients with Fanconi anemia show a decrease in αII-Sp[10,12]. These cells, as well as HeLa cells with siRNA-induced αII-Sp reduction, show increased susceptibility to DNA interstrand cross-linking agents[13,14]. Additionally, nuclear αII-Sp appears critical for telomere stability after DNA damage. αII-Sp colocalizes with telomeric proteins after cells are treated with an interstrand cross-linking agent and is required for the DNA damage repair protein XPF to localize to telomeres after interstrand cross-links are induced[15].

In addition to this role of DNA interstrand crosslink repair and chromosome stability in the nuclear interior, it is suspected that αII-Sp may serve a function in the nucleoskeleton as well[16–18]. Within the nucleus, αII-Sp has been shown to associate with structural proteins

including lamin A, actin, emerin and nuclear myosin via co-immunoprecipitation[17,19]. These associations with structural proteins, along with the understood role of spectrins in erythrocyte membrane stabilization, led to the hypothesis that spectrin proteins help to regulate the mechanics of the nucleus. However, a direct functional mechanical role has not been demonstrated for spectrins.

It is increasingly appreciated that nuclear structure and stiffness correlate with cell functionality[20–22]. While lamins in the nucleoskeleton have been shown to be a primary component to nuclear stiffness[23–25], a potential spectrin network may also play a critical role in regulating the mechanical properties of the nucleus[18]. In this chapter we aim to address the mechanical role of nuclear spectrin. We reduce the level of αII-Sp via RNA interference and then probe mechanical changes of chromatin using live cell intranuclear particle tracking and test the mechanics of the whole nucleus using a live cell compression assay. While the loss of αII-Sp is associated with inhibited DNA damage repair, we find that reduction αII-Sp has no impact on the rheology of the chromatin interior. Reduction in αII-Sp does not appear to alter nuclear size, but αII-Sp does impact the resilience of the nucleus, as evident by a failure to return to initial nuclear area after being compressed; control cell nuclei return to their initial nuclear area after being compressed. Thus, the mechanical role of spectrins in the nucleus appears to be at the inner nuclear membrane, similar to their role at the plasma membrane. Unlike lamin filaments that provide stiffness, spectrins seems to provide resilience to the cell nucleus.

Materials and Methods

Cell Culture and Transfection

HeLa cells (ATCC, Manassas, VA) were cultured at 37°C and 5% CO_2 in low glucose Dulbecco's Modified Eagle Medium (DMEM, Cat # 11885) supplemented with 10% fetal

bovine serum and 1% penicillin/streptomycin (all from Thermo Fisher, Waltham, MA). Cells were transfected with Lipofecatamine3000 transfection reagent (Thermo Fisher, Waltham, MA) based on manufacturers protocols. Media was changed 5 hours after transfection. αII-spectrin knock-down was achieved using a short hairpin RNA (shRNA) vector targeted against the nonerythroid αII-spectrin gene, *SPTAN1* (RHS4430-200292631, Dharmacon, Lafayette, CO, USA). The shRNA vector backbone contains a green fluorescent protein (GFP) reporter protein to assess which cells in a given field of view took up the knock-down vector. The knock-down control vector used was a scramble control vector with the same backbone and reporter as the *SPTAN1* knock-down vector but targeted against no mRNA sequence in any mammalian genome (RHS4346, Dharmacon, Lafayette, CO). All spectrin knock-down experiments were performed 4 days after transfection with the αII-Sp knock-down vector or the scramble control vector. For all experiments, cells which took up the αII-Sp knock-down vector and expressed GFP are referred to as knock-down spectrin (KDSp) cells. Cells which took up the scramble control vector and expressed GFP are referred to as knock-down control (KDC) cells. For the particle tracking experiments, cells were transfected with a red fluorescent protein tagged telomeric protein TRF1 (RFP-TRF1) and imaged 24 hours later. RFP-TRF1 was prepared by Patricia Opresko, University of Pittsburgh from EYFP-TRF1[26], and the EYFP tag was removed with AgeI and EcoRI and replaced with the tagRFP gene from pTagRFP-C vector (Envrogen, Moscow, Russia). KDSp cells were transfected with the αII-Sp knock-down vector 4 days prior to imaging, and subsequently transfected with RFP-TRF1 24-hours prior to imaging.

Western Blot and Nuclear Isolation

Since the vector backbones used for transfection contain puromycin resistance, puromycin (2 μg/mL) (Thermo Fisher, Waltham, MA) was added to the dishes 48 hours after

transfection for western blot experiments. After appropriate transfection and growth with puromycin, cells were scraped from 60mm dishes, and lysed with ice cold Radioimmunoprecipitation assay (RIPA) buffer (Thermo Fisher, Waltham, MA) supplemented with protease inhibitor. In the case of nuclear isolation, nuclei were isolated using Nuclei EZ Prep nuclei isolation kit (Sigma Aldrich, St. Louis, MO), prior to lysing. Total protein concentration was measured via absorbance at 562 nm using a Nanodrop 2000c device (Thermo Scientific, Waltham, MA). Samples were prepared in bicinchoninic acid (BCA) reagent. Total protein was used as a loading control versus other proteins because spectrin levels could influence levels of structural proteins (lamins, actins, tubulins), and since nuclei were isolated many metabolic loading controls could not be used. Once total protein concentration was measured, sample volume was adjusted such that the same mass of protein was added to each well for the whole cell western blot experiments. Similarly, the same total protein mass was added to each well for the isolated nuclei experiment. Thus, the relative band widths of the wells in the whole cell experiments may be compared, and the relative band widths of the wells in the isolated nuclei western blot experiments may be compared, but the relative band widths between these two experiments should not be compared. Protein samples were diluted in Laemmli buffer (Bio Rad, Hercules, CA) with 5% 2-Mercapotethanol (Bio Rad, Hercules, CA), heated for 5 minutes at 95°C, and run on a Mini-PROTEIN TGX 7.5% gel (Bio Rad, Hercules, CA) at 200V. Protein was transferred onto PVDF membranes (iBlot Gel Transfer Stacks, Thermo Fisher, Waltham, MA) using an iBlot Gel Transfer Device (Thermo Fisher, Waltham, MA). Protein staining was performed using WesternBreeze anti-mouse Chemiluminescent kit (Thermo Fisher, Waltham, MA) according to manufacturer's protocol. The primary antibody against αII-spectrin

(sc-376849, Santa Cruz Biotechnology, Dallas, TX) was diluted 1:100. Bands were visualized using an ImageQuant LAS 4000 device (GE, Fairfield, CT).

Immunofluorescence

Cells were grown on coverslips, fixed with a 4% formaldehyde solution (Thermo Fisher, Waltham, MA), subsequently permeabilized with a 0.2% triton X-100 solution (TJ Baker Chemical, Center Valley, PA), and blocked with a 0.2% bovine serum albumin (BSA) solution (BSA from Sigma-Aldrich, St. Louis, MO). The primary mouse antibody (sc-376849, Santa Cruz Biotechnology, Dallas, TX) was diluted 1:100 in 0.2% BSA solutions and cells were incubated in this solution for 1 hour. The secondary antibody, donkey anti-mouse Alexa Fluorophore 647 (A31571, Thermo Fisher, Waltham, MA) was diluted 1:200 in 0.2% BSA and cells were incubated in this solution for 1 hour. Nuclei were stained with Hoechst 33342 (Life Technologies, Grand Island, NY). Analysis of the intensity of the αII-Sp channel was performed in ImageJ. The average αII-Sp intensity within each cell which took up the given vector was compared to the average αII-Sp intensity of control cells which did not take up (no GFP expression) the vector in each field of view (i.e. side-by-side control). In order to perform side by side controls, puromycin was not added for these experiments.

Cell Imaging

Cells were imaged with a 63x (1.4 NA) oil immersion inverted microscope (DMI6000, Leica, Buffalo Grove, IL) with a DFC350 camera. For live cell imaging experiments, cells were imaged in a live cell imaging chamber (PeCon, Erbach, Germany) actively maintained at 37°C and 5% CO_2 (PeCon, Erbach, Germany).

Live Cell Compression Assay

HeLa cells were grown in glass bottom dishes (P35G-1.5-14-C, MatTek Corporation, Ashland, MA) and transfected with the appropriate vector. Cell nuclei were stained with Hoechst 33342, and propidium iodide (PI) (Invitrogen, Carlsbad, CA) was added to the media prior to imaging to reject cells whose membranes burst during compression. Cells were subjected to unconfined compression, and images were taken before application of weight, during compression, and after release of compression. A 50g static mass was placed over an area of 0.5 cm^2, with a silicon spacer placed between the stiff mass to evenly distribute the force over the given area. Transfected cells were detected by a GFP reporter protein. Only cells with high levels of GFP expression were used for knock-down spectrin (KDSp) or knock-down control (KDC) data. Cells not expressing GFP, in the same field of view as the KDSp cells were used as side-by-side controls. The exposure time and intensity were increased to assure that side-by-side control cells were not expressing low levels of the GFP reporter. Cells not treated with any vector or transfection reagent were used as wild type (WT) controls. Projected nuclear area was measured based on the Hoechst nuclear stain using ImageJ. For analysis, nuclear area was normalized to the initial nuclear area of a given cell. A 1-way ANOVA followed by Tukey's pairwise comparison test was performed to determine significant differences between normalized nuclear area increase for each condition. To obtain the side-by-side control puromycin was not used for compression experiments. For the compression assay, samples sizes were as follows: n = 35 WT nuclei, n = 13 side-by-side control nuclei, n = 10 KDC nuclei, and n = 12 KDSp nuclei.

Intranuclear Particle Tracking

HeLa cells were grown in glass bottom dishes (P35G-1.5-14-C, MatTek Corporation, Ashland, MA) and cells were transfected with RFP-TRF1, which is visualized as fluorescent

speckles within the nucleus when expressed. The motion of these speckles was tracked over time, and mean square displacement (MSD) was calculated. Cells were imaged as described above. Images were gathered at 3-minute time intervals for 1 hour. Cells were imaged for an additional hour to assure cell viability, but only the first hour was used for analysis. Single point 2-D particle tracking analysis was performed on these images in MATLAB using custom Laptrack71 software developed by Ge Yang as previously published[27,28]. Using this software, nuclei were cropped and aligned at each frame to remove rigid body motion such that only intranuclear motion was captured. Only points which persisted for the entire hour of imaging were tracked and used for analysis. Student's t-test was performed to test for statistical differences between MSD at each lag time. Sample sizes for intranuclear particle tracking analysis were as follows: n = 12 WT cells, with 37 total points tracked and n = 17 KDSp cells, with 65 total points tracked.

Results

Confirmation of αII-Spectrin Knock-Down

In order to determine the mechanical effects of nuclear spectrin proteins, we aimed to compare cells with decreased levels of nuclear αII-Sp to control cells. We investigated cells with reduced levels of αII-Sp since complete loss of αII-Sp is lethal to cells[14]. The gene *SPTAN1*, which codes for αII-Sp, was chosen as the knock-down target since it is the only gene which codes for α-spectrins in non-erythrocytes, while up to 5 genes code for β spectrins[29]. Knock-down of αII-Sp was used to assess the mechanical impact of a potential nucleoskeletal spectrin network, since sufficient knock-down of αII-Sp would cause disruption of this network, and potentially alter the mechanical properties of the nucleus. Knock-down treatments were performed via transient transfection with a shRNA vector targeted against αII-Sp. While we

aimed to isolate and identify the role of nuclear spectrin, αII-Sp is also present at the plasma membrane. As no nucleoskeletal-specific αII-Sp isoform is known, αII-Sp levels were decreased both in the cytoskeleton as well as in the nucleus with the shRNA, which we confirmed by western blot analysis, shown in Figure 2.1 for both whole cell and isolated nuclear lysates. The level of αII-Sp in KDSp cells was compared to that in non-treated, WT cells, and KDC cells, which were treated with a scramble control vector with the same backbone as the αII-Sp knock-down vector. KDSp and KDC were treated with antibiotic (see Methods) to isolate cells which had taken up the vector. These results indicate that αII-Sp levels were decreased in the whole cell, as well as the nucleus of KDSp cells. With the shRNA vector, KDSp isolated nuclei had approximately a 68% reduction of αII-Sp compared KDC nuclei, as determined by western blot area analysis in ImageJ. By comparison, KDSp whole cells had a 51% reduction of αII-Sp compared to KDC whole cells. Interestingly, bands of lower molecular weight proteins were present in all of the whole cell lysates, but were not observed in the isolated nuclei lysates, even after prolonged exposure for chemiluminescence (Figure 2.1, Figure 2.2). This indicates that cytoskeleton-specific αII-Sp isoforms may exist, which are not present in the cell nucleus.

To further confirm decreased levels of αII-Sp, immunofluorescence (IF) experiments were run. While several antibodies against αII-Sp were tested, none were found to exclusively label nuclear αII-Sp. The αII-Sp knock-down vector and the scramble control vector contain a GFP reporter protein to visually determine which cells have taken up the plasmid. Figure 2.3 A and B, compare the normalized intensity of αII-Sp KDC cells to KDSp cells (no antibiotic). The αII-Sp IF intensity was decreased in KDSp (expressing GFP) cells, relative to cells which did not take up the vector in the same field of view. KDC (expressing GFP) cells had similar levels of αII-Sp to cells which did not take up the vector in the same field of view. The relative intensities

of cells which took up a given vector compared to cells which did not take up the vector, are quantified in Figure 2.3 C. Based on this quantification, it is estimated that αII-Sp levels in KDSp cells were decreased to approximately 50% of those in KDC cells or in the side-by-side controls. These results, combined with the western blot results, show that cells treated with the αII-Sp knock-down vector, which express GFP, have decreased levels of nuclear αII-Sp, and therefore can be used for analysis in future experiments to determine the role of αII-Sp in nuclear mechanics.

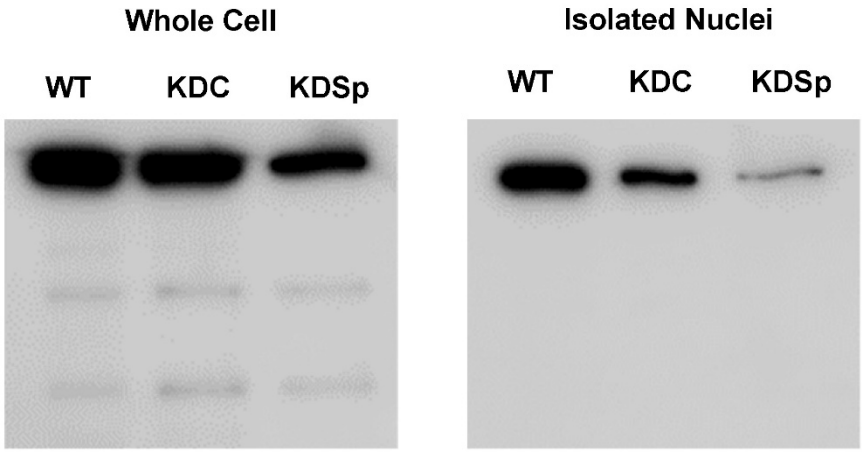

Figure 2.1: Western blot showing αII-spectrin protein level decreases in whole cells, and isolated nuclei

Bands below the primary band in whole cells (left) demonstrate αII-spectrin isoforms may be present in the cytoskeleton which are not seen in the nucleus (right).

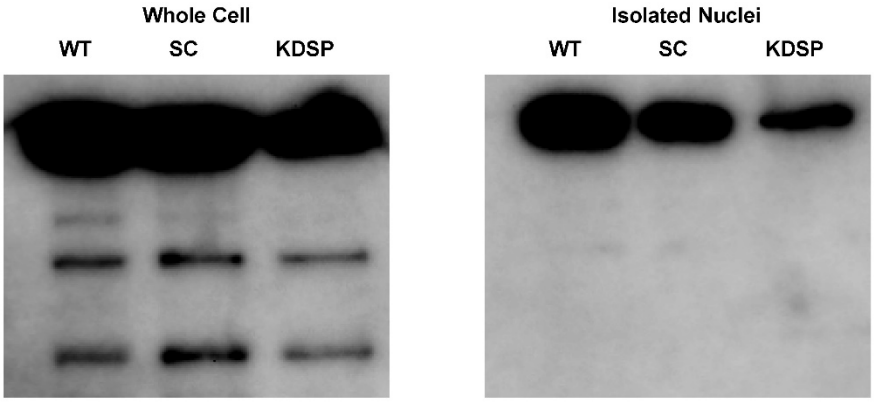

Figure 2.2: Western blot showing αII-spectrin protein level decrease in whole cells, and isolated nuclei, increased exposure time

Bands below the primary band in whole cells demonstrate αII-spectrin isoforms present in the cytoskeleton which are not seen in the nucleus. This image is the same as that shown in Figure 2.1, but exposure time was increased to emphasize the lower molecular weight bands.

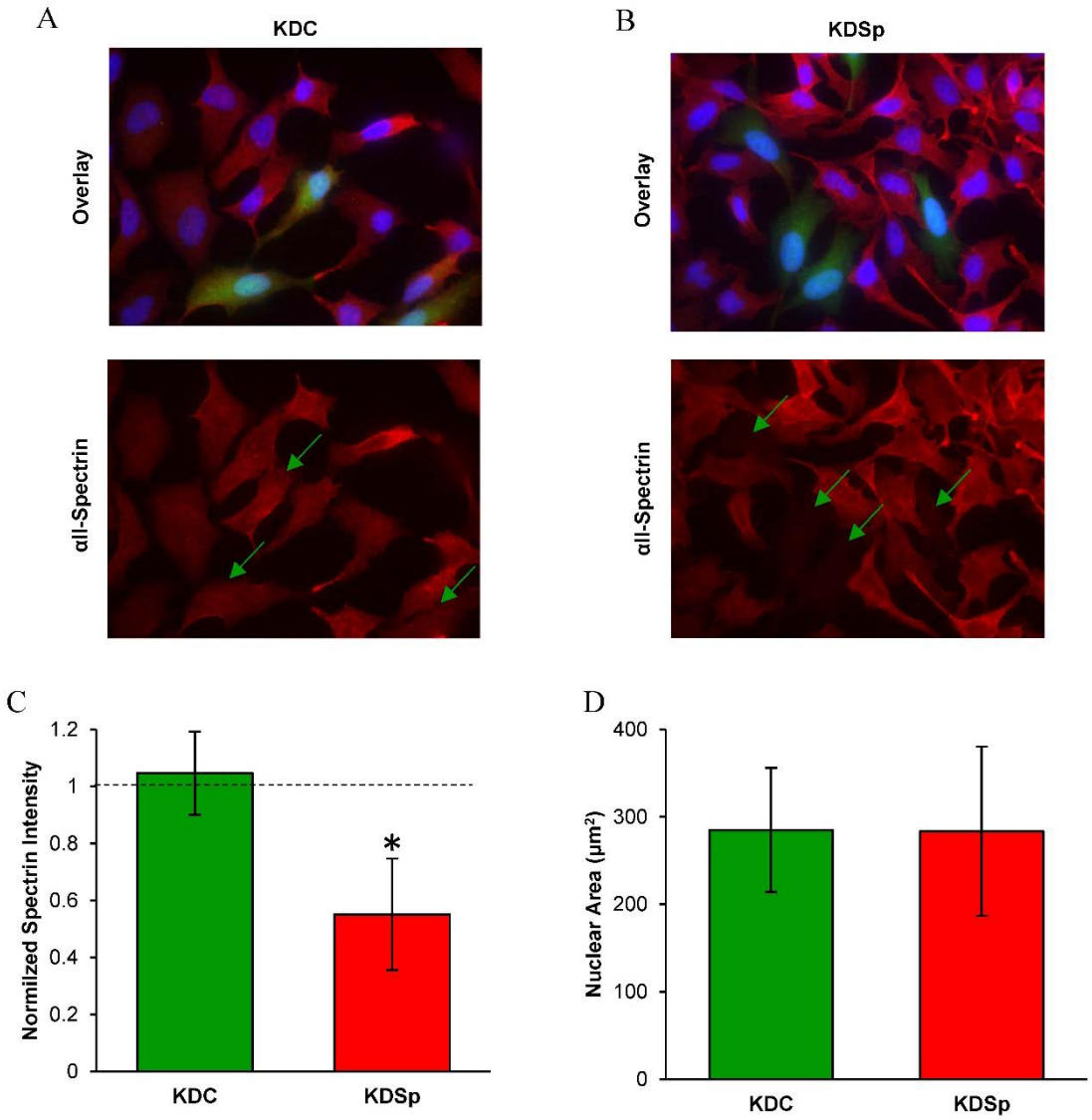

Figure 2.3: Immunofluorescence (IF) and quantification of fluorescence of KDSp and KDC cells

*(**A**) IF of scramble control (KDC – green) cells which express control levels of αII-Sp is shown. Green arrows show locations in the αII-Sp channel of cells which express the GFP-reporter and thus have taken up the given vector. (**B**) IF images of αII-Sp which demonstrate decreased αII-Sp levels in cells which have taken up the knock-down vector (KDSp – green) are shown. (**C**) Quantification of intensity of αII-spectrin channel from IF images is shown. Average intensity of the αII-Sp channel*

*was calculated for cells which had taken up a given vector and divided by the average intensity of the αII-Sp channel of non-transfected cells in each field of view (n = 12 fields of view for each condition). Error bars are standard deviation between fields of view. Asterisk denotes significant difference (p < 0.05). (**D**) A comparison of initial nuclear area (i.e. no compression) between KDC and KDSp cells is shown. No significant difference in nuclear area was detected in these cells as measured by Student's t-test. n = 19 KDSp nuclei, and n = 28 KDC nuclei. Error bars represent standard deviation.*

Intranuclear Movement is Unaffected in αII-Spectrin Depleted Cells

Previously, it was shown that loss of αII-Sp was associated with impaired DNA damage repair and telomere function following DNA interstrand crosslinks[14,15]. Thus, we hypothesized that there may be a structural role of this protein within the chromatin. Since chromatin structure and stability often influence mechanics, we hypothesized that reduction of αII-Sp would alter intranuclear rheology. To measure intranuclear movement, cells were transfected with a RFP-tagged telomeric protein TRF1 (RFP-TRF1). The fluorescent nuclear speckles of TRF1 were tracked over time and mean squared displacement (MSD) was calculated. Figure 2.4 A shows a nucleus transfected with RFP-TRF1. The tracks of high intensity speckles are overlaid on the fluorescent image in Figure 2.4 B. A plot of intranuclear MSD versus lag time comparting WT cells to KDSp cells is shown in Figure 2.4 C. KDSp cells show no change in MSD of intranuclear movement compared with WT cells. Thus, it appears that the decreased levels of αII-Sp have no effect on motion of the chromatin inside the nucleus.

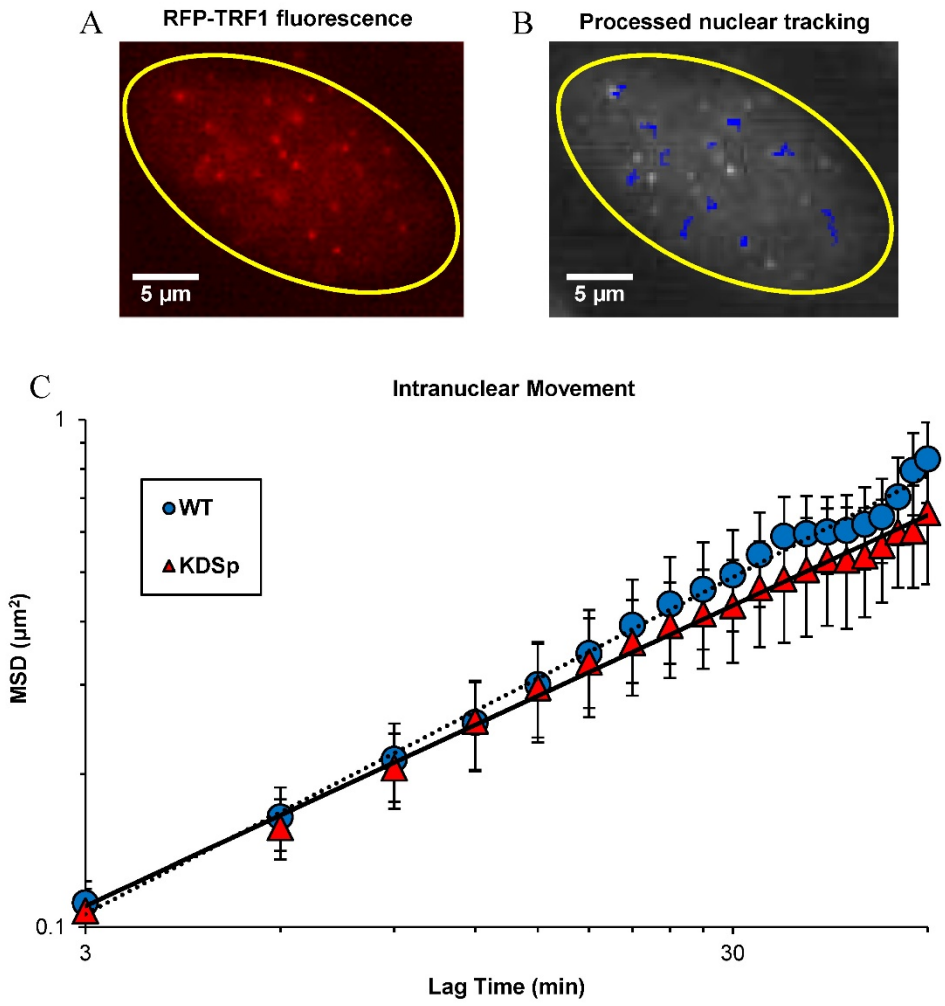

Figure 2.4: Intranuclear particle tracking analysis

*(**A**) An example of a cell nucleus (yellow outline) expressing RFP-TRF1 is shown. This telomeric protein appears as punctate fluorescent speckles in the nucleus which are tracked at 3-minute time intervals for 1 hour. (**B**) Tracks (blue overlay) of these chromatin-bound proteins demonstrate Brownian motion. (**C**) A plot of mean squared displacement (MSD) vs. lag time for αII-spectrin knock-down*

cells compared to wild type (non-treated) cells is shown. Interestingly, no significant difference is seen in MSD between groups for any lag time, indicating no changes in intranuclear movement when spectrin levels are decreased. n = 12 WT cells, with 37 total points tracked and n = 17 KDSp cells, with 65 total points tracked.

αII-Spectrin Depleted Cell Nuclei Show Decreased Resilience to Applied Force

Once decreased levels of nuclear αII-Sp were confirmed, we aimed to determine the mechanical role of αII-Sp in the nucleus. First, we investigated the impact of decreased αII-Sp on nuclear size in cultured cells. HeLa cells were transfected with the *SPTAN1* shRNA, and no significant difference in projected nuclear area was detected between KDSp and KDC cells at the same confluency, as shown in Figure 2.3 D. We then compressed the cells and observed nuclear deformation inside live cells. Briefly, a static load was placed on top of a population of cells, such that they underwent unconfined compression. Images were taken before compression, while being compressed (weight on), and once compression was released (weight removed), which were then used to determine nuclear area. Relative nuclear area was calculated by comparing nuclear area to the initial nuclear area before compression of a given cell. Propidium iodide (PI) was added to the media prior to compressing the cells to verify cell and cell membrane viability following compression. Only cells with intact membranes (i.e. those not stained by PI) upon removal of the weight were used for analysis. A representative image of WT control cell nuclei before, during, and after compression is shown in Figure 2.5. This image shows the increase in nuclear area during compression and return to initial area upon release. Additionally, a cell in the release frame is stained with PI, indicating a compromised membrane, and would not be used for analysis. A representative fluorescent image comparing KDSp to KDC treated cells is shown in

Figure 2.6. Cells expressing the GFP reporter are those which had taken up the vector. Cells which did not express GFP in the KDSp treated cells were used as side-by-side control cells, to assure that changes in nuclear area were not an artifact of changes in force distribution between experiments. Quantification of increase in nuclear area, normalized to initial nuclear area, for KDSp cells and 3 sets of control cells (WT, side-by-side, and KDC) under compression, followed by release of compression, is shown in Figure 2.7. KDSp cells appeared to increase in nuclear area the same extent as control cells, but upon release of compression, the KDSp cell nuclei did not return to their initial nuclear area, while control cells all return to their initial nuclear area. This suggests a potential spring-like role of αII-Sp, which allows nuclei to return to original area after deformation. However, given the similar extent of nuclear area increase during compression, αII-Sp appears to play a negligible role in regulating nuclear stiffness. We also investigated the role of the nucleoskeletal protein emerin in nuclear mechanics with the compression assays by treating cells with an emerin knock-down vector. Unlike spectrin, emerin does not appear to impact nuclear resilience (data given in Appendix A). Regression analysis comparing the deformation of each nucleus with its recovery shows the power of this compression technique (Figure 2.7 B). For each sample (KDSp and all of the controls), larger deformed area correlated with larger area after release of compression. All samples had the same regression slope implying that dilation under compression and regression was not treatment-specific. However, the zero-strain intercept was very different between samples. Both the side-by-side control and KDC regressed to the same point, suggesting that the presence of the transfection agent may alter the cell or nucleus in some way. These controls were slightly different than the WT (no treatment control), but all controls showed a negative intercept

suggesting that at a limit of no compression there is a nuclear contraction or pre-stress in cells that may be mediated by the spectrin network. In KDSp cells, the intercept is at zero.

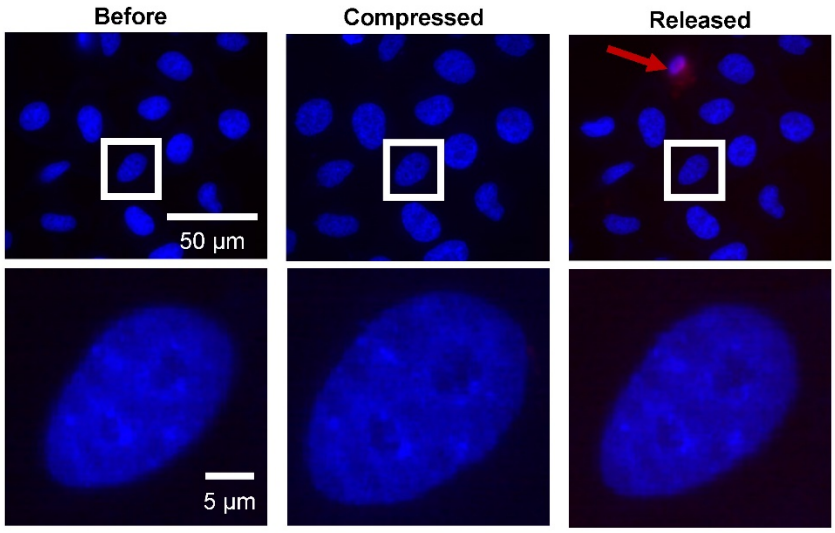

Figure 2.5: Example of nuclear area increase, and subsequent decrease in wild type control cells after compression, and release of compression

Nuclei are stained with Hoechst. Propidium iodide (PI) was added to media for compression assays to assure cell membrane remained intact for the entire experiment. In the release frame, a PI stain is seen in one cell, indicated by a red arrow. This cell would not be used for analysis.

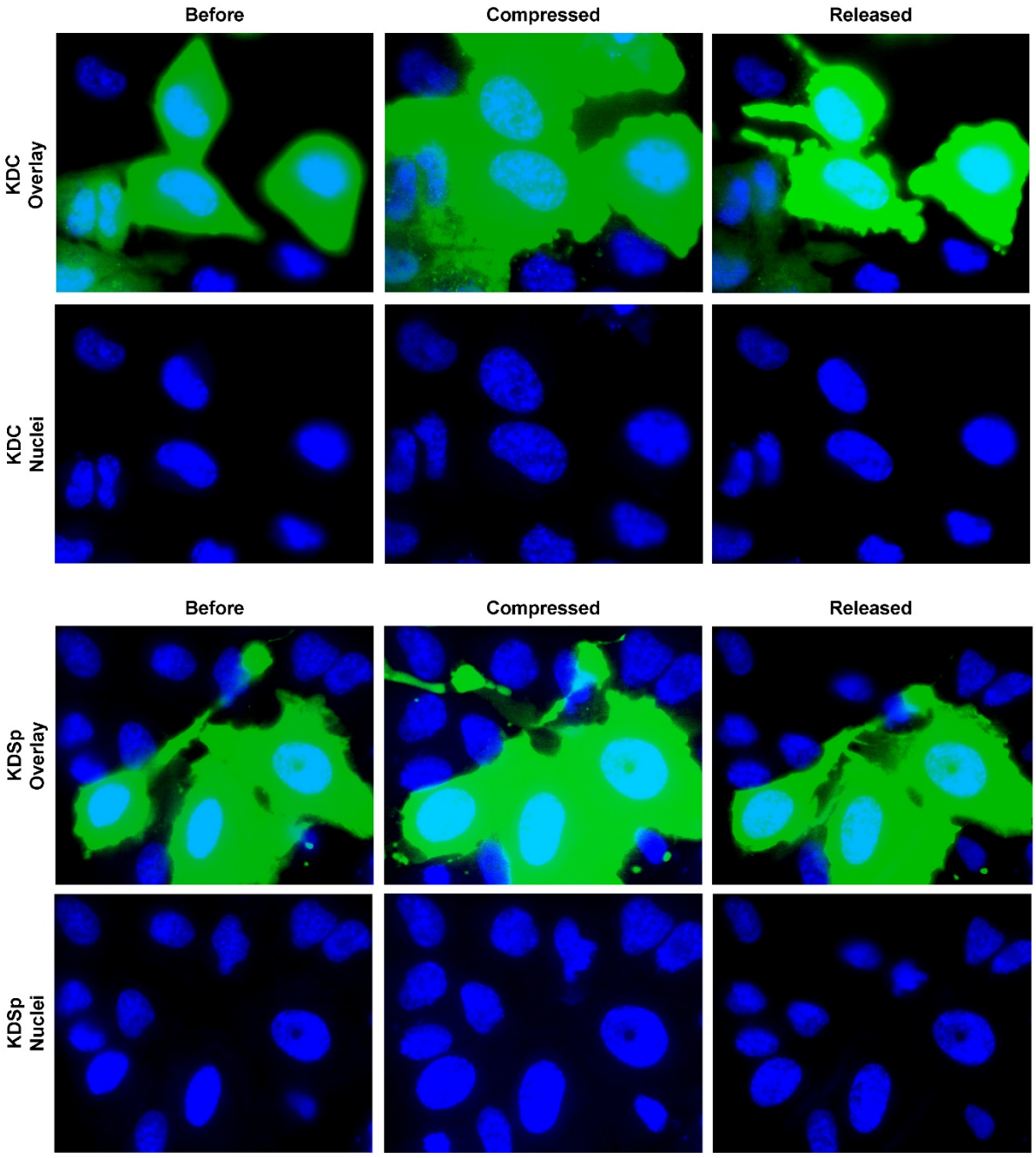

Figure 2.6: Images of live cell compression assay comparing KDSp to KDC

Images are taken before, during, and after application of a 50g static weight, and nuclear area was calculated. The GFP reporter is expressed in cells which have taken up the given vector.

Thus, these cells could easily be distinguished for analysis. Control cells which did not take up the knock-down vector are designated as side-by-side control cells in Figure 2.7. PI stain was added and only cells with intact membranes, which persisted for the entire assay were used for analysis. Nuclei are stained with Hoechst 33342.

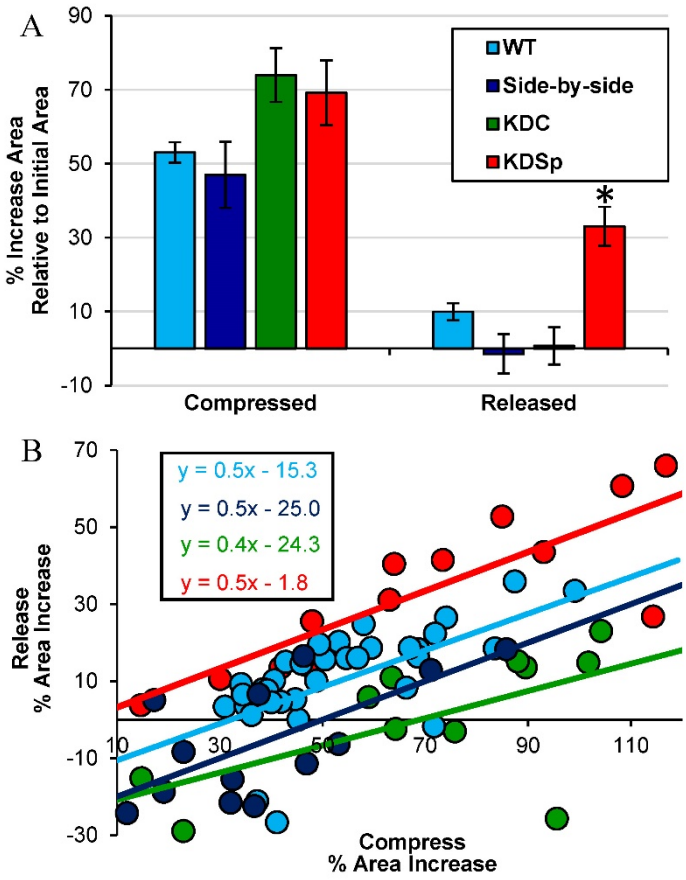

Figure 2.7: Quantification of nuclear area for the various treatment groups after compression assay

*(**A**) KDSp cells (red) fail to return to their initial nuclear area, in contrast to the various control groups (KDC, side-by-side, WT) which all return to their initial nuclear area upon removal of the static weight. Side-by-side cells are cells which*

*did not take up the spectrin knock-down vector but were in the same field of view as the KDSp cells. This control demonstrates that the failure to return to initial area was not an artifact of experimental variability. WT cells are control cells which did not receive any transfection treatment. Error bars show standard error of the mean. Asterisk denotes significant difference detected using a 1-way ANOVA followed by Tukey's pairwise comparison ($p < 0.01$). (**B**) Individual data points of each nucleus are shown for each sample comparing strains under compression (x-axis) to the strain of release (y-axis) normalized to the original size. In each case, high compression strain maps with larger strain after removal of the compressive force. In many control cases, removal of force in nuclei under small strains resulted in a shrinking of the nucleus (blue and green points). Compression of KDSp cells also resulted in the largest nuclear dilation. Regression analysis of the data (inset box) shows similar slopes for all samples, similar intercepts for transfected samples and largely divergent offset for KDSp cells.*

Discussion

Spectrin networks are known to be present at the lipid membranes of many biological systems, such as erythrocytes, the cell cytoplasm, and various intracellular organelles[8,9]. Because of the association of spectrin with lipid bilayers, and the presence of spectrin proteins in the nucleus, it has been proposed that a spectrin network may exist in the nucleoskeleton[18]. Furthermore, this network may provide elasticity to the nucleus playing a similar role as it does in the more well-characterized systems. We too show the presence of spectrin in the nucleus (Figure 2.1), and proceed to test the role of this potential nucleoskeletal spectrin network by knocking down αII-Sp followed by mechanical test. We demonstrate the potential presence of

unique spectrin isoforms present in the cytoskeleton which do not reside in the nucleus. This can be seen in Figure 2.2, where additional protein bands are seen in the western blot of whole cell lysates but not in the isolated nuclear lysates. When nuclear spectrin levels are decreased, and thus this potential nucleoskeletal spectrin network is decreased, we see a change in the nuclear elastic restorative response to compression. Mainly, nuclei with decreased spectrin do not return to their initial nuclear area after release of compression. This suggests a mechanical role of a nucleoskeletal spectrin network. As demonstrated by the compression experiments, a disruption of this network appears to cause a reduction in elasticity of the nucleus. Regression analysis of the data shows a net negative restoration force at a limit of zero compression, suggesting that nuclei are "primed" to have reduced area. This may be related to shape change from flat spread cells to a more spherical phenotype due to loss of cell-substrate adhesions or from nuclear prestress. However, this priming (i.e. nuclear prestress) appears related to the αII-Sp network.

Proper nuclear mechanics are essential to cell function; as physical forces are known to alter genome expression. Generally, physical forces can be propagated from outside cells, through the cytoskeleton, to the nucleus via the linker of the nucleoskeleton and cytoskeleton (LINC) complex[30]. Any changes to nuclear mechanics can impact the effect that physical forces have on the nucleus and ultimately gene expression based on the idea of mechanotransduction[31]. Since spectrin appears to contribute to the resilience of the nucleus, it may play a critical role in cells which undergo high levels of stress such as myocytes subjected to repeated contraction and relaxation cycles, endothelial cells subjected to shear stress and pressure changes, and cells which migrate through tight interstitial spaces which require drastic nuclear deformations. This recovery after deformation, referred to here as resilience (also called plasticity), has very recently

been tested in numerous cell types[32]. Nucleoskeletal stability as well as resilience appears to be important during cell crawling through tight interstitial spaces[33].

In addition to testing the changes in nuclear mechanics via live cell compression assays, we also probed changes in genome mechanics in cells with reduced levels of αII-Sp using live cell intranuclear particle tracking. Previous studies have demonstrated that cells with reduced levels of αII-Sp had increased susceptibility to DNA damage and decreased ability to repair DNA damage[14]. Based on these studies, we suspected that αII-Sp reduced cells may show altered genome motion. Additionally, cells with decreased αII-Sp, and thus lacking a percolated nucleoskeletal spectrin network, may have changes in mechanotransduction arising from changes in nuclear mechanics. However, cells with decreased αII-Sp showed no difference in intranuclear movement relative to wild type control for the conditions measured. Since it is proposed that αII-Sp is involved in DNA interstrand crosslink repair it seems likely that in the absence of large-scale DNA damage induction the intranuclear motion is largely unchanged between wild type control and KDSp cells. It is possible that KDSp cells would not be able to repair the induced damage, thus leading to changes in intranuclear motion. Additionally, no external force was applied to cells during particle tracking experiments. In order to show changes in intranuclear movements due to mechanotransduction, KDSp cells may need to be exposed to forces such as shear flow in order for mechanotransduction related changes to be large enough to measure via particle tracking. In addition to spectrin, the role of the nucleoskeletal protein emerin was also examined. These studies are shown in Appendix A and demonstrate that emerin does not appear to play a mechanical role in the nucleoskeleton when analyzed using the methods presented here.

In conclusion, this work suggests the role of a nucleoskeletal spectrin network in providing elasticity to the non-erythrocyte cell nucleus. This was evident from data obtained via

live cell compression assays, in which nuclei with reduced levels of αII-Sp failed to return to their initial nuclear area after release of compression, while control nuclei returned to their initial area. αII-Sp may play an important role in mechanotransduction for cells undergoing high levels of stress; however, with no externally applied force, changes in intranuclear motion appear minimal between control cells and αII-Sp reduced cells. The nucleoskeleton is composed of many interacting proteins, which play important roles in maintaining cell function. Here we begin to uncover a new mechanical phenotype of the cell nucleus provided by a lesser-studied nuclear protein, αII-spectrin.

Acknowledgements

We would like to thank Dr. Stephen Spagnol for his assistance in experimental design and insights on the project. The authors would like to acknowledge the lab of Ge Yang (Carnegie Mellon University, Biomedical Engineering) for providing the particle tracking software as well as insight on how to best utilize this technique. We would also like to acknowledge Patricia Opresko (University of Pittsburgh, Department of Environmental and Occupational Health) for providing the EYFP-TRF1 and for preparing the RFP-TRF1 vector used for particle tracking. Finally, we would like to acknowledge Katherine Wilson, Daniel Simon, Zhixia Zhong and Alexandre Ribeiro for intellectual contributions to this project. This work was funded by NSF-CMMI-1300476 (to K.N.D) and NIH-EB003392 (to T.J.A). We also acknowledge NIH-ES025606 to Opresko for the production of the TRF1 vector.

References

1. Marchesi, V. T. & Steers Jr, E. Selective Solubilization of a Protein Component of the Red Cell Membrane. *Science.* **159,** 203–204 (1968).

2. Boey, S. K., Boal, D. H. & Discher, D. E. Simulations of the erythrocyte cytoskeleton at

large deformation. I. Microscopic models. *Biophys. J.* **75,** 1573–83 (1998).

3. Li, J., Dao, M., Lim, C. T. & Suresh, S. Spectrin-Level Modeling of the Cytoskeleton and Optical Tweezers Stretching of the Erythrocyte. *Biophys. J.* **88,** 3707–19 (2005).

4. Li, J., Lykotrafitis, G., Dao, M. & Suresh, S. Cytoskeletal dynamics of human erythrocyte. *Proc. Natl. Acad. Sci. U. S. A.* **104,** 4937–42 (2007).

5. Bennett, V. & Healy, J. Organizing the fluid membrane bilayer: diseases linked to spectrin and ankyrin. *Trends Mol. Med.* **14,** 28–36 (2008).

6. Metral, S. *et al.* AlphaII-Spectrin Is Critical for Cell Adhesion and Cell Cycle. *J. Biol. Chem.* **284,** 2409–18 (2009).

7. Zhong, Z., Booth-Gauthier, E. A. & Dahl, K. N. αII Spectrin Stabilizes Stress Fibers and Actin–Membrane Interactions. *Cell. Mol. Bioeng.* **4,** 106–115 (2011).

8. Beck, K. A., Buchanan, J. A., Malhotra, V. & Nelson, W. J. Golgi spectrin: Identification of an erythroid beta-spectrin homolog associated with the Golgi complex. *J. Cell Biol.* **127,** 707–723 (1994).

9. Beck, K. A. Spectrins and the Golgi. *Biochim. Biophys. Acta* **1744,** 374–82 (2005).

10. McMahon, L. W., Walsh, C. E. & Lambert, M. W. Human alpha Spectrin II and the Fanconi Anemia Proteins FANCA and FANCC Interact to Form a Nuclear Complex. *J. Biol. Chem.* **274,** 32904–32908 (1999).

11. Young, K. G. & Kothary, R. Spectrin repeat proteins in the nucleus. *BioEssays* **27,** 144–52 (2005).

12. Brois, D. W. *et al.* A deficiency in a 230 kDa DNA repair protein in Fanconi anemia complementation group A cells is corrected by the FANCA cDNA. *Carcinogenesis* **20,** 1845–1853 (1999).

13. Howlett, N. G., Taniguchi, T., Durkin, S. G., D'Andrea, A. D. & Glover, T. W. The Fanconi anemia pathway is required for the DNA replication stress respone and for the regulation of common fragile site stability. *Hum. Mol. Genet.* **14,** 693–701 (2005).

14. McMahon, L. W., Zhang, P., Sridharan, D. M., Lefferts, J. A. & Lambert, M. W.

Knockdown of alphaII spectrin in normal human cells by siRNA leads to chromosomal instability and decreased DNA interstrand cross-link repair. *Biochem. Biophys. Res. Commun.* **381,** 288–293 (2009).

15. Zhang, P., Herbig, U., Coffman, F. & Lambert, M. W. Non-erythroid alpha spectrin prevents telomere fragility after DNA interstrand cross-link damage. *Nucleic Acids Res.* **41,** 5321–5340 (2013).

16. Holaska, J. M., Kowalski, A. K. & Wilson, K. L. Emerin caps the Pointed End of Actin Filaments: Evidence for an Actin Cortical Network at the Nuclear Inner Membrane. *PLoS Biol.* **2,** E231 (2004).

17. Sridharan, D. M., McMahon, L. W. & Lambert, M. W. AlphaII-Spectrin interacts with five groups of functionally important proteins in the nucleus. *Cell Biol. Int.* **30,** 866–78 (2006).

18. Simon, D. N. & Wilson, K. L. The nucleoskeleton as a genome-associated dynamic 'network of networks'. *Nat. Rev. Mol. Cell Biol.* **12,** 695–708 (2011).

19. Holaska, J. & Wilson, K. An emerin 'proteome': purification of distinct emerin-containing complexes from HeLa cells suggests molecular basis for diverse roles including gene regulation, mRNA splicing, signaling, mechano-sensing and nuclear architecture. *Biochemistry* **46,** 8897–8908 (2007).

20. Dahl, K. N., Ribeiro, A. J. S. & Lammerding, J. Nuclear Shape, Mechanics, and Mechanotransduction. *Circ. Res.* **102,** 1307–18 (2008).

21. Charras, G. & Sahai, E. Physical influences of the extracellular environment on cell migration. *Nat. Rev. Mol. Cell Biol.* **15,** 813–824 (2014).

22. Martins, R. P., Finan, J. D., Guilak, F. & Lee, D. A. Mechanical Regulation of Nuclear Structure and Function. *Annu. Rev. Biomed. Eng.* **14,** 431–455 (2012).

23. Lammerding, J. *et al.* Lamins A and C but Not Lamin B1 Regulate Nuclear Mechanics. *J. Biol. Chem.* **281,** 25768–80 (2006).

24. Shimi, T. *et al.* The A- and B-type nuclear lamin networks: microdomains involved in

chromatin organization and transcription. *Genes Dev.* **22,** 3409–3421 (2008).

25. Shimi, T., Kittisopikul, M., Tran, J., Goldman, A. E. & Adam, S. A. Structural Organization of Nuclear Lamins A , C , B1 and B2 Revealed by Super-Resolution Microscopy. *Mol. Biol. Cell* **26,** 4075–4068 (2015).

26. Opresko, P. L. *et al.* The werner syndrome helicase and exonuclease cooperate to resolve telomeric D loops in a manner regulated by TRF1 and TRF2. *Mol. Cell* **14,** 763–774 (2004).

27. Yang, G., Cameron, L. a, Maddox, P. S., Salmon, E. D. & Danuser, G. Regional variation of microtubule flux reveals microtubule organization in the metaphase meiotic spindle. *J. Cell Biol.* **182,** 631–9 (2008).

28. Spagnol, S. T. & Dahl, K. N. Active cytoskeletal force and chromatin condensation independently modulate intranuclear network fluctuations. *Integr. Biol.* **6,** 523–31 (2014).

29. Machnicka, B., Grochowalska, R., Bogusławska, D. M., Sikorski, a F. & Lecomte, M. C. Spectrin-based skeleton as an actor in cell signaling. *Cell. Mol. Life Sci.* **69,** 191–201 (2012).

30. Wang, N., Tytell, J. D. & Ingber, D. E. Mechanotransduction at a distance: mechanically coupling the extracellular matrix with the nucleus. *Nat. Rev. Mol. Cell Biol.* **10,** 75–82 (2009).

31. Lammerding, J. *et al.* Lamin A/C deficiency causes defective nuclear mechanics and mechanotransduction. *J. Clin. Invest.* **113,** 370–378 (2004).

32. Bonakdar, N. *et al.* Mechanical plasticity of cells. *Nat. Mater.* 1–6 (2016). doi:10.1038/nmat4689

33. C.M. Denais, R. M. Gilbert, P. Isermann, A. L. McGregor, M. te Lindert, B. Weigelin, P. M. Davidson, P. Friedl, K.Wolf, J. L. Nuclear envelope rupture and repair during cancer cell migration. *Science.* **352,** 353–358 (2016).

Chapter III: Progerin Micro-Aggregates as a Model for Lamina Wrinkles Associated with Hutchinson-Gilford Progeria Syndrome

Introduction

Hutchinson-Gilford progeria syndrome (HGPS) is a rare genetic disease that causes premature aging in children[1]. It is caused by an autosomal dominant mutation in the *LMNA* gene, which codes for the structural proteins of the nuclear lamina, lamins A and C[1,2]. Lamin A is an intermediate filament protein required to maintain the mechanical integrity of the nuclear lamina meshwork, which is closely associated with the inner nuclear membrane (INM)[3,4]. The *LMNA* mutation specific to most forms of HGPS is caused by a loss of 50 amino acids in the tail domain from a mutation that creates a cryptic splice site in exon 11[5]. This altered processing of *LMNA* and formation of progerin occurs at extremely low but perceivable levels in wildtype cells as well, leading to a similar cellular phenotype in aged cells[6].

Normal lamin A undergoes a series of posttranslational modifications including C-terminal farnesylation that increases affinity and binding kinetics of lamin A at the INM[7]. Following proper localization, mature lamin A undergoes proteolysis, which results in a mature non-farnesylated protein. However, the final cleavage does not occur in the HGPS variant lamin because the cleavage region is in the deleted 50 amino acid regime, resulting in a permanently farnesylated protein variant called progerin or Δ50 lamin A[8]. Ultimately, progerin expression leads to an accumulation of structural proteins in the lamina (progerin as well as the retention of other lamins), altered nuclear shape, redistribution of the heterochromatin, alterations in gene expression and nuclear structural instability[9–13].

Structurally, progerin expressing cells have altered nuclear morphologies that have been described as blebs, wrinkles or folds[10,12,14,15]. In addition to altered nuclear shape, HGPS is associated with increased lamina stiffness[10,12,13]. Similar nuclear structural abnormalities and stiffness changes between cells from patients with HGPS[10] and cells exogenously expressing progerin[13] have been observed, but patient cells require numerous passages for the protein to accumulate to detectable levels[12]. However, a major confusion in the field is how an increase in a structural protein and a stiffening of the lamina correlates with a blebbed nuclear lamina, which is seemingly related to lamina fragility.

The goal of this chapter is to put forth a new model of the progerin lamina that can describe the shape defect of the nucleus due to overexpression of progerin. We use orthogonal methods to show that the expression of progerin causes micro-aggregates leading to wrinkles and ultimately mechanical dysfunction of the nuclear lamina. We investigate strains imposed by endogenous cellular forces and by forces in cells under confinement. We also provide mechanical models and theory related to the thickening of the lamina with the change in the two-dimensional bending modulus of the lamina network. In addition to suggesting the mechanism of lamina wrinkles associated with HGPS, we comment on how the altered lamina nano- and micro- structure may impact cytoskeletal force transmission through the cell. These combined structural effects may have important functional consequences related to the disease and highlight the benefit of applying physical models to study biological systems to determine aspects of disease states.

Materials and Methods

Cell Culture and Transfection

For HeLa studies, HeLa (ATCC, Manassas, VA, USA) cells were cultured in DMEM low glucose medium supplemented with 10% FBS at 37°C and 1% P/S penicillin streptomycin (ThermoFisher, Waltham, MA, USA). Cells were passaged onto glass coverslips (VWR, Radnor, PA, USA) in 35 mm tissue culture dishes (Corning, Corning, NY, USA). For rDNA expression, cells were transfected using Lipofectamine 3000 transfection reagent (ThermoFisher, Waltham, MA, USA) as per manufacturer's recommendations. Media was changed after 5 hours, and cells were incubated for an additional 24-72 hours prior to experiments to allow for adequate expression and localization. Cells were transfected with DsRed-lamin A (DsRed-LA) or DsRed-progerin from[13].

For human umbilical vein endothelial cell (HUVEC) studies, primary HUVECs (passages 3-6, Lonza, Basel, Switzerland) were grown in EGM-2 medium (Lonza, Basel, Switzerland). To express progerin in HUVECs an adenovirus was developed to express human influenza hemagglutinin-tagged progerin (HA-progerin, kind gift of Bryce Paschal[16]); adenovirus was prepared by Vector Biolabs (Malvern PA). The lowest level of adenovirus that infected nearly 100% of cells was used. To overexpress wild-type lamin A in HUVECs, lamin A adenovirus (based on RefSeq BC014507) was purchased from Vector Biolabs and used at an identical titer level as progerin. For actin depolymerization studies, latrunculin A (Tocris, Bristol, United Kingdom) was added at 10 μM for reported times before cell fixation and labelling.

Micropatterning

HUVECs were seeded on micropatterned lines of width 20 or 40 μm, as previously described[17]. Briefly, the stamps used to micropattern fibronectin lines of 20 or 40 μm were made

with polydimethylsiloxane (PDMS). Stamps were coated with fibronectin and were pressed onto a prepared coverslip. Once stamped, the coverslips were washed and treated with Pluronic F-127 to limit cell adhesion to only the fibronectin lines. Cells were then seeded onto the coverslip.

Cell Fixation and Labelling

Cells were fixed using 3.7% formaldehyde in phosphate buffered saline (PBS) and permeabilized using 0.2% Triton X-100 in PBS. For fluorescence microscopy experiments, cells were stained with 0.1 μg/mL Hoechst 33342 (ThermoFisher, Waltham, MA, USA) for DNA labeling. HUVECs were stained with anti-lamin A antibody (cat # sc-7292, Santa Cruz Biotechnology, Dallas, TX, USA) for control cells or anti-HA antibody (cat # 901501, Biolegend, San Diego, CA, USA) for progerin-expressing cells with an Alexa Fluor 488 fluorescent secondary (cat # A-21202, Thermo Fisher, Waltham, MA, USA). HUVECs were also stained with rhodamine phalloidin (cat # PHDR1, Cytoskeleton, Denver, CO, USA).

Imaging and Analysis

HUVECs were imaged using a Zeiss 710 LSM confocal at 63x and 1.4NA. Images were processed using ImageJ. Fixed HeLa cells were imaged on a Nikon Eclipse TS100-F widefield fluorescence microscope with a 50x (1.4NA) oil immersion oil objective. Live HeLa cells were imaged on a Leica DMI6000 inverted microscope using a 63x (1.4 NA) oil immersion objective. During imaging the microscope environment was regulated by a Pecon live-cell imaging chamber heated to 37^{o}C. Methodologies for analysis of data shown in Figure 3.1 are presented in Figure 3.2.

Simulations of Inclusions

All modelling was completed in Comsol Multiphysics 5.3 using the two-dimensional (2D) plane stress module. The lamina was modelled as a uniform 2D elastic material of 50 kPa. We chose this number based on Vaziri and Mofrad[18] with updates based on a new understanding of lamina thickness to be 10-100 of nm based on super-resolution microscopy (from[19] and our own data); although scaling neglects the need for an absolute stiffness. Circular inclusions were modelled as linear elastic materials within the lamina. For this study we approximated an infinite sheet by modeling a 4 μm by 4 μm square region of the membrane with a small inclusion ranging from 0.05 μm to 0.4 μm in diameter with varying stiffness. Unconfined 25% uniaxial strain in the x-direction (aside constraint holding the midline at y = 0) with Poisson ratio $\nu = 0.49$ resulted in a stiffness profile around the y=0 axis. Von Mises stresses are shown, and peak midline stresses are reported.

Results

Cultured Cells Show Variable Lamina Deformations Under No Force

Not all nuclei show circular projected shapes when imaged from below. Invaginations are common from the microtubule organizing center (MTOC) and other forces via cytoskeletal stresses on the nucleus. Abnormal nuclear shape is associated with progerin expression[10,12,14], and we aimed to focus on structures associated with the nuclear lamina. In order to investigate the underlying causes for the invaginations and dysmorphic shapes in the control (DsRed-lamin A) and progerin (DsRed-progerin) expressing HeLa cells (Figure 3.1 A), we measured the angles associated with lamina invaginations and their corresponding intensities. No significant difference in the the average angle of the invaginations between the control (89° ± 19°) and progerin expressing (83° ± 16°) nuclei was detected. We then compared the intensities within the

invagination, normalized to the intensity of the nuclear lamina, between control and progerin expressing nuclei (Figure 3.2). We found the intensity at these angles of invaginations was higher in DsRed-progerin expressing cells (Figure 3.1 B). We originally hypothesized that there would be a correlation between intensity of the invagination and the angle; however, we did not see any such correlation for either control or progerin-expressing nuclei (Figure 3.2 B). Previous reports focused on patient cells have shown similar classifications of progerin expression, cell shape, mean curvature, and intensity[20].

Our data suggest that DsRed-lamin A (DsRed-LA) expressing cells typically had lower values of lamin intensity within invaginations (compared to the rest of the nuclear periphery), suggesting a slight dilation of the lamina network at the invagination. The intensity values at invagination sites of DsRed-progerin expressing nuclei were statistically greater than 1 (compared to the rest of the nuclear periphery), suggesting lamin accumulation at these invaginated regions and likely a different mechanism of deformation than the control nuclei.

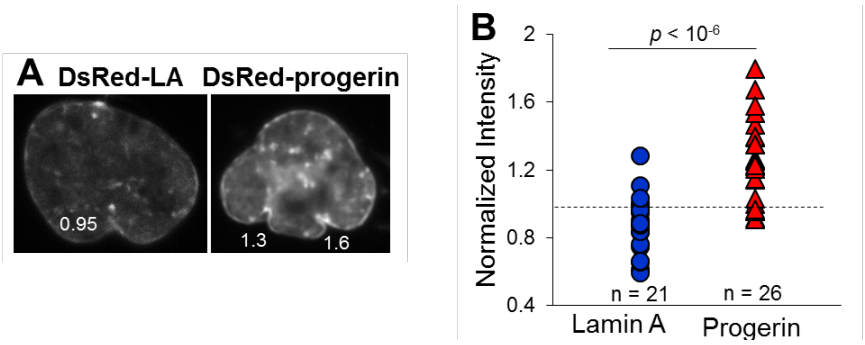

Figure 3.1: Fluorescence microscopy images of transfected HeLa cells and intensity of invagination quantification

*(**A**) HeLa cells expressing DsRed-lamin A (control) and DsRed-progerin (progeria) with the normalized intensity of invaginations are shown. (**B**) Normalized intensity values for*

*control and progeria cells are shown. Control cells demonstrate average lamin intensity levels below 1 ($p < 0.001$ compared to 1) in the invaginations, whereas progerin expressing cells show average lamin intensity levels above 1 within the invagination, relative to the rest of the lamina ($p < 10^{-5}$ compared to 1). The numbers of cells, n, per condition is given in **B**. Statistical significance between samples was determined by Student's t-test.*

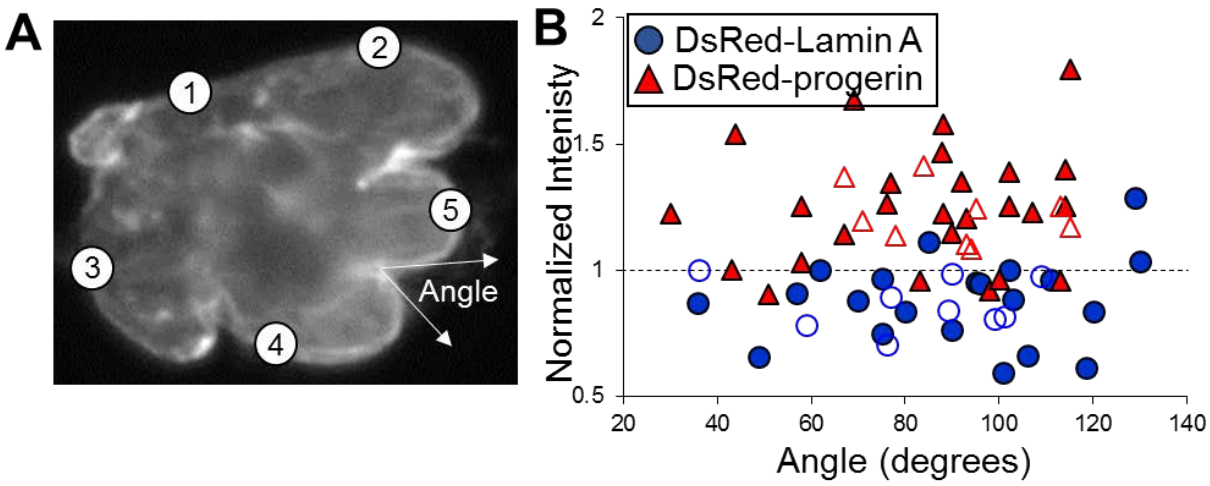

Figure 3.2: Methodology of measuring the angle and intensity of lamina invagination

*(**A**) We measured the angle of the invagination as well as the intensity of the lamina in that region using ImageJ. We then normalized the invagination intensity to line segments in 5 sections that did not contain obvious defects. (**B**) Comparison of normalized intensity versus invagination angle shows no correlation. Open circles and triangles represent samples wherein the entire nuclear periphery was considered for normalization rather than 5 sections from cells with no bright aggregates such as the ones shown in image **A**. These samples fell within the distribution.*

Micro-aggregate Model of the HGPS Nuclear Lamina

The energy of bending for an elastic two-dimensional surface that bends into a third dimension can be calculated based on previous works by Israelachvili[21]. Lamina networks are

mostly elastic[22–24], and weak bending is a type of deformation that costs significantly less energy than stretching. The bending modulus, κ, of a general single elastic sheet is defined according to:

$$\kappa = \frac{1}{12} K_{stretch} h^2$$

Where h is the thickness and $K_{stretch}$ is the dilation modulus[21]. For the lamina of progerin expressing cells, the $K_{stretch}$ would increase[10] and the local thickness, h, of the lamina increases significantly with progerin accumulation, as has been shown by electron and light micrographs[9,10]. Thus, κ would be much higher for progerin expressing cells over control cells; $\kappa_{progerin} >> \kappa_{control}$. Micropipette aspiration (MPA) has previously confirmed the increased lamina stiffness of nuclei from cells exogenously expressing progerin[13]. In addition, increased lamin stiffness has been observed in nuclei from patients with HGPS measured by MPA[10] and by stretching[12].

The resulting energy, e_{bend}, to bend around a segment radius of curvature, R, can be described as[21]:

$$e_{bend} = \frac{1}{2} \kappa \frac{1}{R^2}$$

The energy required to bend the progerin expressing lamina should be much higher than a control lamina, and therefore the deflections out of plane should be much smaller than control lamina ($R_{progerin} << R_{control}$). However, the intrinsic angles associated with inward bending do not change as shown with Figure 3.1, ($R_{progerin} \approx R_{control}$). Thus, another mechanism governing the wrinkling of the progerin lamina must be occurring. As discussed throughout, our alternative theory is that increased lamin accumulation in the invaginations is a cause of the wrinkle rather than a result of the localized bending.

Endothelial Cells Confined to One Dimensional Patterns Show Differential Lamina Deformation

To examine the role of extracellular perturbation on nuclear lamina reorganization, we considered cellular responds to growth on patterns. Endothelial cells (HUVECs) were grown on patterned lines of 20 μm or 40 μm in order to ascertain the extent of deformation of the lamina network under cell confinement. Previously, patterning on lines of this thickness has been shown to exert forces on the nucleus from the cytoskeleton[17,25,26]. On 20 μm lines, nuclei are oblate and orient in the direction of the stripes (Figure 3.3 and Figure 3.4). This orientation has been shown to be a direct function of the cellular confinement to patterning[25]. There are some folds in control lamina, but these coincide with actin filament structures (Figure 3.3 A, C, D). Progerin expressing cells show numerous folds and wrinkles in the nuclear lamina, but these dysmorphic structures do not align or coregister with confocal actin filament structures at a similar plane (Figure 3.3 E, F, H).

We quantified the dysmorphic structures, or wrinkles observed in the lamina, visualized in Figure 3.3 along the length of the nucleus and compared them to the orientation of the nucleus (see schematic in Figure 3.5 A). Earlier studies have suggested that cells under extreme loading conditions or, in this case confinement, may propagate wrinkle formation[26]. Lamin networks that are healthy have been found to deform uniformly under similar conditions[25]. For cells patterned on 20 μm stripes, wrinkle length observed in the lamina (seen in Figure 3.3) was not found to be statistically different for control and progerin-expressing endothelial cells (Figure 3.6 A). As an additional control, we also overexpressed wild-type lamin A in cells to ensure that the results were from progerin expression and not from either increased lamin A or from viral treatment. Levels of exogenous lamin A, measured from confocal immunocytochemistry, were 204 +/- 43% higher compared to wildtype cells. Endothelial cells grown on wider, 40 μm stripes without

progerin did not show any wrinkles. Conversely, progerin expressing cells, on 40 µm stripes, had wrinkles of statistically similar length to cells without progerin grown on 20 µm stripes (Figure 3.7 A).

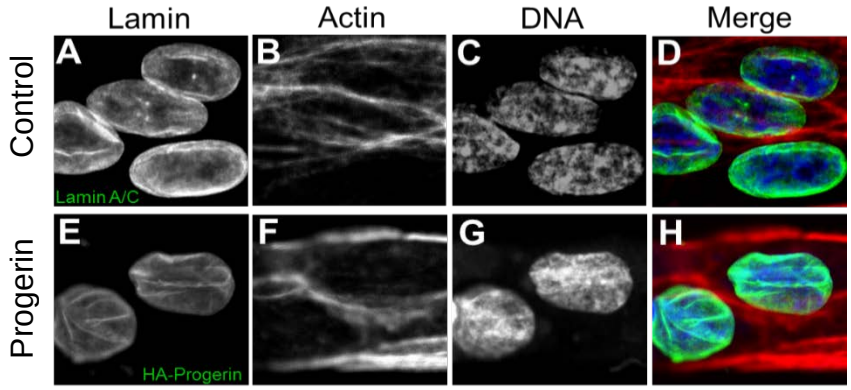

Figure 3.3: Confocal fluorescence microscopy sections for cells patterned on lines. *Fixed HUVEC were stained for Lamin (control) or HA (Progerin), and all cells were stained for actin (phallodin) and DNA (Hoechst 33342). (**A**) Lamin A/C (control) stained with a lamin A/C antibody is shown. (**B**) Control cells stained for actin to check the orientation of folds against the filament structures are shown. (**C**) Lamin A control cells with Hoechst staining for DNA are shown. (**D**) Merge of the lamin and actin channels shows nuclear alignment with the stripes and lamin folds coincident with the actin filaments is shown. (**E**) Progerin cells stained with anti-HA to label HA-progerin express more wrinkles. (**F**) Progerin cells stained for actin to show the orientation of folds against the filament structures. (**G**) Progerin cells with Hoechst staining for DNA are shown. (**H**) Merge of the lamin and actin shows lamin folds distinct from actin filaments. For both conditions the z-resolution for the lamin channel (488nm) was chosen at 3.5 µm, actin channel (561 nm) 1.9 µm and DNA channel (405 nm) 1.3 µm.*

In cells on 20 μm stripes, we also considered the orientation of the wrinkles (Figure 3.5 B). Our data indicate that most of the wrinkles in control nuclear lamina structures lie in the direction of the primary orientation of the cells with more than half at 0-20° (Figure 3.6 B). This is in agreement with the organized actin cytoskeleton along the length of the stripes visible in the overlay images (Figure 3.3 D, H). Conversely, progerin expressing cells displayed angles ranging from 40-90° for many of these wrinkles. For progerin expressing cells on 40 μm stripes, there is an increased number of wrinkle formations in the range of 80-90° which is nearly normal to the applied force from the actin cytoskeleton (Figure 3.7 B).

To further compare control versus progerin expressing cells, we considered cells on 20 μm stripes. In cells confined on the stripes, we depolymerized actin using latrunculin A, fixed cells at increasing time, and imaged the nuclear lamina in control and HA-progerin expressing cells. The actin depolymerized within a minute as expected but the wrinkles in nuclei took some time to be removed, likely due to the stiff mechanics of the nucleus. We plotted the length of wrinkles versus time after actin depolymerization treatment to determine if there was a difference in the loss of wrinkles. From the plot (Figure 3.6 C), the wrinkle loss in both cases was modelled as an exponential decay. After 1 hour of latrunculin A treatment, nuclear rupture in a small number of nuclei (7% of control nuclei, 0% of lamin A expressing nuclei) was observed as visualized by DNA present outside of the nucleus. Interestingly, more of the progerin expressing nuclei (90%) appeared to rupture. Fits of exponential decay of control, exogenous-lamin A and HA-progerin are shown in Figure 3.6D. Progerin expressing cells show a slower loss of wrinkles on a timescale of 111 min versus the scales of 45 min and 55 min for

control and exogenous-lamin A, respectively. Thus, despite the fact that wrinkles are maintained longer, progerin expressing cells appear to be more susceptible to rupture under these conditions.

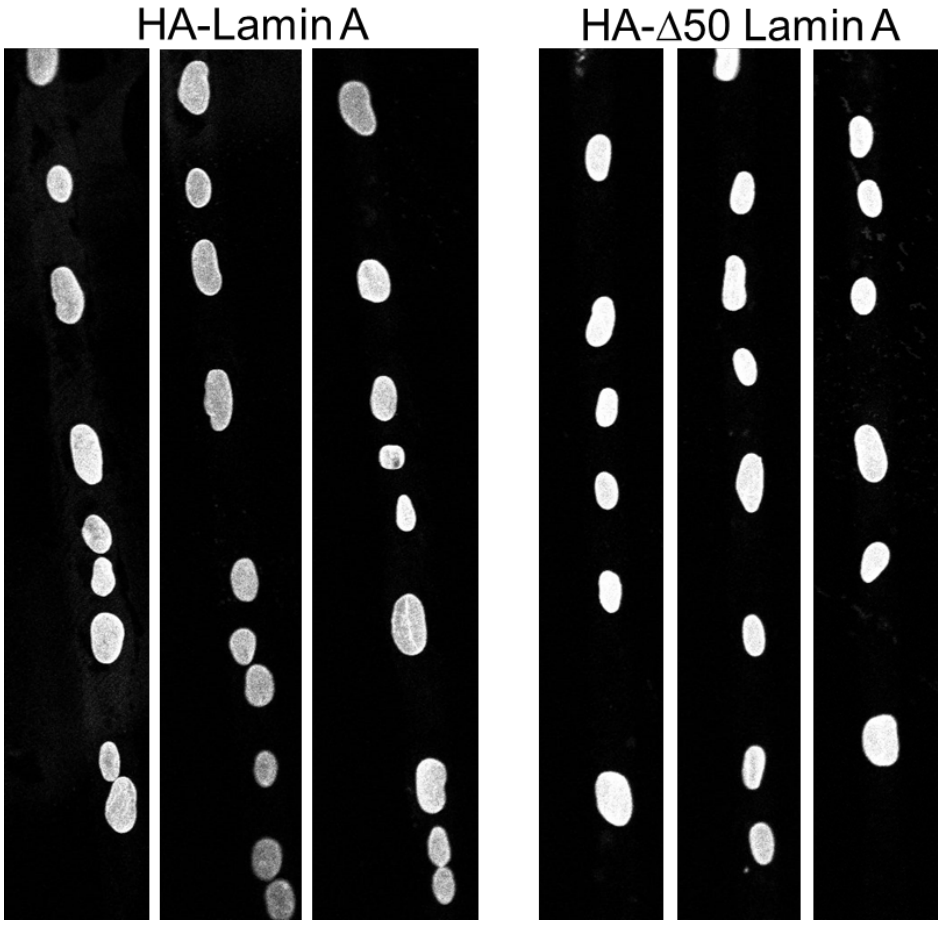

Figure 3.4: Low resolution imaging of HUVEC cells grown on 20 μm stripes

DAPI imaging of nuclei in cells aligned on patterned stripes of HUVEC grown on 20 μm stripes diameter stripes demonstrate similar overall alignment and spacing of nuclei.

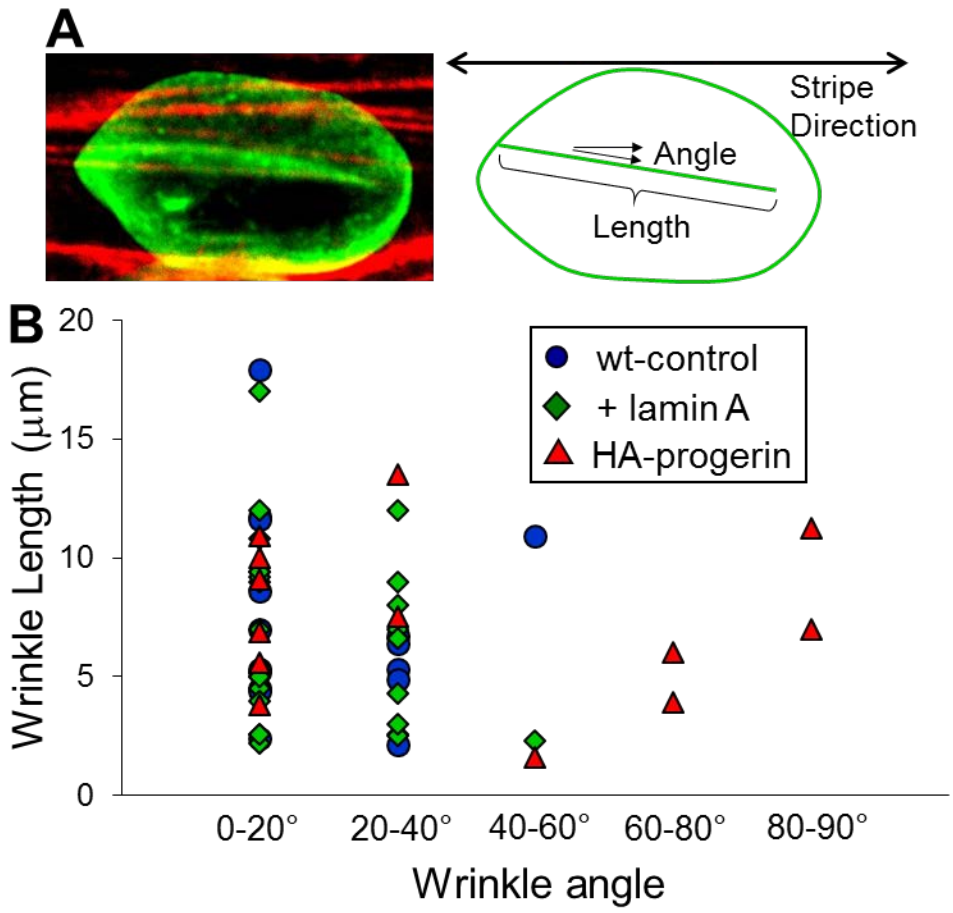

Figure 3.5: Methodology of measuring the angle and length of wrinkles

*(**A**) The length of the wrinkle and the angle of the wrinkle with respect to the stripe were measured. (**B**) Comparison of wrinkle length versus wrinkle angle was plotted, and no correlation was observed.*

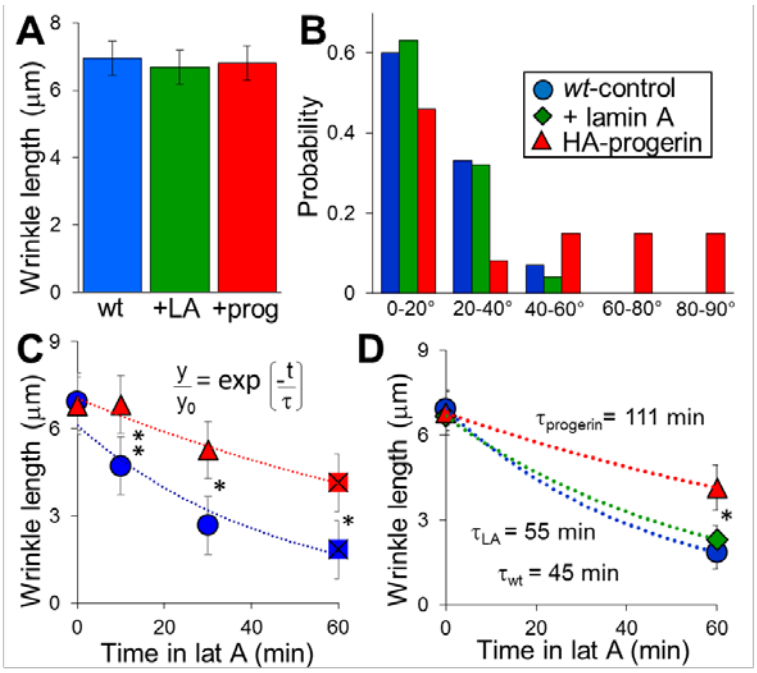

Figure 3.6: Formation of wrinkles for cells under one-dimensional confinement

*(**A**) Length of wrinkles for control, exogenous lamin A or HA-progerin expressing endothelial cells cultured on 20 μm diameter stripes appeared statistically similar ($p > 0.05$). (**B**) On 20 μm diameter stripes, wrinkles in control cells and exogenous lamin A expressing cells (+ lamin A) primarily aligned with the stripe axis whereas HA-progerin-expressing cells did not show preferred orientation. (**C**) On 20 μm diameter stripes, data for treatment with latrunculin A and fixation at different time points were fit to an exponential decay. (**D**) Fits of the exponential decay and the differential decay constants for control and exogenous lamin A versus HA-progerin cells are shown. Fits appear similar for 4 points as 2 points. 30-50 cells per condition were considered. For C and D, ** indicates $0.001 < p < 0.05$; * indicates statistically different with $p < 0.001$; otherwise $p > 0.05$ as detected by Student's T-test, or 1-way ANOVA followed by Tukey's pairwise comparison.*

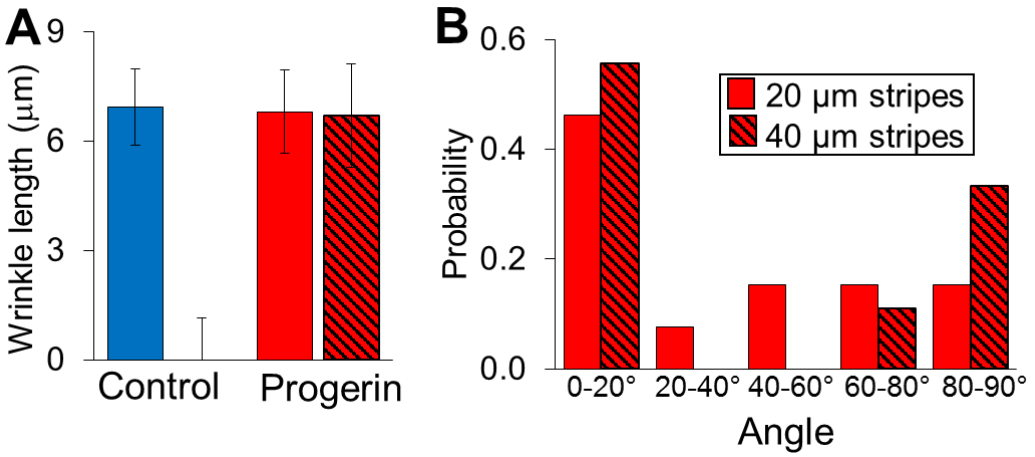

Figure 3.7: Wrinkle comparison on 40 μm stripes versus 20 μm stripes

*(**A**) The Length of deformations or wrinkles for control or HA-progerin expressing endothelial cells on 20 μm or 40 μm diameter stripes is shown. On 40 μm stripes, no wrinkles were observed in control cells, in contrast to cells expressing progerin. (**B**) For progerin-expressing cells, orientation preference of the wrinkles is further lost as the stripe diameter widens. 30-50 cells per condition were considered.*

Simulations of Stiffened Inclusions Show Stress Fields Consistent with Wrinkling

To consider the physical aspects of wrinkle formation from the presence of a micro-aggregate, we utilized simulations to model a stiffened region within a uniform lamina. We approximated the stiffness of the lamina (50 kPa, see Methods), added a stiffened inclusion within the uniform field (black circle), and then uniaxially strained in the x-direction and pinned along the black line at y=0 (Figure 3.8). We then tracked the peak stress along the midline outside of the inclusion. High stresses in deviation from the bulk would lead to asymmetries that could initiate out of plane bending. We found that the size of the inclusion (from 50-400 nm) did not influence the peak midline stress (Figure 3.9). However, an increase in the ratio of stiffness of the inclusion to the bulk stiffness led to greater midline stresses (Figure 3.8). Thus, a stiffened

inclusion of nearly any size leads to larger-scale stress features in the bulk of materials under strain. The wrinkles observed in nuclei exposed to intracellular forces could be caused by single point defects of increased micro-aggregates.

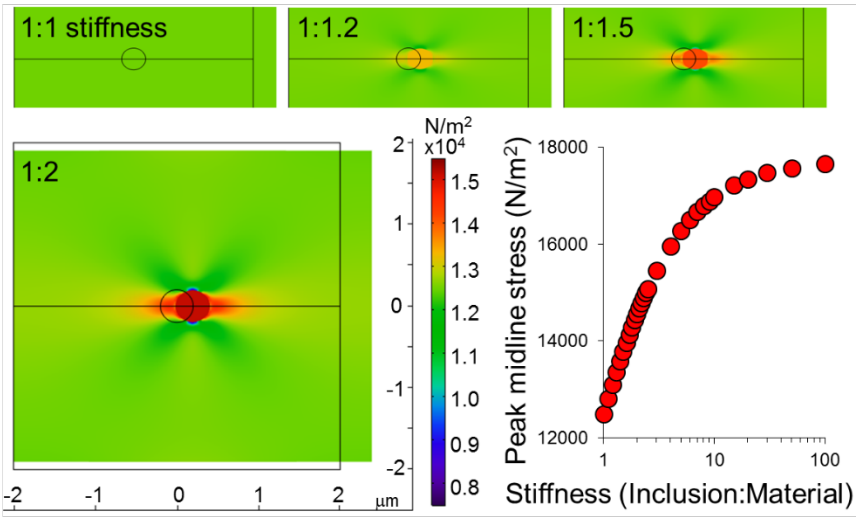

Figure 3.8: Strain on an inclusion of increased stiffness causes a line of increased stress normal to the imposed strain

Comsol simulation of a homogeneous structure with a stiffened inclusion is compressed in y and dilated in x. The resulting von Mises stiffness profile is shown for increasing inclusion stiffness (1, 1.2, 1.5 and 2x as stiff as the background material). The peak midline stress in the x-direction outside of the inclusion is plotted as a function of stiffness ratio.

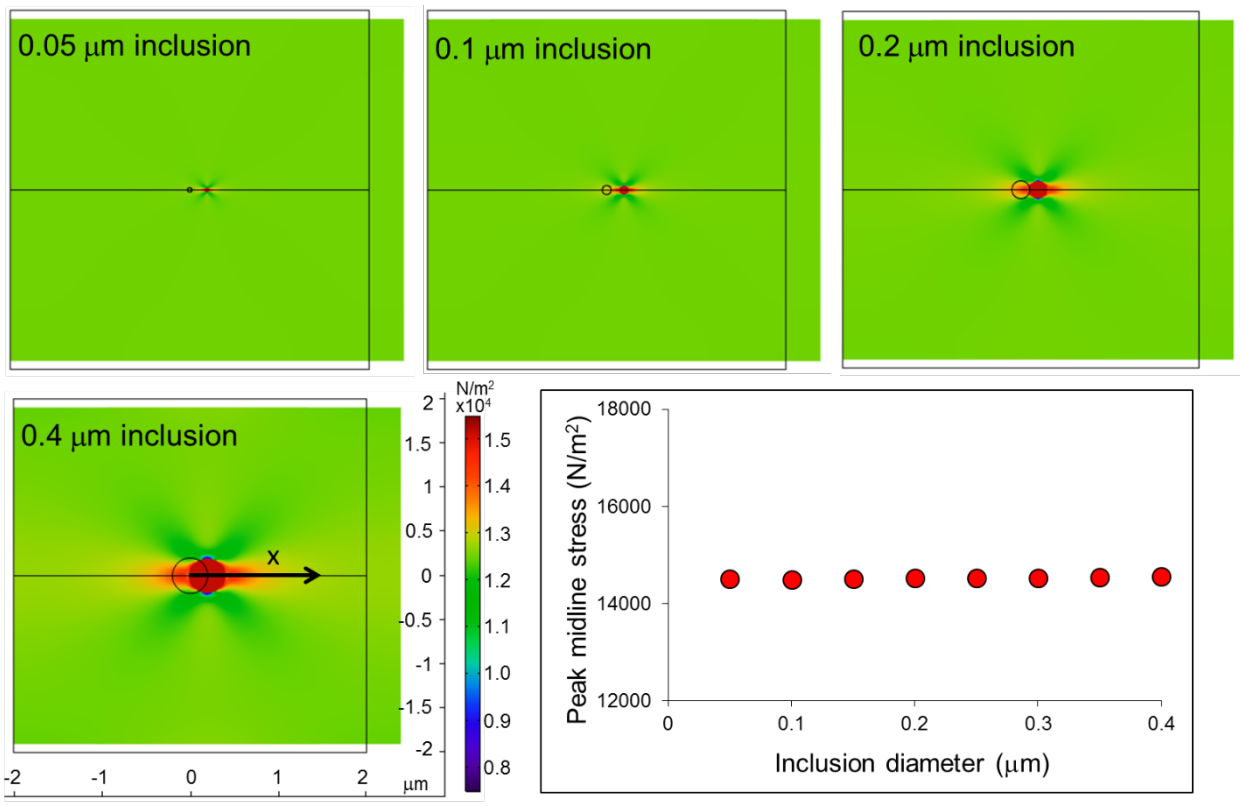

Figure 3.9: Simulations for measuring peak midline stress as a function of inclusion size

Changes in size of an inclusion (1:2 inclusion:material stiffness) meant to mimic a micro-aggregate of progerin shown as 50, 100, 200 and 400 nm in a 4 μm by 4 μm square matching the stiffness of the nuclear lamina (50 kPa) were considered. The inclusion caused a midline stress along the x-axis, and the peak midline stress was independent of the inclusion size.

Discussion

Nuclei in cells from patients with HGPS can exhibit dysmorphic changes labeled as protrusion of the nucleus towards the cytoplasm[9] as well as many other gross nuclear morphological changes[10,14]. There are many changes associated with HGPS nuclei including reduced lamin B1 levels[27], loss of heterochromatin[11], changes in chromatin-lamin binding[28], altered lamin-nuclear envelope association[29], altered nuclear pore complex[30] and changes in nuclear and cytoskeletal binding[26]. Here, we have tried to examine lamina-specific defects

through different cellular manipulations of cells exogenously expressing progerin. Of note by our group and others is that the exogenous expression of progerin, is not identical to HGPS. Defects that result from exogenous expression appear to be more severe due to higher expression levels[13]. However, the physical model we propose here is entirely consistent with the force-induced wrinkling behavior observed in nuclei from patients with HGPS[10]. In previous studies, micropipette aspiration of isolated nuclei from patients demonstrated wrinkling under high stress that was independent of the direction of applied force[10]. Thus, it appears that this model would hold with endogenous expression as well as with exogenous expression.

Several other lamin and nuclear envelope mutations are associated with nuclear dysmorphisms[31], and the term "blebbing" has been used to categorize most of these altered shapes[32]. We suggest here, that the unique aspects of the nuclear shape changes – outward blebbing seen in some nuclear defects[33] versus the wrinkles or folds observed in HGPS – are likely significant markers of the etiology of this mechanical dysfunction. We suggest that the phrase blebbing should be used exclusively for an increase in the size of the nuclear envelope and an outward distention of a particular region of the nucleus. Thus, models developed for other nuclear blebs may not necessarily be applied to progeria[34,35].

Given the differential responses of lamina invaginations (Figure 3.1), responsiveness on patterns (Figure 3.6) and model predictions (Figure 3.8 and Figure 3.9), we suggest in sum that the deformations in the lamina of progeria cells are driven by entirely or significantly different factors than those seen in control cells. In Figure 3.10, we show a schematic that conveys the different mechanisms of nuclear lamina wrinkle formation between progerin and control cells. For control cells, due to a uniform distribution of lamin, stress and exogenous forces cause the nuclear lamina to become thinner due to the elastic properties of the lamina[24] and therefore result

in a slight dilation of the lamina network and lower intensity values at the site of applied force (Figure 3.10 A). Conversely, progerin expressing cells show micro-aggregates of progerin and deformation occurs at these regions rather than at regions of applied force which would always show higher intensities of progerin associated with defects (Figure 3.10 B). We have demonstrated, in Figure 3.1, this increased progerin intensity at the invaginations. Also, this schematic accounts for defects that occur in regions not necessarily associated spatially with the application of force (Figure 3.3 and Figure 3.6, wrinkles not aligned with actin filaments), rather, defects associate with the region of accumulation of progerin. This schematic is consistent with our simulations as well as the concepts of stiffened inclusions demonstrated in many examples throughout biology and materials science. This mechanism of differential stiffness at unique sites of localization has also been shown to be important in branching morphogenesis during development in the lung[36].

Previous models of blebs have suggested that the lamina is restorative and resistant to blebs[34,35]. Finite element analysis of an isotropic elastic shell has predicted folds rather than blebs in shape bifurcation studies but does not address altered nucleoskeleton changes[37]. Also, the nature of intermediate filaments appears to make the lamina resistant to holes and defects from loss of local filament structure[38]. Here, we have shown that control nuclei of cells on stripes lost their wrinkles when internal force was removed; progerin-expressing cells took more than twice as long to lose wrinkles, possibly rupturing before wrinkles were lost. Thus, expression of the micro-aggregates may impact the restorative elastic nature of the nuclear lamina.

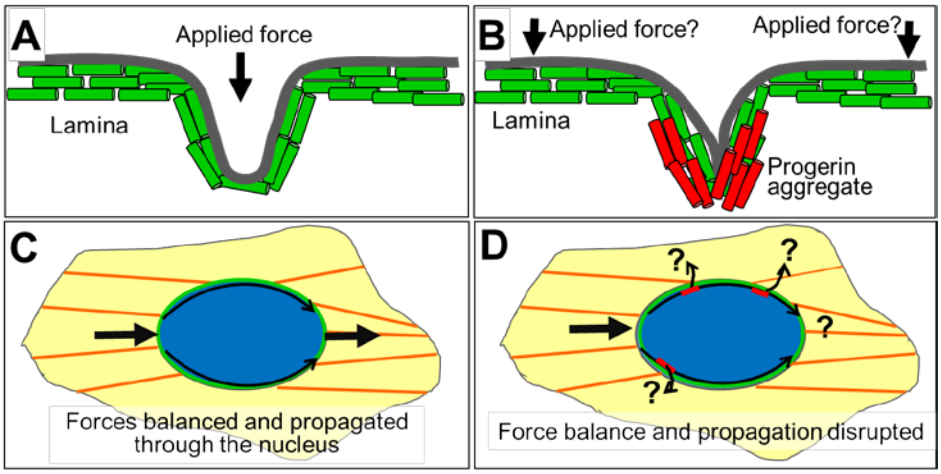

Figure 3.10: Schematic of nuclear lamina under force

*(**A**) The nuclear lamina for control cells experiences a thinning of membrane and dilation of lamin A network. (**B**) The nuclear lamina for progerin expressing cells experiences high stress and buckles at the aggregates irrespective of force application. Wrinkles then emanate from the aggregate location. (**C**) In control cells, cytoskeletal forces are balanced through the nuclear lamina and are propagated from one side of the nucleus to the other. (**D**)Wrinkles or defects in progerin-expressing cells may cause forces to be disrupted along the lamina.*

Implications in Force Transmission Through the Lamina and Nucleus

Collectively, the data and models presented here as many implications in cellular function; wrinkled nuclei will be present in cells with higher progerin expression, which tends to form heterogeneous aggregates. Also, wrinkled nuclei will form in cells with higher internal stresses, such as in cells with constrained alignment, under compression or exposed to shear stress. One particularly important implication for the progerin-expressing nucleus would be the integrated set of proteins that interconnect the cytoskeleton with the nucleoskeleton called the

LINC (linker of nucleus to cytoskeleton) complex. The LINC complex is important in balancing forces throughout the cell and transmitting forces across the cell (Figure 3.10 C)[39,40]. Disrupting the LINC complex prevents forces from being transmitted to the inside of the nucleus[41] and from being transmitted from one side of the cell to the other[42]. It is unclear if LINC components are altered in HGPS cells. However, even if LINC complexes are maintained, we suggest that improper distribution of forces across the nuclear lamina (from the non-isotropic distribution of lamins associated with progerin expression) could modify propagation of force throughout the cell (Figure 3.10 D). This may be in-part why the wrinkles form away from the direction of the actin filaments in progerin expressing cells (Figure 3.3 and Figure 3.6). Thus, in HGPS, and in aspects of normal cellular aging[6], accumulated nuclear lamina defects may prevent proper force transmission through cells.

In conclusion, our findings reveal that the abnormal nuclear morphology observed in HGPS and progerin expression is a consequence of both structure and mechanics. Excessive accumulation of progerin at the nuclear lamina causes wrinkles and invaginations observed in numerous cellular conditions. We suggest that these altered shapes are a result of micro-aggregates rather than a uniform stiffening of the lamina.

Acknowledgements

We would like to thank Kranthidhar Bathula, and Dr. Daniel E. Conway (Virginia Commonwealth University, Biomedical Engineering), who designed and conducted the HUVEC and patterned lines experiments and helped analyze results. Additionally, we would like to thank Dr. Rebecca E. Taylor (Carnegie Mellon University, Mechanical Engineering) for performing the Comsol simulations, Pragna S. Vellala for help conducting the HeLa experiments, and Chris Lemmon (Virginia Commonwealth University, Biomedical Engineering) for assistance with

micropatterning. We acknowledge support from NSF-CMMI-1300476 (Dahl), NIH-EB003392 (Dahl and Armiger), American Heart Association 16SDG27370007 (Conway), NSF-CMMI-1653299 (Conway), and the Thomas F. and Kate Miller Jeffress Memoria Trust (Conway).

References

1. De Sandre-Giovannoli, A. *et al.* Lamin a truncation in Hutchinson-Gilford progeria. *Science* **300,** 2055 (2003).

2. Eriksson, M. *et al.* Recurrent de novo point mutations in lamin A cause Hutchinson–Gilford progeria syndrome. *Nature* **423,** 293–298 (2003).

3. Dahl, K. N. & Kalinowski, A. Nucleoskeleton mechanics at a glance. *J. Cell Sci.* **124,** 675–678 (2011).

4. Zwerger, M., Ho, C. Y. & Lammerding, J. Nuclear Mechanics in Disease. *Annu. Rev. Biomed. Eng* **13,** 397–428 (2011).

5. Scaffidi, P. & Misteli, T. Good news in the nuclear envelope: Loss of lamin A might be a gain. *Journal of Clinical Investigation* **116,** 632–634 (2006).

6. Scaffidi, P. & Misteli, T. Lamin A-dependent nuclear defects in human aging. *Science* **312,** 1059–1063 (2006).

7. Young, S. G., Fong, L. G. & Michaelis, S. Prelamin A, Zmpste24, misshapen cell nuclei, and progeria—new evidence suggesting that protein farnesylation could be important for disease pathogenesis. *J. Lipid Res.* **46,** 2531–2558 (2005).

8. Dahl, K. N., Kalinowski, A. & Pekkan, K. Mechanobiology and the microcirculation: Cellular, nuclear and fluid mechanics. *Microcirculation* **17,** 179–191 (2010).

9. Goldman, R. D. *et al.* Accumulation of mutant lamin A causes progressive changes in nuclear architecture in Hutchinson-Gilford progeria syndrome. *Proc. Natl. Acad. Sci.* **101,** 8963–8968 (2004).

10. Dahl, K. N. *et al.* Distinct structural and mechanical properties of the nuclear lamina in Hutchinson-Gilford progeria syndrome. *Proc. Natl. Acad. Sci. U. S. A.* **103,** 10271–6 (2006).

11. Shumaker, D. K. *et al.* Mutant nuclear lamin A leads to progressive alterations of epigenetic control in premature aging. *Proc. Natl. Acad. Sci.* **103,** 8703–8708 (2006).

12. Verstraeten, V. L. R. M., Ji, J. Y., Cummings, K. S., Lee, R. T. & Lammerding, J. Increased mechanosensitivity and nuclear stiffness in Hutchinson-Gilford progeria cells: Effects of farnesyltransferase inhibitors. *Aging Cell* **7,** 383–393 (2008).

13. Booth, E. A., Spagnol, S. T., Alcoser, T. A., Dahl, K. N. & Matter, S. Nuclear stiffening and chromatin softening with progerin expression leads to an attenuated nuclear response to force. *Soft Matter* **11,** 6412–6418 (2015).

14. Choi, S. *et al.* Computational image analysis of nuclear morphology associated with various nuclear-specific aging disorders. *Nucleus* **2,** 570–579 (2011).

15. Scaffidi, P. & Misteli, T. Reversal of the cellular phenotype in the premature aging disease Hutchinson-Gilford progeria syndrome. *Nat. Med.* **11,** 440–445 (2005).

16. Datta, S., Snow, C. J. & Paschal, B. M. A pathway linking oxidative stress and the Ran GTPase system in progeria. *Mol. Biol. Cell* **25,** 1202–1215 (2014).

17. Arsenovic, P. T. T. *et al.* Nesprin-2G, a Component of the Nuclear LINC Complex, Is Subject to Myosin-Dependent Tension. *Biophys. J.* **110,** 34–43 (2016).

18. Vaziri, A. & Mofrad, M. R. K. Mechanics and deformation of the nucleus in micropipette aspiration experiment. *J. Biomech.* **40,** 2053–62 (2007).

19. Turgay, Y. *et al.* The molecular architecture of lamins in somatic cells. *Nature* **543,** 261–264 (2017).

20. Righolt, C. H., Van 't Hoff, M. L. R., Vermolen, B. J., Young, I. T. & Raz, V. Robust nuclear lamina-based cell classification of aging and senescent cells. *Aging (Albany. NY).*

3, 1192–1201 (2011).

21. Israelachvili, J. *Intermolecular and Surface Forces*. *Intermolecular and Surface Forces* (2011). doi:10.1016/C2009-0-21560-1

22. Dahl, K. N., Engler, A. J., Pajerowski, J. D. & Discher, D. E. Power-law rheology of isolated nuclei with deformation mapping of nuclear substructures. *Biophys. J.* **89,** 2855–64 (2005).

23. Dahl, K. N., Kahn, S. M., Wilson, K. L. & Discher, D. E. The nuclear envelope lamina network has elasticity and a compressibility limit suggestive of a molecular shock absorber. *J. Cell Sci.* **117,** 4779–86 (2004).

24. Rowat, A. C., Lammerding, J. & Ipsen, J. H. Mechanical properties of the cell nucleus and the effect of emerin deficiency. *Biophys. J.* **91,** 4649–64 (2006).

25. Versaevel, M., Grevesse, T. & Gabriele, S. Spatial coordination between cell and nuclear shape within micropatterned endothelial cells. *Nat. Commun.* **3,** (2012).

26. Hale, C. M. *et al.* Dysfunctional connections between the nucleus and the actin and microtubule networks in laminopathic models. *Biophys. J.* **95,** 5462–75 (2008).

27. Dreesen, O., Ong, P. F., Chojnowski, A. & Colman, A. The contrasting roles of lamin B1 in cellular aging and human disease. *Nucleus* **4,** 283–290 (2013).

28. Bruston, F. *et al.* Loss of a DNA binding site within the tail of prelamin A contributes to altered heterochromatin anchorage by progerin. *FEBS Lett.* **584,** 2999–3004 (2010).

29. Chojnowski, A. *et al.* Progerin reduces LAP2α-telomere association in hutchinson-gilford progeria. *Elife* **4,** 1–21 (2015).

30. Kelley, J. B. *et al.* The Defective Nuclear Lamina in Hutchinson-Gilford Progeria Syndrome Disrupts the Nucleocytoplasmic Ran Gradient and Inhibits Nuclear Localization of Ubc9. *Mol. Cell. Biol.* **31,** 3378–3395 (2011).

31. Burke, B. & Stewart, C. L. Functional architecture of the cell's nucleus in development,

aging, and disease. *Curr. Top. Dev. Biol.* **109,** 1–52 (2014).

32. Luke, Y. *et al.* Nesprin-2 Giant (NUANCE) maintains nuclear envelope architecture and composition in skin. *J. Cell Sci.* **121,** 1887–1898 (2008).

33. Pfleghaar, K. B. *et al.* Gene-rich chromosomal regions are preferentially localized in the lamin b deficient nuclear blebs of atypical progeria cells. *Nucleus* **6,** 66–76 (2015).

34. Funkhouser, C. M. *et al.* Mechanical model of blebbing in nuclear lamin meshworks. *Proc. Natl. Acad. Sci.* **110,** 3248–3253 (2013).

35. Wren, N. S., Zhong, Z., Schwartz, R. S. & Dahl, K. N. Modeling nuclear blebs in a nucleoskeleton of independent filament networks. *Cell. Mol. Bioeng.* **5,** 73–81 (2012).

36. Varner, V. D., Gleghorn, J. P., Miller, E., Radisky, D. C. & Nelson, C. M. Mechanically patterning the embryonic airway epithelium. *Proc. Natl. Acad. Sci.* **112,** 9230–9235 (2015).

37. Kim, D.-H. D.-H. *et al.* Volume regulation and shape bifurcation in the cell nucleus. *J. Cell Sci.* **128,** 457–457 (2016).

38. Qin, Z. & Buehler, M. J. Flaw tolerance of nuclear intermediate filament lamina under extreme mechanical deformation. *ACS Nano* **5,** 3034–3042 (2011).

39. Kaminski, A., Fedorchak, G. R. & Lammerding, J. The cellular mastermind(?) - Mechanotransduction and the nucleus. *Prog. Mol. Biol. Transl. Sci.* **126,** 157–203 (2014).

40. Neelam, S., Dickinson, R. B. & Lele, T. P. New approaches for understanding the nuclear force balance in living, adherent cells. *Methods* **94,** 27–32 (2016).

41. Spagnol, S. T., Dahl, K. N. & Noel Dahl, K. Active cytoskeletal force and chromatin condensation independently modulate intranuclear network fluctuations. *Integr. Biol.* **6,** 523–31 (2014).

42. Alam, S. G. *et al.* The nucleus is an intracellular propagator of tensile forces in NIH 3T3 fibroblasts. *J. Cell Sci.* **128,** 1901–1911 (2015).

Chapter IV: Determining Mechanical Features of Modulated Epithelial Monolayers Using Subnuclear Particle Tracking

Introduction

Generation and propagation of forces by cells within monolayers is critical in development and disease[1]. Generally, the mechanobiology of monolayers and collective cellular behavior is of increasing interest since cells integrate forces for communication, in addition to chemical signaling[2]. Important aspects of collective cellular behaviors are regulated in response to mechanical differences within an intact cellular monolayer environment. Current methods to measure cellular forces typically require an external, physiologically deformable probe or substrate, as in traction force microscopy[3], or require drastic alterations to cell architecture, as in stress fiber ablation[4]. Additionally, many of the current techniques are more easily performed on isolated cells, as opposed to cell monolayers.

Previously, we have developed a particle tracking technique in which fluctuations of probes bound to chromatin are measured as readouts of cell force propagation[5]. Details on previous applications of the technique are provided in the Materials and Methods. Here, we describe the use of chromatin dynamics to detect cellular force propagation (a technique termed Sensors from IntraNuclear Kinetics (SINK)) and investigate the force response of cells to disruption of the monolayer and changes in substrate stiffness. SINK provides previously unattainable information about monolayer force dynamics. Unlike traction force microscopy in which actin-myosin forces are transmitted to focal adhesions, integrins and ultimately the extracellular matrix[6], SINK is based on actin-myosin forces transmitted to the linker of the nucleoskeleton and cytoskeleton (LINC) complex through the nucleoskeleton and into the

chromatin of the nucleus[7]. Thus, SINK can be utilized to investigate systems previously unreachable by current force measurement techniques, or in similar systems to further understand the extent that forces impact the cell nucleus, and ultimately gene expression.

Here, we use SINK to compare measurements in intact cell monolayers with either (*i*) modulated substrate stiffness or (*ii*) single cells mechanically decoupled from the monolayer. Using this intracellular technique, we can determine (*i*) the maximum effective stiffness that the monolayer can sense and (*ii*) the lateral length scale that the cells can mechanically perturb.

Materials and Methods

Cell Culture, Transfection, and Chemical Treatment

NRK-52E rate kidney epithelial cells (Kind Gift Y. Wang Carnegie Mellon University) were used in all experiments and cultured in DMEM high glucose media (ThermoFisher), supplemented with 5% FBS (ThermoFisher) and 1% Penicillin-Streptomycin (ThermoFisher) at 37°C and 5% CO_2. Live cell imaging with Hoechst 33342 allowed us to confirm that contamination was not present during experiments. All cells were cultured on uncoated glass for imaging applications with the exception of cells grown on polyacrylamide gels (to examine changes in substrate stiffness) which are described in a later section. To visualize chromatin fluctuations, cells were transfected with a green fluorescent protein tagged upstream binding factor (GFP-UBF) plasmid[8]. Upstream binding factor is a transcription factor involved in ribogenesis and binds to chromatin. To disrupt the LINC complex, cells were transfected with a dominant negative Klarsicht, ANC-1, Syne Homology (DN-KASH) plasmid tagged with red fluorescent protein used in[5] (Kind Gift, G. Luxton, University of Minnesota) to disrupt the LINC complex. Lipofectamine 3000 (ThermoFisher) was used for transfection according to manufacturer's protocol; cells were imaged 24 hours after transfection. For experiments which

required cells transfected with GFP-UBF to be either adjacent, or distant, to DN-KASH expressing cells, monolayers were first transfected with DN-KASH. After 4 hours, cells were washed with PBS, media was changed, and cells were re-transfected with the GFP-UBF. For isolated, monolayer control, and Y-27632 treated monolayers, cells were co-transfected with LifeAct-Tag RFP to visualize actin filaments in live cells (Figure 4.1). As expected, cell shape and actin filaments were altered after treatment with Y-27632 which is a ROCK inhibitor and therefore decreases cell contractility. For Y-27632 experiments, cells were treated for 1 hour prior to imaging, at a concentration of 50 µM. Y-27632 remained in the media during imaging.

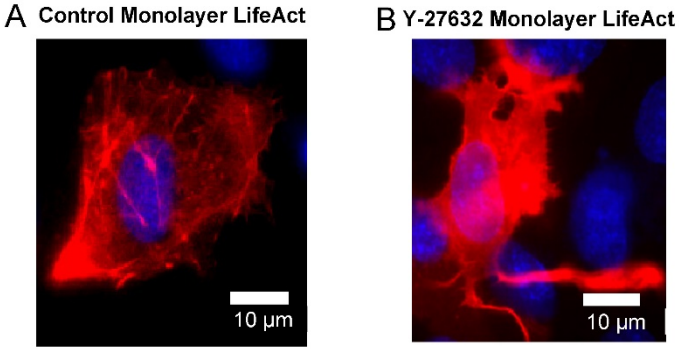

Figure 4.1: Monolayer control and Y-27632 treated cells actin visualization

*(**A**) A control cell in a monolayer with the nucleus stained with Hoechst (blue), and actin visualized with life act tag-RFP (red) is shown. Individual stress fibers were observed. (**B**) A cell in a monolayer after treatment with Y-27632 with the nucleus stained with Hoechst (blue), and actin visualized with life act tag-RFP (red) is shown. Individual stress fibers were largely lost, and a change in cell shape was observed.*

Cell Imaging and Fluorescent Labeling

For SINK analysis live cells were imaged in a live cell imaging chamber (PeCON), maintained at 37°C and 5% CO_2. Cells were imaged using a 63x, 1.4 NA, oil immersion inverted widefield fluorescence microscope (DMI6000, Leica) with a DFC350 camera. All cells were treated with Hoechst 33342 (Life Technologies) to visualize nuclei. When applicable, cells were fixed using 4% formaldehyde solution (ThermoFisher), and permeabilized using 0.2% Triton-X. For actin visualization in fixed cells, cells were stained using Oregon Green or Rhodamine Phalloidin (ThermoFisher). Immunofluorescence against E-cadherin was performed by blocking with a 0.2% BSA (Sigma-Aldrich) solution in PBS for 20 minutes, followed by incubation with the primary mouse E-cadherin antibody (BD Biosciences, Mfr. No. 610181) at a 1:100 dilution in 0.2% BSA for 1 hour. The secondary antibody used was either donkey anti-mouse Alexa Fluorophore 647 (ThermoFisher, A31571), or goat anti-mouse Alexa Fluor 488 (ThermoFisher R37120), at a 1:200 dilution in 0.2% BSA and incubated for 1 hour. Confocal images were acquired on a Zeiss LSM700, with a 63X, 1.4 NA, oil immersion objective.

Image Processing and SINK method

Live cell, time series images were acquired at 3-minute time intervals for 1 hour. Only the green (GFP-UBF) channel, and bright field channel were acquired for this time to minimize phototoxicity. Brightfield images were obtained to assess the viability of target, and adjacent cells throughout the length of imaging. Additionally, if gaps between cells in the monolayer became apparent during imaging, these cells were not analyzed. Prior to time series imaging, single images were taken with all necessary channels for analysis (i.e. to confirm cotransfection etc.). Additionally, images were taken 1 hour after the hour-long time series was acquired to assure cells remained viable during and after imaging. If cells of interest died or divided during

imaging, or an hour after imaging, these data were not used for analysis to assure that artifacts of cell death and division were not captured. After image acquisition, images were processed using custom MATLAB software developed by Ge Yang, as previously published[9]. Briefly, nuclei were aligned to remove rigid body motion such that only intranuclear motion of GFP-UBF punctate regions was captured. In order to assure single, unique points were tracked and to minimize artifacts of z-drift or particles moving in and out of focus in the z-direction, only particles which persisted throughout the entire movie were tracked and used for analysis. No changes in size of particles was observed during imaging. For the particles tracked for a given condition, the ensemble average MSD was calculated according to Eqn 1 below.

$$MSD(\tau) = \langle (x_{t+\tau} - x_t)^2 + (y_{t+\tau} - y_t)^2 \rangle, (1)$$

In which τ is the lag time, x_t and y_t are the x and y coordinates of the particle at a given time t, and $x_{t+\tau}$ and $y_{t+\tau}$ are the x and y coordinates of the particle after a given lag time τ. The ensemble average of the data for each condition was taken, after outliers were removed. Data in which the MSD for a given track was 3 standard deviations above the mean was considered an outlier. Outliers were removed to minimize the potential artifact in which a different punctate region was tracked between the beginning and end of imaging, and thus may lead to a significantly increased MSD. Outliers accounted for at most 6% of the total points tracked, as seen in Table 4.1. Curve fitting was performed using the MATLAB curve fitting toolbox (using the Trust-Region Algorithm), in which mean squared displacements were fit to a power law of the form shown in Eqn 2, and the inset of Figure 4.2E.

$$MSD = D_{eff}\tau^{\beta}, (2)$$

Where MSD is the mean squared displacement, τ is the lag time, and the fitting parameters D_{eff} and β are known as the effective diffusivity and diffusive exponent respectively.

In previous work, we demonstrate that the parameters D_{eff} and β appear to be modulated by independent phenomena[5]. In live cell nuclei, the diffusive exponent, β, appears to be altered by active forces. This was demonstrated by reducing myosin-II activity with blebbistatin, in which a reduction in β was observed. Additionally, force propagation to the nucleus was reduced by disrupting the LINC complex using DN-KASH and again a decrease in β was observed. In cases in which chromatin was decondensed (via daunomycin or trichostatin A treatment), a decrease in D_{eff} was observed with no significant change in β detected. In this work, we further confirm the force responsiveness of β by treating cells with Y-27632 (a ROCK inhibitor) or decoupling the LINC complex with DN-KASH. In both cases we note a decrease in the parameter β. In previous works we have demonstrated similar results using SINK, regardless of the probe being tracked, provided it is bound to the genome (i.e. not an inert particle)[5]. For this work, we chose GFP-UBF as the particle of interest because we were interested in bulk chromatin dynamics. Because GFP-UBF expresses as bright punctate regions throughout the entire nucleus, it presents an ideal particle for tracking in terms of brightness and number.

For heterogeneous DN-KASH experiments, the closest distance (edge to edge) between a DN-KASH expressing nucleus and the nucleus of interest was taken to be the distance to a DN-KASH expressing cell. These distances were measured for every cell of interest, and the data were binned into 10 μm intervals. Distances were measured using the Leica Application Suit – Advanced Fluorescence software. Nuclear area was measured for cells in all conditions, and no significant difference between nuclear area for any condition was detected using a 1-way ANOVA ($p > 0.05$). All data showing number of cells, number of tracks, nuclear area, and β for each condition is presented in Table 4.1.

Polyacrylamide Gel Synthesis

Polyacrylamide (PA) gels were synthesized similar to previously published methods[10,11]; however, here Sulfo-SANPAH was used as the protein-substrate linker. Activated glass coverslips were coated with PA gels of varying elastic moduli, using acrylamide to bisacrylamide ratios of 5%:0.1%, 7.5%:0.35% and 12%:0.28% for a stiffness of 2.5, 10, and 30 kPa respectively. Gels were then coated with Sulfo-SANPAH at 0.2 mg/ml (BioVision), and UV treated for 30 minutes, followed by coating with 0.1 mg/ml rat tail type 1 collagen (Corning) for cell adhesion. For comparison we also present the monolayer data on an uncoated glass substrate. While extracellular matrix coating likely influences cellular forces, we found it interesting that uncoated glass (orders of magnitude stiffer than 30kPa) demonstrated the largest MSD within the nucleus, and β. While glass can be coated in collagen, the differences in surface chemistry between polyacrylamide and glass likely influence interfacial interactions with collagen, and the cells would, in turn, experience a different binding surface regardless. Nevertheless, the main finding presented for this section is the stiffness response of motion within the nucleus, which is clearly demonstrated with the different stiffness PA gels.

Statistics

Error bars shown on MSD versus lag time plots are standard error of the mean of the population of tracks for a given experimental group. If a given MSD data point was greater than 3 standard deviations from the mean of that population at 60 minutes, the track was removed from analysis. Error bars on the bar graphs of β are the 95% confidence intervals based on the fit of this parameter. Values were considered significantly different if the 95% confidence intervals did not overlap.

Table 4.1: Number of cells, tracks, nuclear area, and β for each condition

Experiment	Number of cells	Total Tracks (w/ Outliers)	Total Tracks (w/o Outliers)	Nuclear Area (μm^2)	Std. Dev. Of Nuclear Area	β
Monolayer Control (Glass)	11	86	84	155	54	0.9461
Isolated	9	58	55	150	30	0.6925
Monolayer DN-KASH (CoTransfected)	12	65	64	127	34	0.5929
Monolayer Y-27632	19	104	101	124	60	0.5885
Monolayer 2.5 kPa	12	176	173	131	24	0.4407
Monolayer 10 kPa	21	298	287	131	40	0.5305
Monolayer 30 kPa	16	241	235	148	38	0.6875
Monolayer DN-KASH 0-10 μm	17	193	185	125	36	0.5901
Monolayer DN-KASH 10-20 μm	10	95	93	106	22	0.6626
Monolayer DN-KASH 20-30 μm	13	135	132	116	41	0.6988
Monolayer DN-KASH 30-40 μm	7	51	50	106	30	0.8136

Results and Discussion

Active Cellular Forces Increase Intranuclear Dynamics

SINK does not require isolated cells, and we present studies here on epithelial cell (NRK-52E) monolayers. We tracked GFP-tagged upstream binding factor (GFP-UBF) and quantified intranuclear motion as mean square displacement (MSD). With extensive processing and nuclear alignment, punctate regions of GFP-UBF within the nucleus were tracked over time (Figure 4.2A-D). The MSD of these tracks were then averaged and power-law fits (of the form of Eqn 2 in Materials and Methods) of the MSD versus lag time (τ) yielded β, the force generation exponent (Figure 4.2 E, F). Details of this equation and fitting are provided in Materials and Methods. We have shown previously that the fitting parameters β and D_{eff}, indicative of the force propagation through cells and related to the chromatin condensation state, respectively, are affected by independent cellular phenomena[5], and we have successfully performed SINK on a variety of cells types[5,8,12]. Here, we reduced force generation in NRK-52E epithelial cell monolayers with the Rho-associated protein kinase (ROCK) inhibitor Y-27632 (Figure 4.1 for

characterization) and physically decoupled the nucleus from the cytoskeleton using a dominant negative Klarsicht, ANC-1, Syne Homology (DN-KASH) domain construct to reduce LINC complex connectivity (Figure 4.3, and Figure 4.4 for characterization), via displacement of nesprins[13]. Both Y-27632 treated and DN-KASH transfected cells showed reduced intranuclear movement, and the force generation exponent β was similar despite the independent mechanisms used to reduce the propagation of cell force (Figure 4.2F). Increased agitation within cells from active forces is also observed in the cytoplasm based on stochastic motion of tracer particles, driven by molecular motor activity on the cytoskeleton[14]. Additionally, due to connections through the LINC complex, motor forces propagate to the nucleus and affect subnuclear movements[15]. In addition to the work described here, we previously demonstrated this propagation of active force in endothelial cells with inhibition of myosin II with blebbistatin, ATP depletion, and physical disruption of the LINC complex using DN-KASH, wherein all cases showed a reduction of the force generation exponent, β[5]. While a quantitative force value cannot currently be extracted using this technique, we have shown that chromatin motion and the parameter β are responsive to changes in force propagation. We demonstrate the utility of SINK for probing complex systems in the following sections.

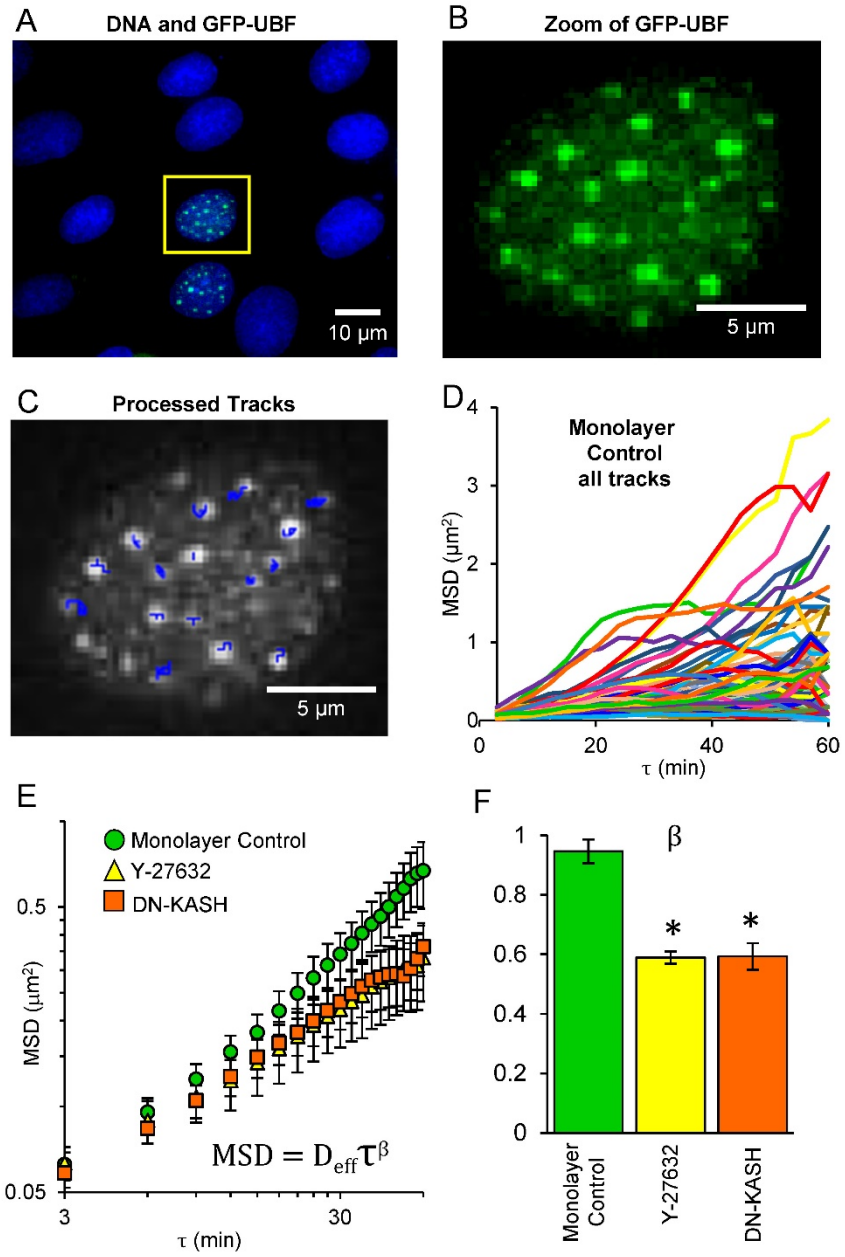

Figure 4.2: SINK method and mechanisms of intracellular force propagation reduction

(A) *Monolayer of NRK-52E epithelial cells with 2 cells expressing GFP-UBF (green) is shown. DNA (blue) was stained with Hoechst. (**B**) Magnified image of outlined nucleus in **A** showing only the GFP-UBF channel is shown. (**C**) Processed frame of **B** after imaging nucleus at 3-minute time intervals for 60 minutes is shown. Tracks of points are shown as blue overlay. Nuclei*

*were aligned prior to tracking of points. (**D**) Tracks from all points in all nuclei for the control monolayer data plotted on linear coordinates are shown. (**E**) MSD average of intranuclear movement vs. lag time (τ) was plotted on log-log coordinates for control cells in a monolayer (green), cells in a monolayer treated with Y-27632 (yellow), and cells in a monolayer transfected with DN-KASH (orange). Error bars represent standard error. Data were fit to a power law of the form shown in the inset. (**F**) Comparison of the force generation exponent (β) for control cells in a monolayer, Y-27632 treated monolayers, and DN-KASH monolayers. Reduction of either cell force generation (Y-27632), or nuclear connectivity (DN-KASH) resulted in decreased β. Asterisk denotes significant difference based on the curve fit ($p < 0.05$). Error bars represent 95% confidence interval for the fitting of β.*

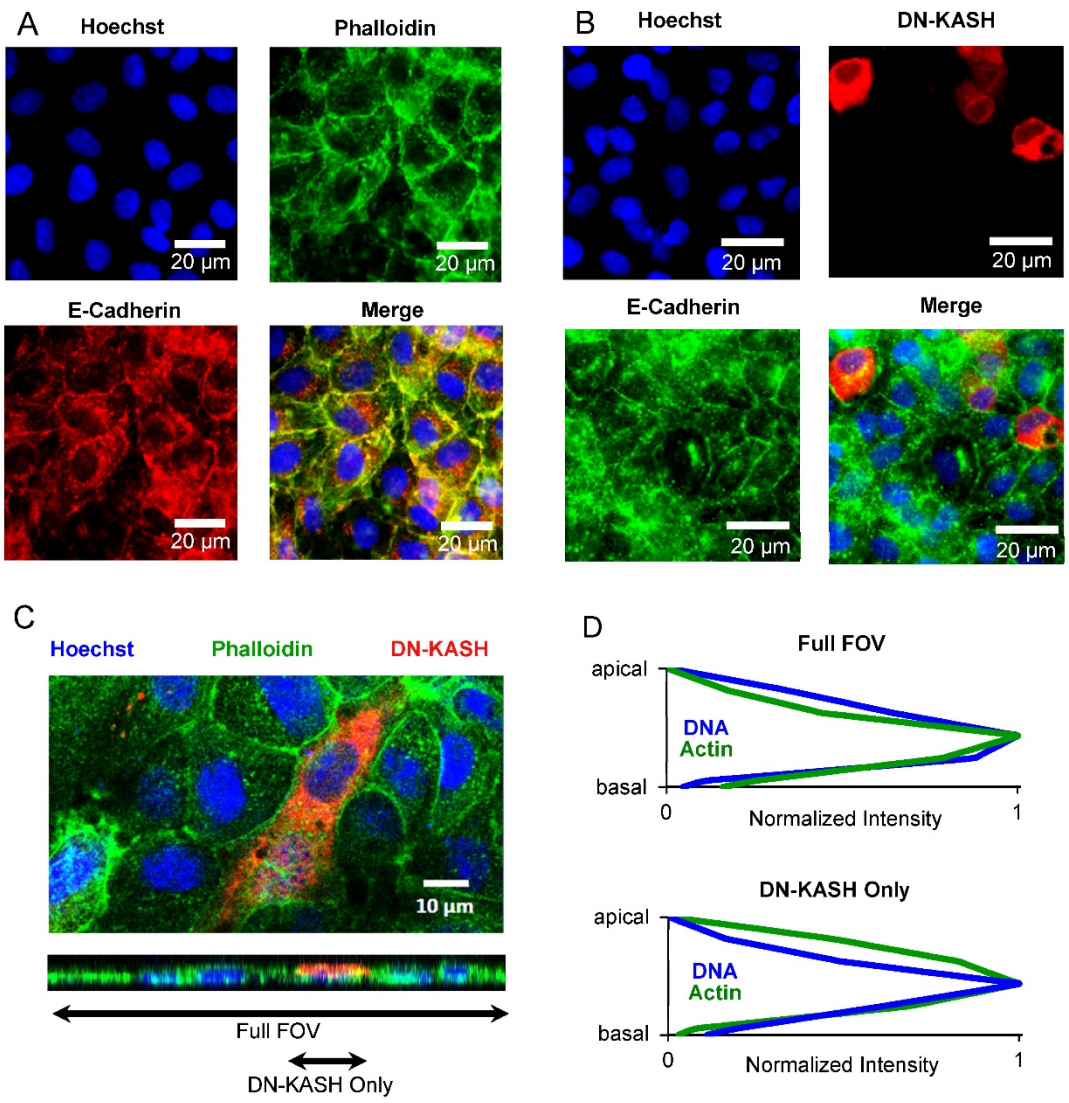

Figure 4.3: DN-KASH expression does not appear to alter E-cadherin expression or actin distribution

*(**A**) Monolayer control cells show normal E-cadherin expression. Nuclei were stained with Hoechst (blue), actin was visualized with Oregon Green Phalloidin (green), and E-Cadherin was visualized via immunofluorescence (red). (**B**) Monolayer cells, expressing DN-KASH (red) show normal E-Cadherin expression (green). Nuclei were stained with Hoechst (blue). E-Cadherin was visualized via immunofluorescence. (**C**) Monolayer cells, expressing DN-KASH (red) show normal actin distribution (green).*

*Nuclei were stained with Hoechst (blue). Actin was visualized using Oregon Green Phalloidin. (**D**) Actin distribution appears similar in DN-KASH expressing cells as in control monolayers, with actin distributed throughout the height of the nucleus. A full field of view, including cells not expressing DN-KASH, is shown as well as the analysis performed only on a cell expressing DN-KASH.*

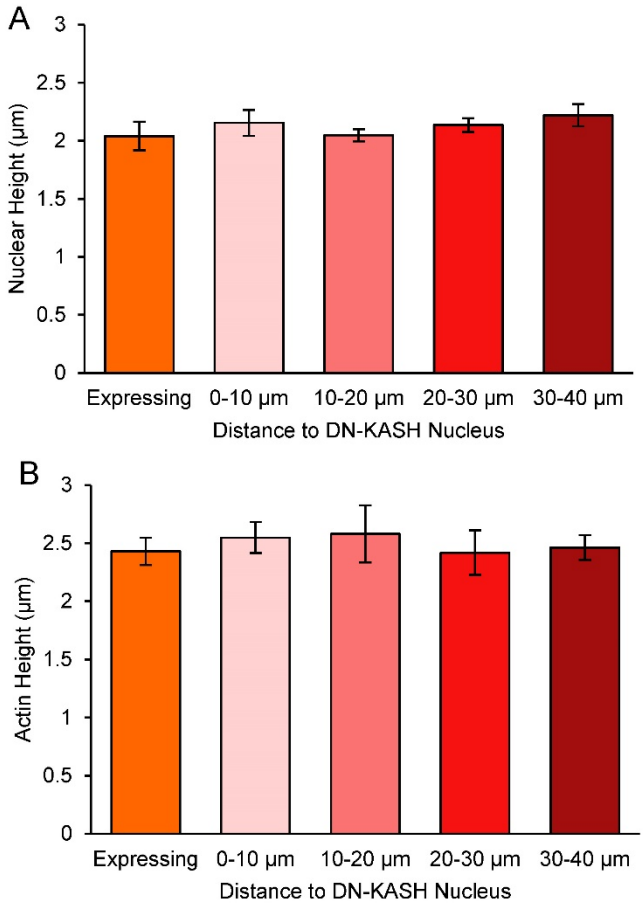

Figure 4.4: Nuclear and actin height of heterogeneous DN-KASH monolayer

*(**A**) Nuclear height was measured for cells expressing DN-KASH and at various distances from DN-KASH expressing cell. No significant difference in nuclear height was detected for any conditions. ($p > 0.05$). Error bars represent standard error of the mean. This is in contrast to work in which DN-KASH expressing and nearby*

*cells showed an increase in nuclear height compared to more distant cells[17]; however differences in cell type, expression level, and time after transfection may affect this parameter. (**B**) Actin height was measured from orthogonal views for cells expressing, or at various distances from DN-KASH expressing cells. No significant difference was detected between any conditions ($p > 0.05$). Analysis for nuclear and actin height was performed in ImageJ. Significant differences were detected using a 1-way ANOVA followed by Tukey's pairwise comparison.*

Sub-confluent Cells Demonstrate Reduced Intranuclear Motion Compared to Monolayer Cells

SINK can be used to investigate epithelial cells in monolayers which can be challenging using other biophysical techniques. We first considered the differences in intracellular force generation between sub-confluent and monolayer cells. Previous studies using traction force microscopy on multicellular systems reported that the traction force generation of two adjoined cells was not the sum of forces of the two isolated cells on the substrate[16]. We define monolayer cells as being in contact with adjacent cells on all sides with actin at the midline of the cell Figure 4.5 A-C) and with developed adherens junctions, as confirmed via immunofluorescence (Figure 4.3). Isolated cells were imaged at sub-confluence where a portion of the cell was not in contact with adjacent cells. In these cells, actin distribution was observed primarily in the basal region of the cell (Figure 4.5 A-C). We used SINK to compare changes in intranuclear movement of GFP-UBF in isolated and monolayer cells; intranuclear movement was increased in a monolayer compared to isolated cells (Figure 4.5 D). When these MSD curves were fit to a power law, the force generation exponent, β, was significantly increased in monolayer cells (Figure 4.5 E). We speculate that the increased force propagation to the nucleus in monolayer

cells compared with isolated cells may be from both the redistribution of force within cells due to changes in actin distribution, as well as increased net force due to increased cell-cell contact.

We observed increased coplanar actin leading to the nucleus in monolayers (Figure 4.5 A-C). This is consistent with previous observations of monolayers wherein cell nuclei were uniform and flatter, with actin throughout the height of the nucleus compared to isolated cells which had less uniform nuclei with primarily basal plane actin[17]. The cell-cell contacts present in monolayers allow for force propagation through adherens junctions rather than only through focal adhesions. Previous studies have shown that the overall contractile moment in clusters of endothelial cells decreased after blocking VE-cadherin[18], suggesting that cells increase their force generation upon forming cadherin junctions. Our results suggest that while some fraction of force generated by cells may by-pass the nucleus, a larger amount of cell-generated force is propagated to the nuclei in monolayer systems compared to the nuclei of isolated cells.

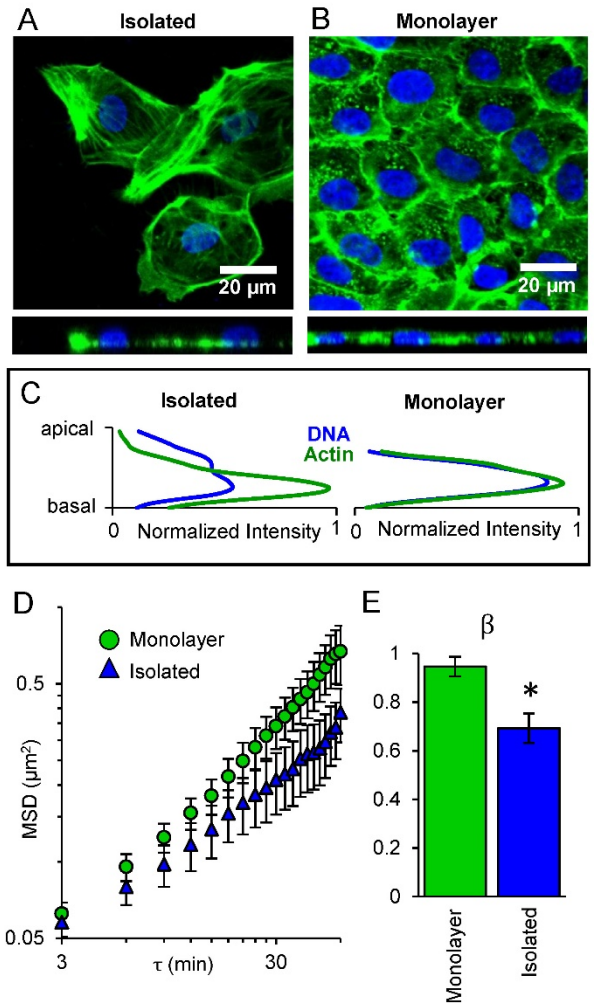

Figure 4.5: Reduction of intranuclear movement and β in isolated cells vs. monolayers

*(**A**) Top view (top) and side view (bottom) of confocal images of isolated cells and (**B**) cells in a monolayer, stained for DNA (blue), and actin (green) are shown. (**C**) Image analysis of apical-basal (z-direction) distribution of actin and DNA shows colocalization in the monolayer but separation in the isolated cells. In isolated cells actin lies primarily along the basal region of cells, while in monolayer cells actin is primarily coplanar with the nucleus. (**D**) MSD of intranuclear movement vs. lag time (τ) plotted on log-log coordinates, comparing monolayer (green) vs isolated (blue) cells is shown. Error bars represent standard error. (**E**) β for monolayer and isolated cells is plotted. Asterisk denotes significant difference based on the curve fit ($p < 0.05$). Error bars represent 95% confidence interval for the fitting of β.*

Intranuclear Motion Changes with Substrate Stiffness in Monolayer Systems

For more than a decade, traction force measurements and analogous studies have shown that individual cells generate increased force on stiffer substrates[19]. We use SINK in NRK-52E epithelial cell monolayers on collagen coated polyacrylamide gels of varying elastic moduli, generated and characterized using our previous methodology[10,11]. As the stiffness of the underlying substrate was increased from 2.5, to 10, to 30 kPa, the intranuclear movement of GFP-UBF in these monolayers also increased. The force generation exponent, β, also increased, indicating a dose-dependent increase in force propagation through cells in a monolayer as their substrate stiffness increases (Figure 4.6). Additionally, these data were compared to cell monolayers grown on glass (not coated with collagen), with an elastic modulus several orders of magnitude greater than that of a 30 kPa gel, where a further increase in MSD, and β, was observed (Fig. 3). Each of these regimes were found to be statistically different suggesting that SINK has sufficient precision to measure substrate stiffness dependent changes in cellular force generation. This result was in slight contrast to traction force microscopy data, which often plateaus on stiffer substrates[20]. In contrast to SINK measurements, traction forces become difficult to measure at high stiffness, as substrate displacements decrease, and cannot be measured on glass substrates. There is evidence to suggest that epithelial monolayers are more responsive to substrate stiffness than sparsely seeded cells[21]. Generally, the trend of increased force generation with increased substrate stiffness is consistent with traction force microscopy data[18,22]. From exponential fitting of our data, we find that cells would generate 90% of the force generated on glass (glass set to 50 GPa, essentially infinite stiffness) on a substrate with an elastic modulus of about 60 kPa. To our knowledge, this is the first example of measuring the effects of substrate stiffness on cellular force propagation to the nucleus in a monolayer system.

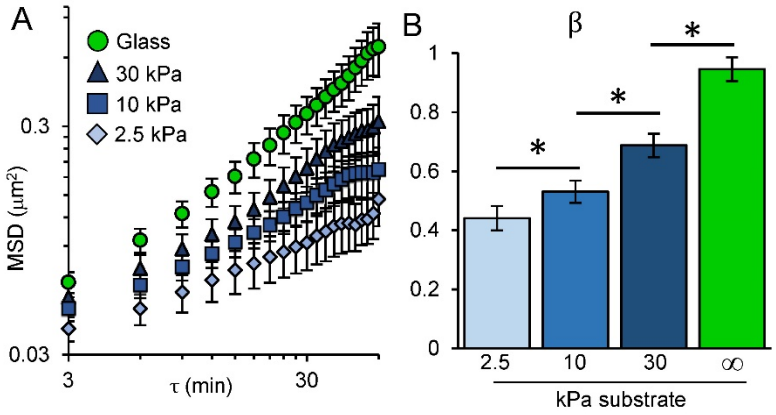

Figure 4.6: Effect of substrate stiffness on intranuclear movement via SINK in monolayers

*(**A**) MSD of intranuclear movement vs. lag time (τ) plotted on log-log coordinates for cells in monolayers seeded on glass (green), or collagen coated polyacrylamide gels with elastic moduli of 30 (dark blue), 10 (blue), or 2.5 (light blue) kPa is shown. Intranuclear movement increases as substrate stiffness increases. Error bars represent standard error. (**B**) Comparison of the force generation exponent (β) for monolayers of varying elastic moduli for curves shown in **A**. Asterisk denotes significant difference based on the curve fit ($p < 0.05$). Error bars represent 95% confidence interval for the fitting of β.*

SINK Method can be Used to Characterize Monolayers with Single Cell Defects

Cancers, cardiovascular plaques and other diseases often stem from the dysfunction of a single cell or cell cluster within a relatively homogeneous monolayer[23,24]. We used SINK to investigate spatial propagation of force from a single cell defect through a monolayer. We decreased cellular force propagation through a cell by expressing DN-KASH, which has previously been shown to reduce force propagation from one side of a cell to the other[7]. For these experiments, monolayers were initially transfected with DN-KASH, media was changed after several hours, and the cell monolayer was transfected again with GFP-UBF (Figure 4.7 A-C). We examined cells co-transfected with DN-KASH and GFP-UBF (Figure 4.7 A) or at

various distances from DN-KASH expressing cells (Figure 4.7 B, C) for SINK analysis. With the addition of the untransfected monolayer data and the co-transfected cells (from Figure 4.2E, F) a trend in the force generation exponent β was observed; β (and MSD) increased in nuclei further from the DN-KASH expressing cell (Figure 4.7 D-F). We saw no significant difference in nuclear height or actin distribution between DN-KASH expressing, nearby or distant cells (Figure 4.3 C,D, and Figure 4.4), suggesting that altered β is from force propagation through cells, not changes in cell architecture. Next, β was normalized and plotted versus distance between the DN-KASH expressing nucleus and the cell in which the SINK analysis was performed. We find that the data can be fit by an exponential, $\beta \approx 1 - \exp(-a/50\mu m)$ consistent with a two-dimensional strain field, where a is the distance between the two nuclei (Figure 4.7 G). For reference, in these systems we find that cells are 7.7 ± 1.1 μm apart (schematically, average of a_1, a_2, etc. from Figure 4.7 D). These results suggest that mechanically compromised cells can affect additional cells in a monolayer, perhaps increasing the probability for disease propagation. It has been shown that cells can sense rigidity in fibrous protein matrices at distances >65 μm as compared to synthetic gel matrices where this distance is only ~5 μm[25]. We have shown here that cells have a mechanical interaction distance greater than 50 μm and, based on this fit, would return to approximately 90% of their control level force propagation at a distance of 100 μm from the compromised cell nucleus. These data are consistent with literature reports that suggest cells within a monolayer respond to physical perturbation (via magnetic twisting cytometer) several cells away from the applied force[26]. Within the context of wound healing, a refined strain field allows for regulation and control of physical properties such as coordinated mechanotransduction[27] (polarization, translocation, division, etc.) as a function of distance from the wound site.

The fitting of spatial data to an exponential suggests that these cells are integrated as colloidal crystals rather than as a continuum material[28]. Based on theory, continuum materials with defects would scale as $1/a^2$ whereas colloidal crystal materials would scale as an exponential[29]. There are numerous analogies of cell monolayers to colloidal crystals: colloidal crystals have weak attraction energy between individual particles and assembly is driven primarily by volume exclusion rather than strong attraction. Thus, fluctuations allow for reorganization and redistribution in void sites and at edges, similar to the self-healing of monolayers. Also, cells can undergo geometric-sensitive changes in structure[30] similar to colloidal crystal phase transitions[31]. Calculation of intercellular forces from traction force microscopy data of cell monolayers utilizes an assumption of a continuum of the monolayer[32]. Our results suggest that this assumption should be modified to include the fact that cells are mechanically communicating as colloids rather than as a continuum.

In conclusion, we demonstrated that bulk, intranuclear movement is responsive to intercellular forces and that the force generation exponent, β, can serve as a relative output of intracellular force propagation through modulated monolayer structures. Additionally, no correlation between nuclear area and β was seen (Figure 4.8). Our results suggest that monolayer cells generate increased force as substrate stiffness increases (consistent with results of single cells[19,33,34]) and that this increased force leads to increased chromatin motion. In these monolayer systems, the data suggest that cells have a maximum stiffness sensing threshold of approximately 60 kPa and would respond similarly to 60 kPa and glass (GPa) substrates. Finally, heterogeneous monolayers arising from aberrant single cell defects appear to integrate similar to colloidal crystal systems with a length scale of ~50 μm.

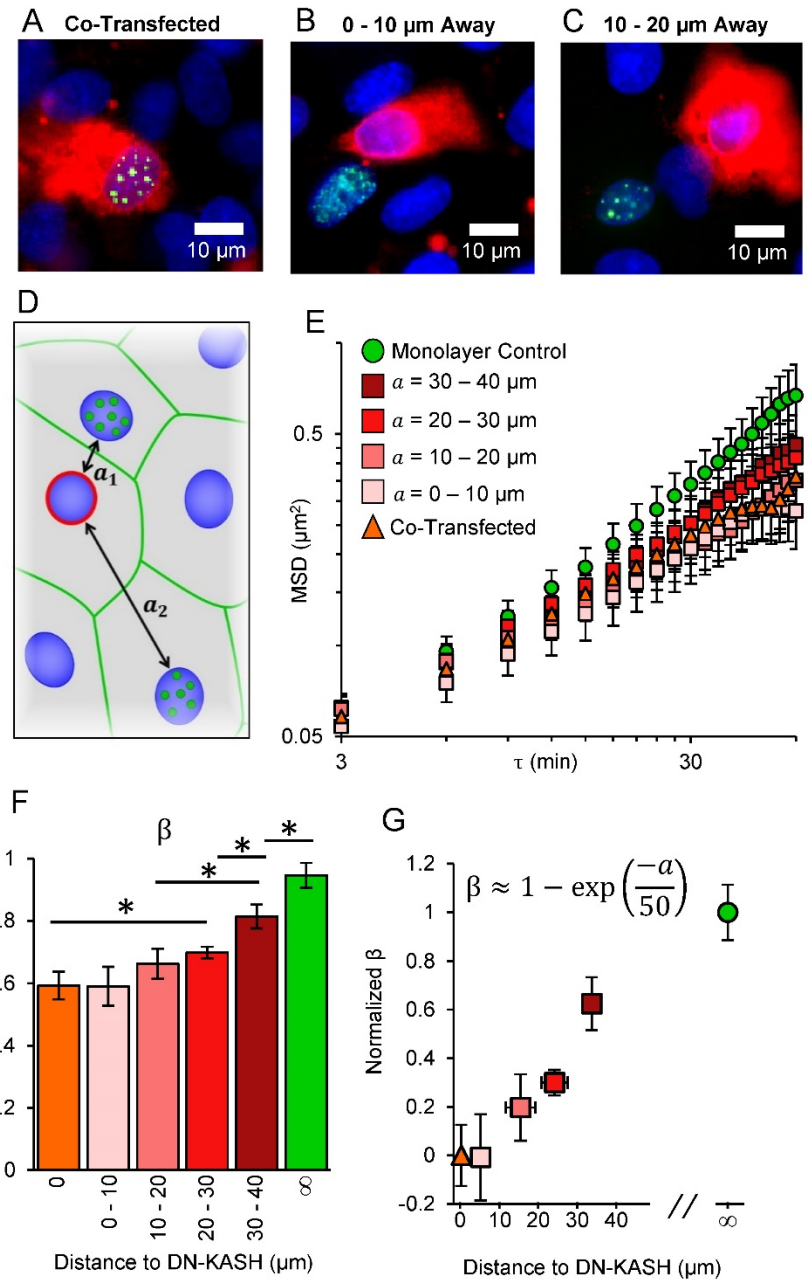

Figure 4.7: SINK method to measure changes in force in heterogeneous monolayers

(A-C) *Images of GFP-UBF (green) expressing nuclei (blue) with DN-KASH (red) being expressed in* ***(A)*** *the same cell* ***(B)*** *a cell 0 – 10 µm away from, or* ***(C)*** *a cell 10 – 20 µm away from the GFP-UBF expressing cell are shown. Distances measured represent nearest nucleus to nucleus distance to a DN-KASH expressing nucleus.* ***(D)*** *A schematic of target cells expressing*

*GFP-UBF (green dots) at various distances (a) from a DN-KASH expressing cell (red outline) is shown. (**E**) A MSD vs lag time plot for DN-KASH expressing cells, cells of varying distances from DN-KASH, and control monolayer cells is shown. Nearby cells demonstrate similar intranuclear motion to co-transfected cells. MSD appears to increase as cells are further from a DN-KASH expressing cell. Error bars represent standard error. (**F**) A comparison of the force generation exponent (β) for nuclei transfected with DN-KASH (orange), or at different distances away from a DN-KASH expressing cell (shades of red) as well as monolayers not transfected with DN-KASH (green) is presented. Error bars represent 95% confidence interval for the fitting of β. (**G**) A plot of the normalized β value vs. distance away from DN-KASH is shown. Initially data appear fairly linear (shades of red); however, since we assumed the control monolayer β value to be significantly far from DN-KASH cells, the data were fit as an exponential of the form $\beta = 1 - \exp(-a/n)$, with a being the distance (in μm) away from a DN-KASH expressing nucleus. The parameter n is a spatial parameter such that forces at a distance n (in μm) no longer feel the majority of the effects of the DN-KASH expressing cell, approximately 50 μm based on the fit. The R^2 for the fit was 0.93. Y-error bars are 95% confidence intervals of β after normalization. X-error bar is the standard deviation of distance away from DN-KASH for the non-adjacent cells.*

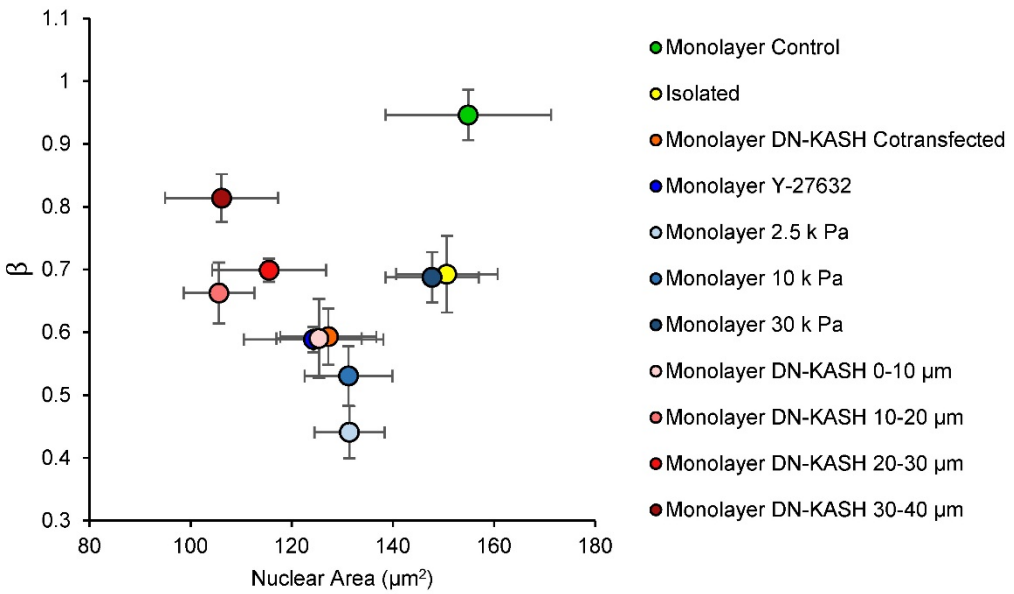

Figure 4.8: β does not correlated with nuclear area

Nuclear area was calculated for each condition and plotted against the corresponding β value. No correlation was observed between β and nuclear area. Additionally, no significant difference between nuclear area was detected for any condition ($p > 0.05$), using a 1-way ANOVA followed Tukey's pairwise comparison. Horizontal error bars are standard error of the mean, vertical error bars are the 95% confidence interval of the fits of β. The values plotted, along with the standard deviation of nuclear area are shown in Table 4.1.

Acknowledgments

We would like acknowledge G. Yang (Carnegie Mellon University) for providing the particle tracking software as well as S. T. Spagnol, A. W. Feinberg, R. Palchesko, Y-L. Wang, S. Wong, and D. Li for their experimental insight. This work was funded by the National Science Foundation [NSF-CMMI-1634888 to K.N.D., NSF-CMMI-1435755 to C.A.R-K., graduate research fellowship 201315546 to M.C.L.], the National Institutes of Health [NIH-EB003392 to T.J.A.], Cornell Sloan Foundation Fellowship and a Ford Foundation Fellowship to M.C.L.

References

1. Saw, T. B. *et al.* Topological defects in epithelia govern cell death and extrusion. *Nature* **544,** 212–216 (2017).

2. Ladoux, B. & Mège, R.-M. Mechanobiology of collective cell behaviours. *Nat. Rev. Mol. Cell Biol.* **18,** 743–757 (2017).

3. Polacheck, W. J. & Chen, C. S. Measuring cell-generated forces: a guide to the available tools. *Nat. Methods* **13,** 415–423 (2016).

4. Kassianidou, E. & Kumar, S. A biomechanical perspective on stress fiber structure and function. *Biochim. Biophys. Acta - Mol. Cell Res.* **1853,** 3065–3074 (2015).

5. Spagnol, S. T., Dahl, K. N. & Noel Dahl, K. Active cytoskeletal force and chromatin condensation independently modulate intranuclear network fluctuations. *Integr. Biol.* **6,** 523–31 (2014).

6. Rape, A., Guo, W. & Wang, Y.-L. The Regulation of Traction Force in Relation to Cell Shape and Focal Adhesions. *Biomaterials* **32,** 2043–2051 (2011).

7. Alam, S. G. *et al.* The nucleus is an intracellular propagator of tensile forces in NIH 3T3 fibroblasts. *J. Cell Sci.* **128,** 1901–1911 (2015).

8. Booth-Gauthier, E. a, Alcoser, T. a, Yang, G. & Dahl, K. N. Force-induced changes in subnuclear movement and rheology. *Biophys. J.* **103,** 2423–31 (2012).

9. Yang, G., Cameron, L. a, Maddox, P. S., Salmon, E. D. & Danuser, G. Regional variation of microtubule flux reveals microtubule organization in the metaphase meiotic spindle. *J. Cell Biol.* **182,** 631–9 (2008).

10. Lampi, M. C. *et al.* Simvastatin ameliorates matrix stiffness-mediated endothelial monolayer disruption. *PLoS One* **11,** 1–20 (2016).

11. Kraning-Rush, C. M., Carey, S. P., Califano, J. P. & Reinhart-King, C. A. Quantifying Traction Stresses in Adherent Cells. in *Methods in Cell Biology* (eds. Asthagiri, A. R. & Arkin, A. P.) **110,** 139–178 (Elsevier Inc., 2012).

12. Armiger, T. J., Spagnol, S. T. & Dahl, K. N. Nuclear mechanical resilience but not

stiffness is modulated by αII-spectrin. *J. Biomech.* **49,** 3983–3989 (2016).

13. Lin, G. G. & Scott, J. G. Linear Arrays of Nuclear Envelope Proteins Harness Retrograde Actin Flow for Nuclear Movement. *Science* **329,** 956–959 (2010).

14. Guo, M. *et al.* Probing the stochastic, motor-driven properties of the cytoplasm using force spectrum microscopy. *Cell* **158,** 822–832 (2014).

15. Tajik, A. *et al.* Transcription upregulation via force-induced direct stretching of chromatin. *Nat. Mater.* **15,** 1–20 (2016).

16. Sim, J. Y. *et al.* Spatial distribution of cell-cell and cell-ECM adhesions regulates force balance while main taining E-cadherin molecular tension in cell pairs. *Mol. Biol. Cell* **26,** 2456–2465 (2015).

17. Neelam, S., Hayes, P. R., Zhang, Q., Dickinson, R. B. & Lele, T. P. Vertical uniformity of cells and nuclei in epithelial monolayers. *Sci. Rep.* **6,** 19689 (2016).

18. Krishnan, R. *et al.* Substrate stiffening promotes endothelial monolayer disruption through enhanced physical forces. *Am. J. Physiol. Cell Physiol.* **300,** C146–C154 (2011).

19. Discher, D. E., Janmey, P. & Wang, Y.-L. Tissue cells feel and respond to the stiffness of their substrate. *Science* **310,** 1139–43 (2005).

20. Ghibaudo, M. *et al.* Traction forces and rigidity sensing regulate cell functions. *Soft Matter* **4,** 1836 (2008).

21. Ng, M. R., Besser, A., Danuser, G. & Brugge, J. S. Substrate stiffness regulates cadherin-dependent collective migration through myosin-II contractility. *J. Cell Biol.* **199,** 545–563 (2012).

22. Andresen Eguiluz, R. C., Kaylan, K. B., Underhill, G. H. & Leckband, D. E. Substrate stiffness and VE-cadherin mechano-transduction coordinate to regulate endothelial monolayer integrity. *Biomaterials* **140,** 45–57 (2017).

23. Lodish, H. *et al.* Tumor Cells and the Onset of Cancer. in *Molecular Cell Biology. 4th edition.* (W. H. Freeman, 2000).

24. Mehta, V. & Tzima, E. A turbulent path to plaque formation Sharks shift their. *Nature*

540, 531–532 (2016).

25. Rudnicki, M. S. *et al.* Nonlinear Strain Stiffening Is Not Sufficient to Explain How Far Cells Can Feel on Fibrous Protein Gels. *Biophys. J.* **105,** 11–20 (2013).

26. Barry, A. K., Wang, N. & Leckband, D. E. Local VE-cadherin mechanotransduction triggers long-ranged remodeling of endothelial monolayers. *J. Cell Sci.* **128,** 1341–1351 (2015).

27. Sunyer, R. *et al.* Collective cell durotaxis emerges from long-range intercellular force transmission. *Science* **353,** 1157–1161 (2016).

28. Alsayed, A. M., Islam, M. F., Zhang, J., Collings, P. J. & Yodh, A. G. Premelting at Defects Within Bulk Colloidal Crystals. *Science* **309,** 1207–1210 (2005).

29. Lipowsky, R. Melting at grain boundaries and surfaces. *Physical Review Letters* **57,** 2876 (1986).

30. Chanet, S. *et al.* Actomyosin meshwork mechanosensing enables tissue shape to orient cell force. *Nat. Commun.* **8,** 15014 (2017).

31. Weeks, E. R., Crocker, J. C., Levitt, A. C., Schofield, A. & Weitz, D. A. Three-dimensional direct imaging of structural relaxation near the colloidal glass transition. *Science* **287,** 627–631 (2000).

32. Tambe, D. T. *et al.* Collective cell guidance by cooperative intercellular forces. *Nat. Mater.* **10,** 469–475 (2011).

33. Han, S. J., Bielawski, K. S., Ting, L. H., Rodriguez, M. L. & Sniadecki, N. J. Decoupling substrate stiffness, spread area, and micropost density: A close spatial relationship between traction forces and focal adhesions. *Biophys. J.* **103,** 640–648 (2012).

34. Califano, J. & Reinhart-King, C. Substrate Stiffness and Cell Area Predict Cellular Traction Stresses in Single Cells and Cells in Contact. *Cell Mol Bioeng* **3,** 68–75 (2011).

Chapter V: Calyculin A Treatment Influences Epithelial Monolayer Response in a Substrate Dependent Manner

Introduction

Cells are able to sense their extracellular environment and have the ability to regulate their gene expression through mechanotransduction[1]. Maintaining proper cellular responses to the extracellular environment proves critical for differentiation, as the stem cell niche provides both physical and chemical factors for determining stem cell fate and is vital for fetal development and organogenesis[2–8]. Additionally, misregulation of the feedback loop between a cell and the extracellular environment represents a possible mechanism for cancer metastasis, as tumors are typically stiffer than the surrounding tissue[9–13]. This increased stiffness, sensed by both healthy and cancerous cells, may cause cells to further misregulate their genome, ultimately leading to disease progression. As cells generate increased forces in stiff environments [14–16], tissue fibrosis and vascular stiffening may ultimately lead to dysfunctional monolayer permeability in these environments (i.e. monolayer cells generating sufficient forces to disrupt cell-cell junctions)[17]. Cancer metastasis, tissue fibrosis, and monolayer permeability are examples that highlight the importance of understanding the complex biophysical factors that ultimately generate and maintain healthy tissues or become misregulated in diseases. Through actomyosin contractions, cells are able to pull on their extracellular environment, which represents one means by which cells probe the physical properties of their environment, as extracellular, cytoskeletal, and nuclear proteins are intimately connected throughout a cell[18]. Further, the ability of cells to sense their neighboring cells is evident through contact inhibition during homeostasis (to control proliferation) and collective migration during wound healing[19,20].

As mechanotransduction is gaining recognition as a key method of genome regulation in many tissue and cell types, we aim to characterize the substrate dependent response of epithelial monolayers to changes in actomyosin contractility.

The rat kidney epithelial cell line, NRK52E, is used as a model cell system in these studies. We first characterize these cells on glass substrates, which is a common substrate for *in vitro* experiments. Then, we probe monolayers grown on polyacrylamide gels of soft (2.5 kPa) and intermediate (30 kPa) elastic moduli, which are closer in stiffness to the *in vivo* environment of kidney cells[21–23]. We aim to determine the substrate dependent responses to the well-characterized phosphatase inhibitor Calyculin A, which ultimately increases cellular contractions. On glass substrates, we also characterize subconfluent cells, as the monolayers appear to begin to shift towards a subconfluent phenotype after Calyculin A treatment on glass. We hypothesize that substrate stiffness, and potentially protein coating, may influence the cellular response to Calyculin A treatment. As epithelial to mesenchymal transition (EMT) is a drastic phenotypic shift in epithelial cells, we characterize outputs representing early markers of EMT and other phenotypic changes. For each substrate condition, we investigate how changes in contractility impact actin distribution, chromatin dynamics, and yes-associated protein (YAP) localization on substrates of various stiffness.

Actin distribution was chosen as a metric since actomyosin contractions represent a means of direct force propagation to the cell nucleus through the linker of the nucleoskeleton and cytoskeleton (LINC) complex[24–27]. As forces propagate through the cytoskeleton and LINC complex, the chromatin fibers within the nucleus can be impacted[28]. Therefore, chromatin dynamics were measured via tracking displacements of a green fluorescently tagged transcription factor, upstream binding factor (GFP-UBF). Tracking this chromatin-bound protein allows direct

visualization of fluctuations of the chromatin fiber and, therefore, a method of visualizing the extent that cell-generated forces influence chromatin motion. Finally, we quantify YAP nuclear to cytoplasmic intensity, as YAP has been demonstrated to be a mechanosensitive protein which is likely involved in various downstream cellular changes such as EMT[29–31]. YAP is a downstream effector of the HIPPO pathway, involved in organ size regulation, cell proliferation, and overexpressed in various cancers[29,32–34]. These metrics collectively provide sensitive tools to probe the extracellular-dependent monolayer response to actomyosin contractions. NRK52E monolayers likely require multiple simultaneous treatments for a complete transition to a mesenchymal phenotype to occur[35,36]. Thus, this work utilizes various methods with sufficient sensitivity to probe contraction-based changes likely occurring prior to completion of EMT or other drastic phenotypic shifts.

Materials and Methods

Cell culture, transfection, and drug treatment

Rat kidney epithelial cells, NRK52E (kind gift Y. Wang CMU) were cultured in Dulbecco's modified Eagle's medium (DMEM), (ThermoFisher) supplemented with 5% Bovine Calf Serum (ThermoFisher) and 1% penicillin/streptomycin (ThermoFisher) at 37 ºC and 5% CO_2. For particle tracking analysis, cells were transfected with green fluorescent protein tagged upstream binding factor (GFP-UBF) using Lipofectamine3000 (Thermofisher) according to manufacturer's protocols. For Calyculin A treatments, cells were treated with 1nM Calyculin A for 30 minutes prior to imaging or fixation. Calyculin A remained in the media during live cell imaging. For imaging, cells were grown on either glass or polyacrylamide substrates. In all cases, with the exception of the subconfluent data, cells were cultured to a confluent monolayer prior to drug treatment and/or analysis.

Imaging, fluorescent labeling, and image analysis

For live cell imaging, cells were imaged in a live cell imaging chamber held at 37 ºC and 5% CO_2. Widefield images were obtained using 63x, 1.4 NA, oil immersion objective on an inverted microscope (DMI6000, Leica) with a DFC350 camera. Confocal images were acquired on a Zeiss LSM700, with a 63X, 1.4 NA, oil immersion objective. In all cases, nuclei were stained using Hoechst 33342 (Life Technologies) according the manufacturer's protocols. For fixed cell imaging, cells were fixed in a 4% formaldehyde (Thermofisher) solution for 15 minutes and permeabilized using a 0.2% triton-x solution for 15 minutes. Actin was stained using Oregon Green Phalloidin (ThermoFisher) according the manufacture's protocols. For YAP immunofluorescent imaging, blocking was performed using a 0.2% BSA (Signma-Aldrich) solution in PBS for 30 minutes. Cells were then incubated using the primary mouse anti-YAP antibody (YAP Antibody 63.7: sc-101199, Santa Cruz Biotechnology) at a 1:100 dilution in 0.2% BSA solution for 1 hour. The secondary antibody used was a Rabbit anti-Mouse IgG Alexa Fluor 488 (A-11059, Invitrogen), at a 1:200 dilution in 0.2% BSA solution for 1 hour.

Nuclear and actin basal to apical intensity distribution analysis was performed using ImageJ. Based on a confocal z-stack orthogonal view, the actin and nuclear channel distributions along the height of the cell nuclei were calculated. These values were then normalized and plotted for nine fields of view. An example of this method is shown in Figure 5.1. Particle tracking was performed using the same method described in Chapter IV. For particle tracking image analysis, live cell images were acquired for one hour at 3-minute increments. Images were taken 1 hour after time series images were acquired to assure cell viability and that cells remained in interphase (e.g. did not divide). The images were analyzed using custom MATLAB software developed by Ge Yang as previously published[37,38]. Nuclei were aligned prior to tracking such that only intranuclear motion was captured. Additionally, only tracks which

persisted throughout the length of imaging were used for analysis. Tracks which exceeded 3 standard deviations from the mean of a given experimental condition were considered outliers and removed from analysis. These points were removed as they appeared likely to be cases in which the software detected two points as a single unique point, which, therefore increased apparent motion. Mean squared displacement (MSD) was calculated, and power law fits of MSD were performed using the MATLAB curve fitting toolbox. All fits obtained had a r^2 value greater than 0.97. YAP localization image analysis was performed using ImageJ. A nucleus mask was obtained via the Hoechst channel. A cytoplasmic mask was obtained using the YAP channel with a hole cut out using the nuclear mask. The average intensity of the YAP channel was measured using each mask, and the nuclear value was divided by the cytoplasmic value to obtain the nuclear to cytoplasmic ratio. An example of this method is shown in Figure 5.2.

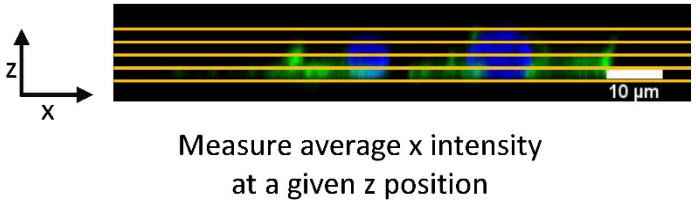

Figure 5.1: Example of calculation of actin distribution

The nuclear and actin basal to apical distribution plots in the results section were determined as follows. For a given orthogonal field of view, the average intensity was calculated for each channel along the length of the image (x-axis) for a given z-position. For comparison, the intensity profiles and cell height were normalized between 0 and 1 for each field of view. Analysis was performed using ImageJ.

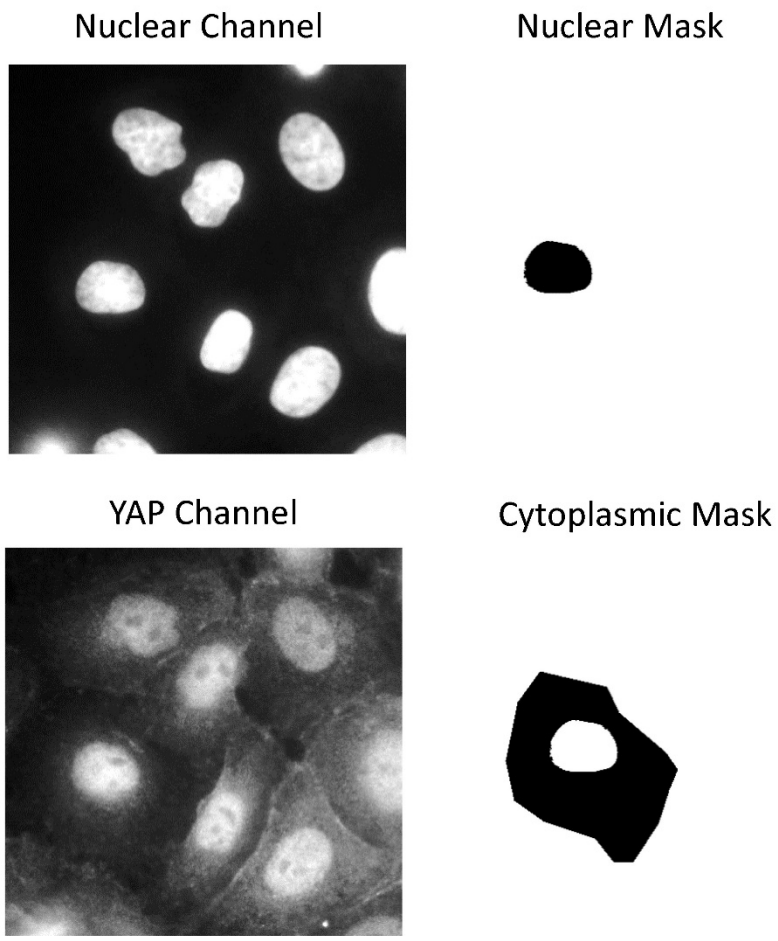

Figure 5.2: Example of the image analysis for calculation of the YAP nuclear to cytoplasmic intensity ratio

For each condition, a nuclear mask was generated from the Hoechst stained channel. A YAP mask was then drawn around the entire cell using the YAP channel. The nuclear mask was subtracted from the entire cell mask to generate the cytoplasmic mask. Each mask was overlaid on the YAP channel, and the average YAP intensity for both the nuclear YAP, and cytoplasmic YAP was calculated. Finally, the average nuclear intensity was divided by the average cytoplasmic intensity to obtain the ratio of the two. Image analysis was performed on ImageJ.

Polyacrylamide gel generation

Polyacrylamide gels were synthesized as previously published and described in Chapter IV[39,40]. Activated glass coverslips were coated with polyacrylamide gels with an acrylamide to bis-acrylamide ratio of 5%:0.1% to obtain an elastic modulus of 2.5 kPa, or with a ratio of 12%:0.28% to obtain an elastic modulus of 30 kPa. Gels were coated with a 0.2 mg/mL Sulfo-SANPAH (BioVision) solution in 50mM HEPES buffer of pH 8, followed by 30 minutes of UV treatment. After Sulfo-SANPAH treatment, gels were coated with 0.1 mg/ml rat tail type 1 collagen (Corning) solution in 50mM HEPES buffer of pH 8 for 2 hours. Gels were exposed to UV light for 30 minutes for sterilization prior to seeding cells. Gels were kept in PBS, with the lid off for sterilization.

Results

In this work, we aim to elucidate the cellular response to increased cytoskeletal contractions, via Calyculin A treatment, for monolayers on various substrates. We investigated monolayer systems of cells grown on glass substrates, soft gels (elastic modulus of 2.5 kPa), and intermediate stiffness gels (elastic modulus of 30 kPa). For each of the investigated substrates, the monolayers were characterized in terms of actin distribution, chromatin dynamics, and YAP nuclear localization. Apical to basal actin distribution was determined through confocal imaging. Chromatin dynamics were investigated through live cell intranuclear particle tracking, and YAP localization was probed via immunofluorescent labeling.

On glass substrates epithelial monolayers approach an isolated phenotype after Calyculin A treatment

As stiff substrates, such as plastic or glass, are commonly employed for *in vitro* cell culture experiments, we first chose to analyze epithelial monolayer responses to increased

cellular contractility on glass substrates. Confocal imaging was used to determine the actin distribution from the apical to basal plane of monolayer control cells, subconfluent control cells, and monolayer cells treated with Calyculin A. Representative fluorescent confocal images stained for actin (green) and DNA (blue) for each experimental condition on glass are shown in Figure 5.3. For these confocal images, the z-slice in which the most actin stress fibers were observed is shown. Increased actin stress fibers were observed in Calyculin A treated monolayers, suggesting the cells are increasing their actomyosin contractions as expected. Orthogonal views were used for image analysis, in which the average intensity of a single channel (actin or nuclear) was determined along a horizontal line at a given z-position for the entire height of the cell. This method is shown in Figure 5.1. For comparison among multiple fields of view and conditions, cell height and intensity were both normalized such that all values fell between 0 and 1. Representative orthogonal views, as well as the plot profile for the actin and nuclear channels, for each condition on glass coverslips are shown in Figure 5.4 A,B,C. Additionally, a Nuclear-Actin Segregation Parameter, defined as the absolute value of the difference between the average normalized nuclear and actin intensities at a given z-height, was calculated as a means to quantitatively compare the various conditions (Figure 5.4 D). On glass, subconfluent cells appear to have rounder and taller nuclei compared to the monolayer control cells, as expected[41]. Additionally, the majority of actin in the subconfluent control cells was localized toward the basal plane of the cell, while in the monolayer cells, actin was present throughout the height of the cell, peaking in intensity at a similar z-height as the peak intensity of the nuclear channel (Figure 5.4 A, B). When monolayer cells on glass are treated with Calyculin A to increase actomyosin contractions, cell shape appeared altered from the control monolayer case. While the nuclei in the Calyculin A treated monolayer remained flat, the actin appeared to

distribute preferentially to the basal plane (Figure 5.4 C). Additionally, in cases where an actin cap could be seen above the nuclei, the actin distribution dropped in between cells, giving them a similar shape to the subconfluent cells (albeit with flattened nuclei). This is in contrast to the glass monolayer control cells in which actin between cells was present throughout the height of the cell.

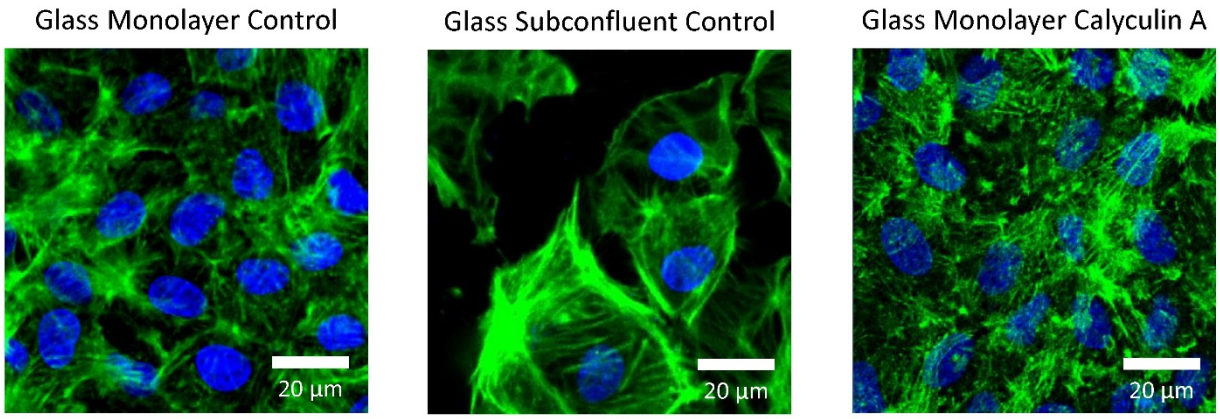

Figure 5.3: Actin stress fibers on glass substrates

Confocal images of actin stress fibers (green) and nuclei (blue) for each condition on glass substrates are shown. The z-slice which contained the most visible stress fibers for each condition is shown. Subconfluent cells appear more spread than the monolayer cells. Upon treatment with Calyculin A, an increase in stress fibers within the monolayer was observed.

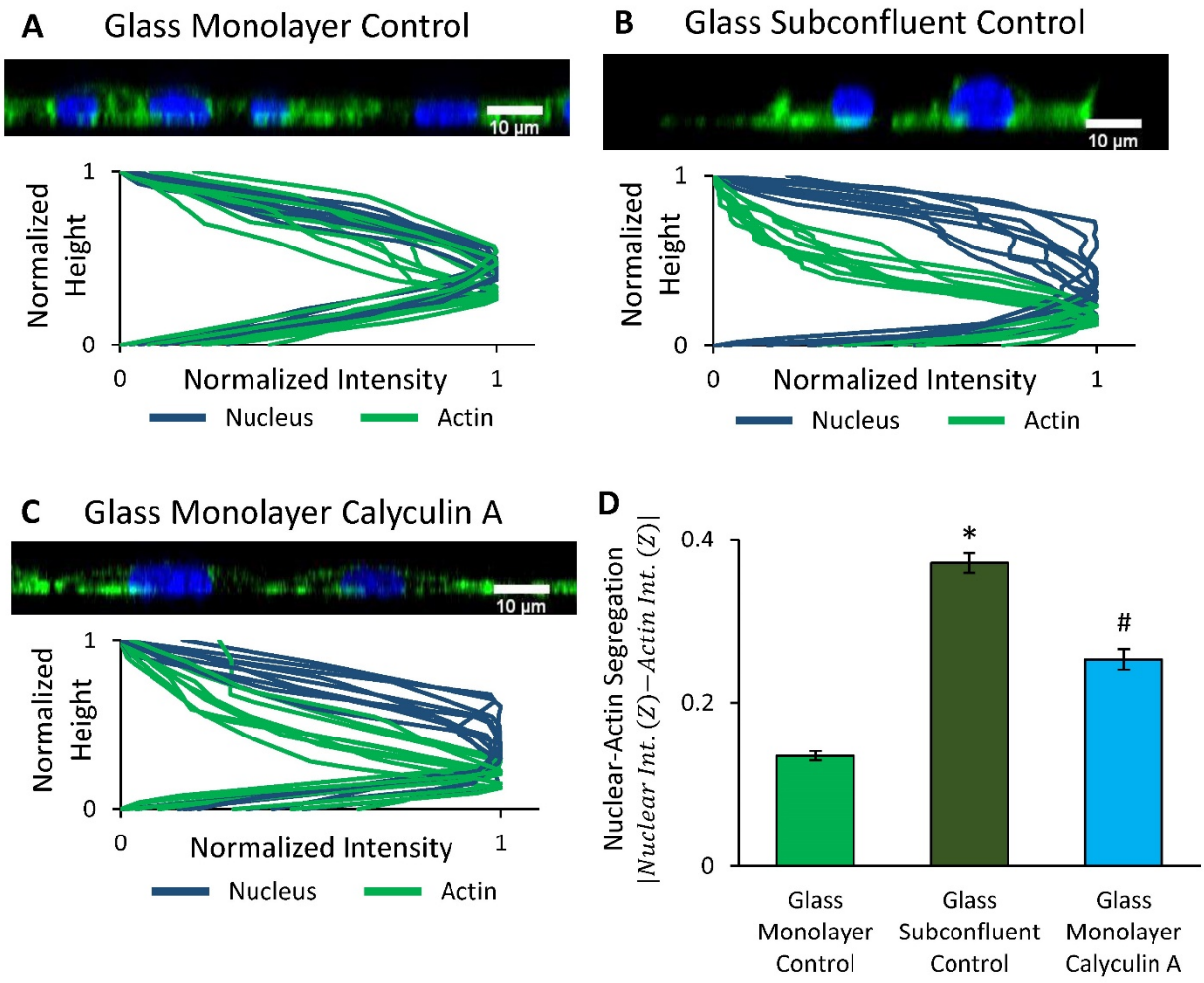

Figure 5.4: Actin distribution for cells on glass substrates

*Representative orthogonal view of the actin (green) and nuclear (blue) channels are shown for (**A**) glass monolayer control, (**B**) glass subconfluent control, and (**C**) glass monolayer Calyculin A treated cells. The intensity distribution plot of each channel along the height of the cell for nine fields of view is also shown. (**D**) A Nuclear-Actin Segregation parameter was calculated for each condition. This parameter is defined as the absolute value of the difference between the nuclear and actin normalized intensities at a given z-position. Thus, if the normalized intensity profiles for the nuclear and actin channels were to overlap perfectly, this parameter would be zero. The larger the separation between the normalized intensity profiles,*

the closer this parameter is to a value of one. The control monolayer appears to have actin distributed throughout the height of the cell, while the subconfluent cells show actin primarily in the basal plane. Upon treatment with Calyculin A the monolayer cells began to approach a subconfluent phenotype. Error bars represent standard error of the mean. A 1-way ANOVA, followed by Tukey's pairwise comparison was used to detect significant differences. Data which do not share a common symbol were found to be significantly different ($p < 0.05$).

Previous work has demonstrated that chromatin is responsive to cellular forces through various mechanisms[28,38,42]. Here, we aimed to elucidate the effect of cell shape (i.e. actin distributions as characterized above) and contractility on chromatin dynamics and suggest that changes in chromatin dynamics due to physical cellular changes are likely routes for mechanotransduction. In order to quantify chromatin dynamics in live cells, cells were transfected with GFP-UBF, which was then tracked over time and quantified as MSD as described in previous publications[38] and in Chapter IV. A nucleus expressing GFP-UBF and associated tracks of GFP-UBF are shown in Figure 5.5 A, B. The chromatin dynamics, based on the ensemble average MSD of GFP-UBF, for each condition on glass are shown in Figure 5.6. The glass monolayer and subconfluent controls are the same data shown previously in Chapter IV, (subconfluent control was termed "isolated" in Chapter IV) which are presented here for comparison with the Calyculin A treated monolayer cells. Additionally, the data were fit to the power law equation $MSD = D_{eff}\tau^{\beta}$, in which τ is the lag-time, D_{eff} is referred to as the effective diffusivity, and β is referred to as the diffusive exponent. We have previously demonstrated that β is affected by active cellular forces, with increased β being indicative of increased active forces within, or propagated to, the nucleus[38] and extended upon this concept in Chapter IV. Monolayers on glass, when treated with Calyculin A, showed a decrease in

chromatin dynamics, compared to the glass monolayer untreated control cells. Since Calyculin A increases cell contractility[43], it was originally hypothesized that Calyculin A treatment would increase chromatin dynamics since cell forces can propagate to the nucleus through the LINC complex[44]. However, the chromatin dynamics observed in the glass monolayer Calyculin A treated cells appear similar to the glass subconfluent control cells. Additionally, both of these groups of cells showed similarities in their actin distribution relative to nuclear height (Figure 5.4 B, C). Thus, we hypothesize that, in both cases, cell contractions are largely by-passing the nucleus even though the Calyculin A treated cells are presumably generating increased basal plane forces.

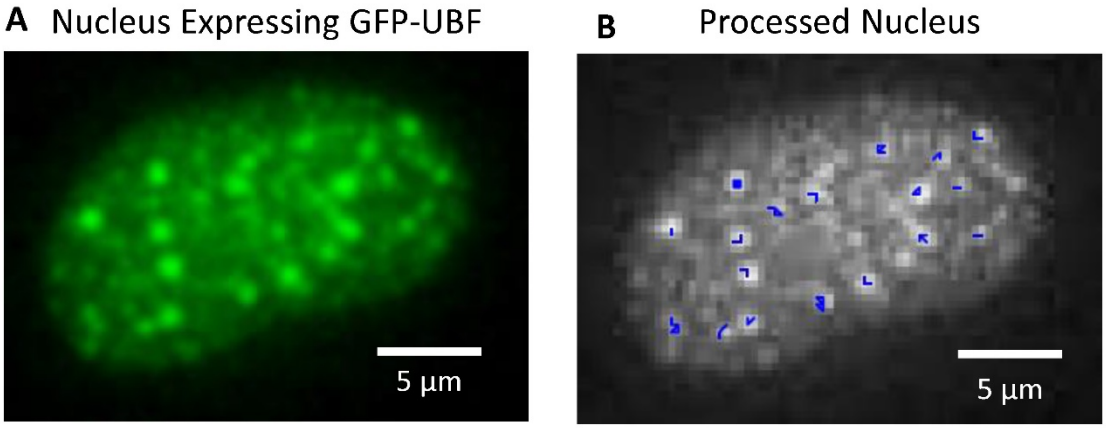

Figure 5.5: Example of image processing for calculation of chromatin dynamics from intranuclear particle tracking

*(**A**) A representative image of a nucleus expressing GFP-UBF (green) is shown. The bright punctate regions of GFP-UBF were tracked over time, at 3-mintue intervals for 1 hour. (**B**) The same nucleus as in (**A**) after it has been processed is shown. The individual tracks of the GFP-UBF punctate regions are shown in blue, overlaid on the original image (greyscale). The nucleus was aligned prior to calculation of the tracks, such that only motion within the nucleus (i.e. chromatin dynamics) was captured, rather than rigid*

body motion of the entire nucleus. Only points which persisted for the entire imaging time were tracked. Additionally, cells were imaged at a time point 1 hour post-tracking (2 hours from the start of imaging), to assure that the cells remained viable and in interphase well after the imaging at 3-minute intervals was completed. Bright field images were also acquired to ensure that monolayer integrity was not disrupted during the imaging process.

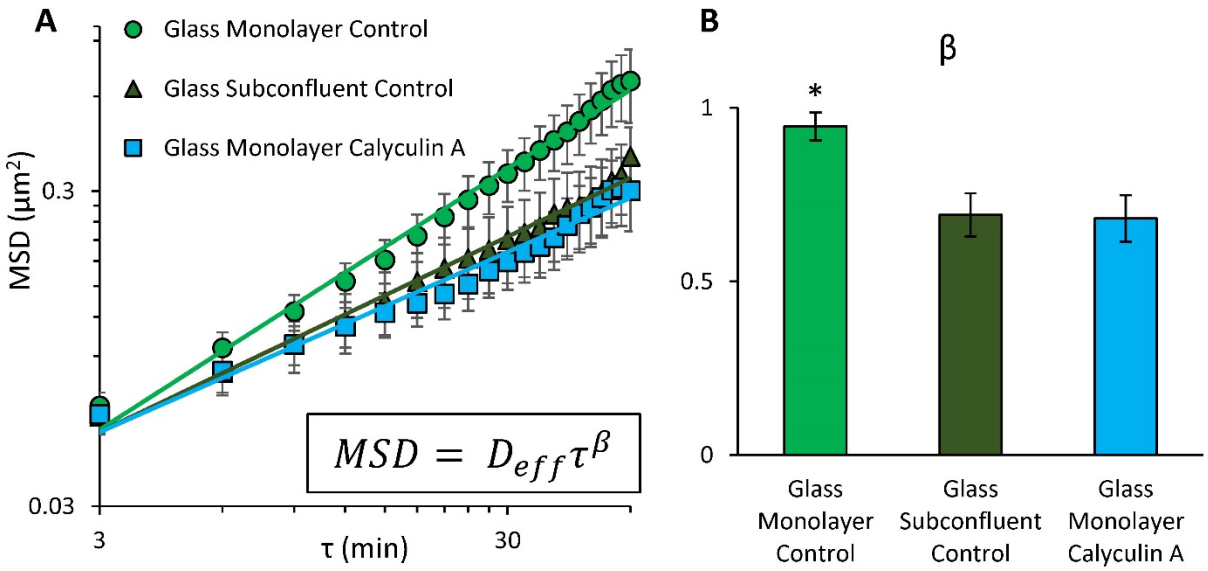

Figure 5.6: Quantification of chromatin dynamics for cells on glass substrates

*(**A**) The ensemble average mean squared displacement (MSD) versus lag-time (τ) plotted on log-log coordinates for each condition on glass substrates is shown. The control monolayer cells displayed increased chromatin dynamics compared to both the subconfluent control, and monolayer Calyculin A treated cells. The MSD data were fit to the form of a power law equation, shown in the inset of (**A**). Error bars represent standard error of the mean. (**B**) The diffusive exponent (β) based on the power law fits for each condition is plotted. We have demonstrated previously in Chapter IV that this parameter is indicative of force propagation to the nucleus. Thus, an increase in β*

*suggests an increase in forces within, or acting on, the nucleus. The monolayer control cells appear to demonstrate increased force propagation to the nucleus, likely due to the changes in actin distribution compared to the other two conditions. Error bars represent the 95% confidence intervals of the power law fit. An * represents a significant difference in* β *(*$p < 0.05$*).*

To test whether the changes in actin distribution and intranuclear motion may coincide with changes in mechanotransduction, we aimed to quantify the localization of the mechanosensitive transcriptional activator YAP in each of the above conditions (Figure 5.7). Representative images of the nuclear and YAP channels for each condition are shown in Figure 5.7 A-C. YAP nuclear to cytoplasmic localization, based on the intensity of the YAP channel, is quantified in Figure 5.7 D. The method of this quantification is shown in Figure 5.2. Our results are consistent with previous reports that YAP localizes to the nucleus in proliferating cells on stiff substrates[45,46] as the glass subconfluent control cells demonstrated the highest level of nuclear to cytoplasmic YAP intensity (Figure 5.7 A, D). Additionally, the glass monolayer control cells had a significant decrease in nuclear to cytoplasmic YAP intensity ratio as expected (Figure 5.7 B, D). Previous reports indicate that apical-basal cell polarity may regulate YAP localization[47]. Additionally, recent work focused on isolated fibroblasts demonstrates the importance of the actin cap in regulating YAP localization, mainly that disruption of the actin cap reduces YAP nuclear localization[48]. Here we demonstrate that monolayer cells treated with Calyculin A with relatively increased basal to apical plane actin distribution and where actomyosin forces appear to partially by-pass the nucleus (as evident from the reduced chromatin dynamics) show increased nuclear YAP localization (Figure 5.7 C, D). This increase was found

to be significantly greater than the untreated monolayer cells, but significantly less than untreated subconfluent cells suggesting that, while cells may be approaching a subconfluent phenotype, aspects of cell-cell contact inhibition are still present. Additionally, while Calyculin A is a phosphatase inhibitor and phosphorylated YAP is excluded from the nucleus[49], Calyculin A may be directly impacting YAP localization. However, if this were the case, Calyculin A treatment would lead to decreased nuclear YAP as compared to the observed increase in nuclear YAP localization. Thus, the cellular mechanosensitivity appears to regulate YAP localization to a greater extent than any potential direct impact of Calyculin A treatment. Consistent with this observation, Das et al. suggests that cytoskeletal integrity (i.e. filamentous actin) is a more potent regulator of YAP localization than direct phosphorylation of YAP in cells without cell-cell contacts[49].

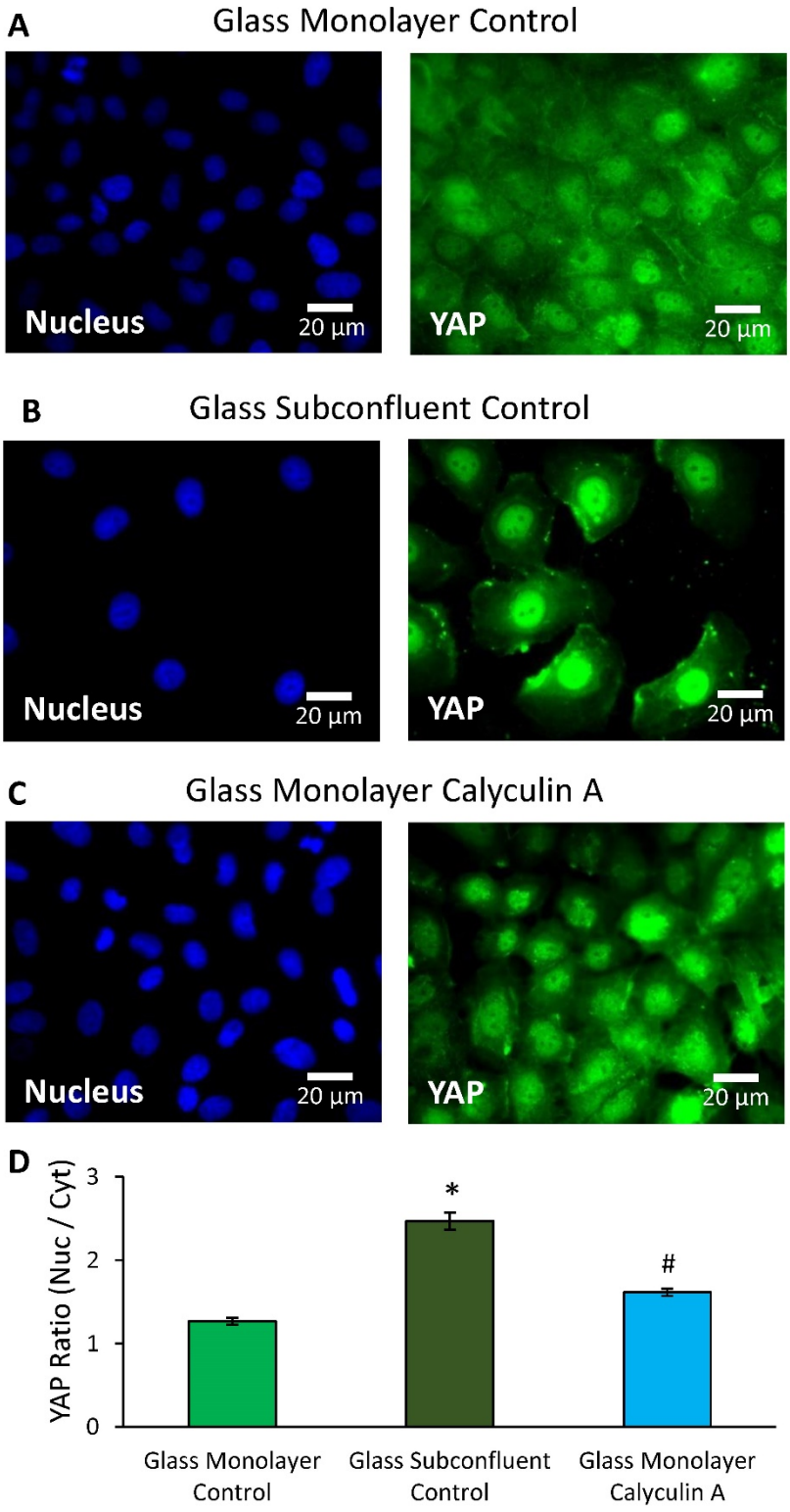

Figure 5.7: YAP nuclear localization for each condition on glass substrates

*(**A**) Representative images of the nuclear (blue) and YAP (green) channels for the glass*

*monolayer control cells are shown. (**B**) Representative images of the nuclear (blue) and YAP (green) channels for the glass subconfluent control cells are shown. (**C**) Representative images of the nuclear (blue) and YAP (green) channels for the glass monolayer Calyculin A treated cells are shown. (**D**) The average ratio of the nuclear to cytoplasmic YAP intensity of 45 cells for each condition is shown. The subconfluent control cells demonstrated the highest YAP nuclear localization, while the Calyculin A treated monolayer condition had an intermediate YAP ratio. Error bars represent standard error of the mean. An ANOVA, followed by Tukey's pairwise comparison was used to detect significant differences. Data which do not share a common symbol were found to be significantly different ($p < 0.05$).*

On soft substrates Calyculin A treatment leads to increased chromatin dynamics with minimal disruption of monolayer integrity

We aimed to characterize how epithelial monolayers respond to changes in contractility when they are grown on soft (2.5 kPa) substrates which are more similar to the *in vivo* elastic modulus of the basement membrane than glass substrates[21–23]. For these experiments, polyacrylamide gels with an elastic modulus of 2.5 kPa, coated in collagen, were generated. Representative confocal images of monolayers on soft gels for control and Calyculin A treated conditions are shown in Figure 5.8. The z-slice in which the most actin stress fibers was seen is shown for each condition. Increased actin stress fibers were observed in Calyculin A treated monolayers, suggesting the cells are increasing their actomyosin contractions as expected. As with the cells grown on glass cover slips, we characterized actin distribution, chromatin dynamics, and YAP localization on soft substrates. On these soft gels, actin appears to be distributed in a similar z-plane as the nucleus, as evident from the orthogonal views and the actin and nuclear intensity plots shown in Figure 5.9. Additionally, no significant difference in the Nuclear-Actin Segregation Parameter was seen (Figure 5.9 C). Next, we quantified chromatin

dynamics to determine if Calyculin A treatment could increase chromatin dynamics through increased cytoskeletal forces being transmitted to the nucleus in these systems. Since actin distribution appears similar in control and treated cells on soft gels, in contrast to the monolayers on glass coverslips, we hypothesized that the increased actomyosin contractions after treatment are transmitted to the nucleus in the soft substrate condition. An increase in chromatin dynamics was observed and, when these data were fit to a power law, the exponent β appeared to increase after Calyculin A treatment (Figure 5.10). Finally, we quantified YAP nuclear localization in control and Calyculin A treated monolayers in order to determine if the increase in forces propagated to the nucleus (as is evident from the increased chromatin dynamics) might increase YAP nuclear localization, as YAP has been shown to be mechanosensitive[45]. As seen in Figure 5.11, no change in nuclear YAP localization was observed. This lack of nuclear YAP localization may be explained by two, non-exclusive, hypotheses. First, the 2.5 kPa substrate stiffness is below the 5 kPa threshold required for YAP localization proposed by Elosegui-Artola[50] and, thus, even with Calyculin A the cells may not be generating significant forces on the nucleus to impact YAP localization. Additionally, in this manuscript, we are investigating a different cell type in monolayers rather than isolated cells and the effects of cell-cell connections may also cause a lack of change in YAP localization.

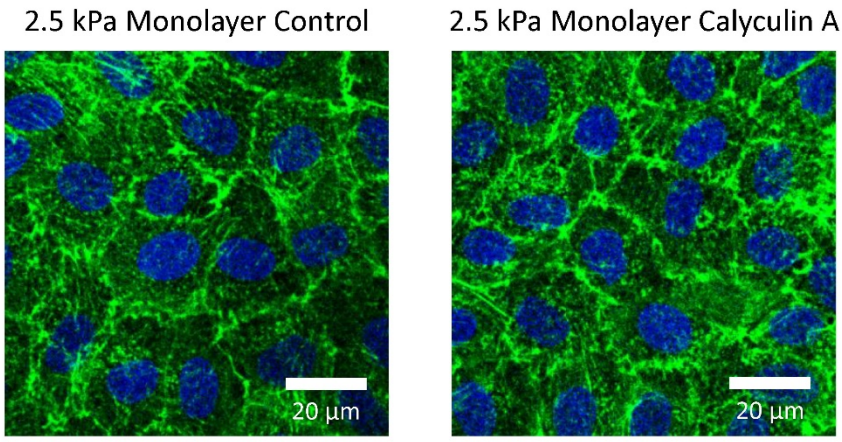

Figure 5.8: Actin stress fibers on 2.5 kPa substrates

Confocal images of actin stress fibers (green) and nuclei (blue) for each condition on 2.5 kPa elastic modulus substrates are shown. The z-slice which contained the most visible stress fibers for each condition is shown. Upon treatment with Calyculin A, a slight increase in stress fibers within the monolayer was noted.

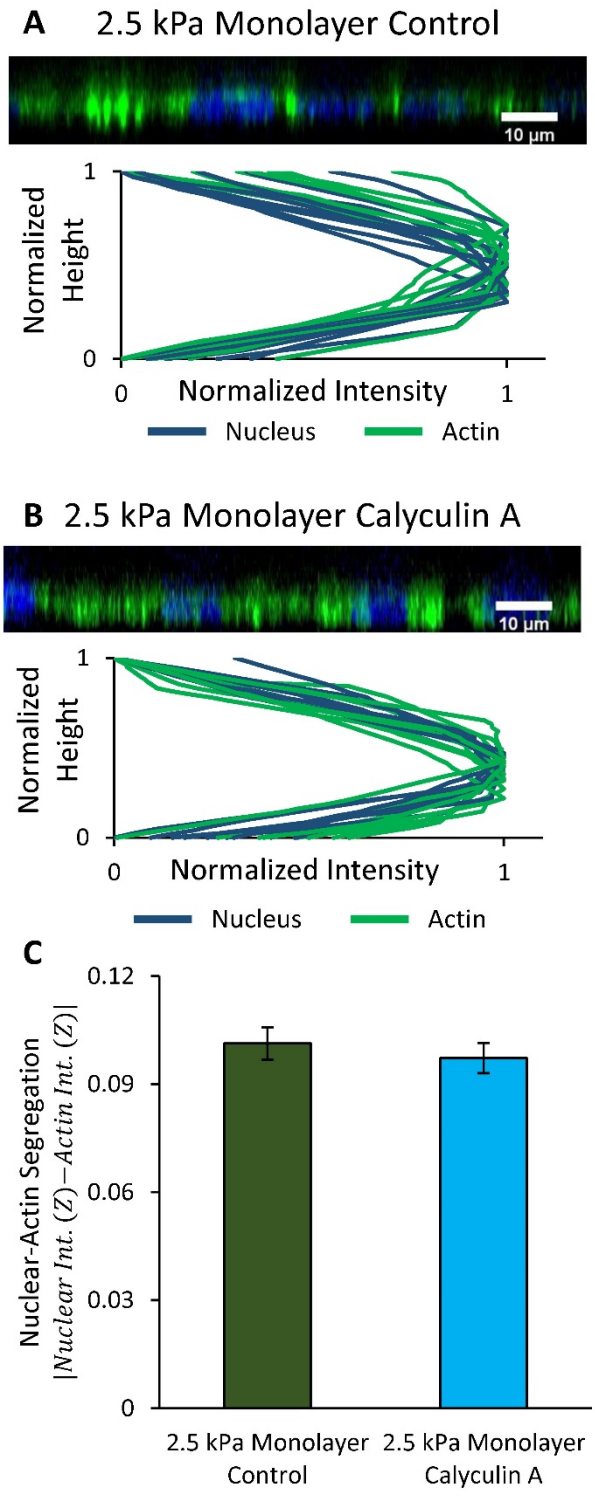

Figure 5.9: Actin distribution for cells on 2.5 kPa substrates

A representative orthogonal view of the actin (green) and nuclear (blue) channels are shown for ***(A)*** *2.5 kPa monolayer control and* ***(B)*** *2.5 kPa monolayer Calyculin A treated cells. The*

*intensity distribution of each channel along the height of the cell for nine fields of view is also shown. (**C**) A Nuclear-Actin Segregation parameter was calculated for each condition. Error bars represent standard error of the mean. Student's t-test was used to detect significant difference. No significant difference between the conditions was detected ($p > 0.05$).*

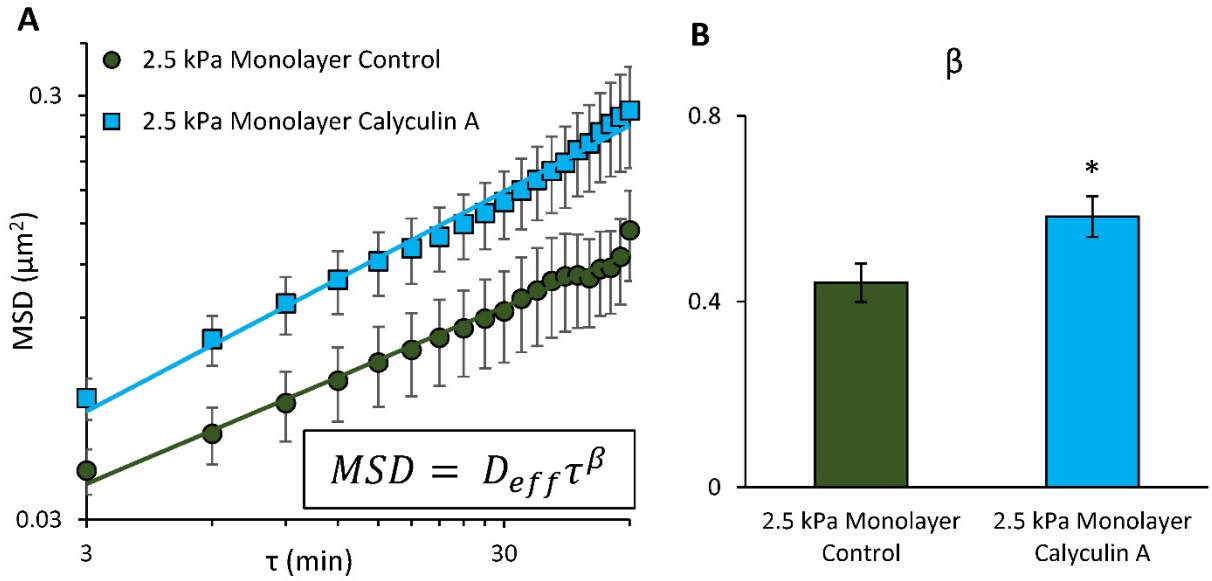

Figure 5.10: Quantification of chromatin dynamics for cells on 2.5 kPa substrates

*(**A**) The ensemble average mean squared displacement (MSD) versus lag-time (τ) plotted on log-log coordinates for each condition on 2.5 kPa substrates is shown. The monolayer cells treated with Calyculin A displayed increased chromatin dynamics compared to the control monolayer cells, in contrast to the changes in chromatin dynamics on glass substrates. The MSD data were fit to the form of a power law equation, shown in the inset of (**A**). Error bars represent standard error of the mean. (**B**) The diffusive exponent (β), based on the power law fits for each condition, is plotted. The monolayer Calyculin A treated cells appear to demonstrate increased force*

*propagation to the nucleus, likely due to the increased contractility from Calyculin A treatment, while actin distribution remains distributed throughout the height of the cell. Error bars represent the 95% confidence intervals of the power law fit. An * represents a significant difference in β ($p < 0.05$).*

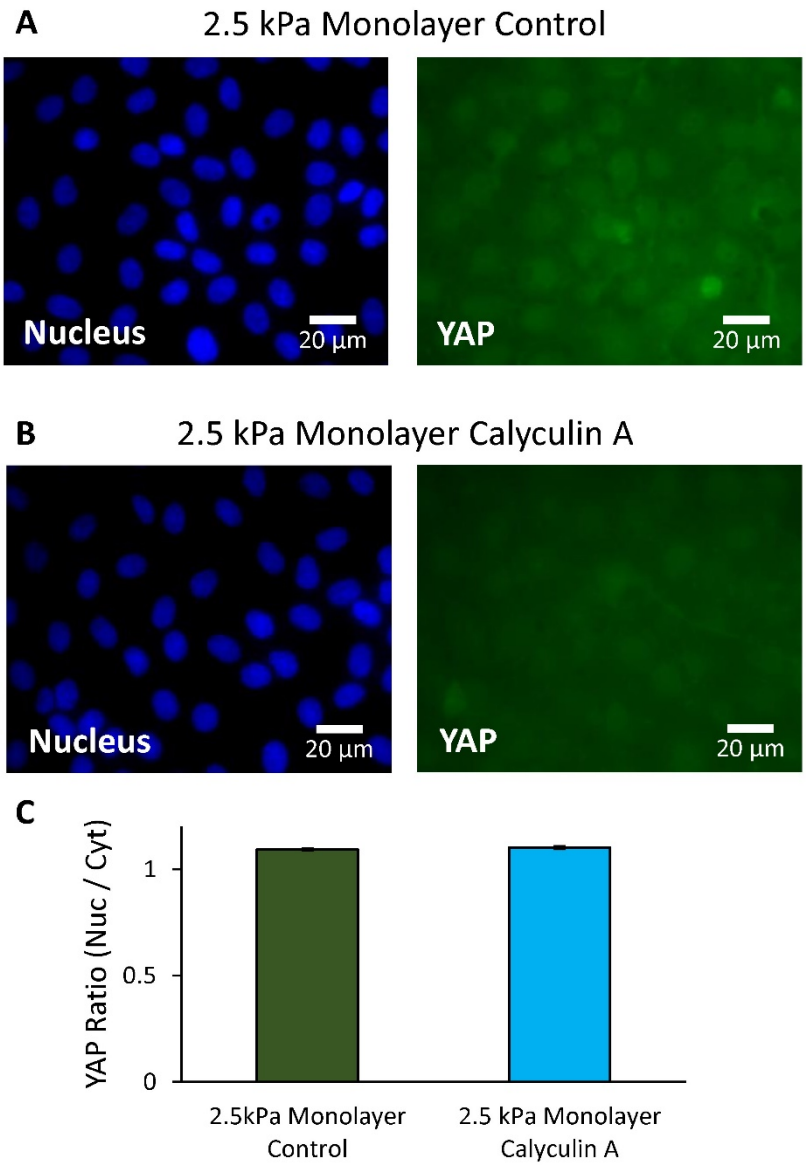

Figure 5.11: YAP nuclear localization for each condition on 2.5 kPa substrates

*(**A**) Representative images of the nuclear (blue) and YAP (green) channels for the 2.5 kPa*

*monolayer control cells are shown. (**B**) Representative images of the nuclear (blue) and YAP (green) channels for the 2.5 kPa monolayer Calyculin A treated cells are shown. (**C**) The average ratio of the nuclear to cytoplasmic YAP intensity of 45 cells for each condition is shown. Error bars represent standard error of the mean. Student's t-test was used to detect significant difference. No significant difference between the conditions was detected ($p > 0.05$).*

On substrates of intermediate stiffness, monolayers demonstrate intermediate behavior following Calyculin A treatment

In order to better understand the differences in the previous data for cells on glass (uncoated) and soft gels (collagen coated), we performed the same experiments on monolayers on stiffer (30 kPa) gels coated in collagen which is between the stiffness of the glass and 2.5 kPa gels. Representative confocal images of monolayers stained for actin (green) and DNA (blue) on 30 kPa gels are shown in Figure 5.12. The z-slice that contained the most visible actin stress fibers for each condition is shown. Increased actin stress fibers were observed in Calyculin A treated monolayers, suggesting the cells are increasing their actomyosin contractions as expected. The actin height distribution images and normalized plots for multiple fields of view are shown in Figure 5.13. The control cells appeared to have increased apical actin (actin cap) perhaps due to the combination of collagen coating on stiff gel, as substrate coatings can influence actin stress fibers[51]. In the Calyculin A treated monolayers, the actin and nuclear intensities were largely co-planar. These differences in actin distribution were subtle, yet the Nuclear-Actin Segregation Parameter was slightly increased for the control cells (Figure 5.13 C); however, unlike in the glass cells, this difference appears to be from increased apical actin rather than increased basal plane actin. Additionally, the actin appears to decrease in z-height, from above the nucleus to in plane with the nucleus, after Calyculin A treatment which is similar to the trend on glass but to a lesser extent.

When investigating the chromatin dynamics on stiff gels, we noticed a slight decrease in the parameter β after treatment (similar to the response on glass); however, the values of MSD between the control and treated cells were not statistically significant ($p > 0.05$) at the majority of lag times (Figure 5.14). Thus, while the interpretation of changes in β is more difficult than in the previously presented conditions, the dynamics appear to trend in a similar fashion to the glass substrate data but with a less dramatic change. Finally, the YAP nuclear localization for Calyculin A treated and control monolayers on 30 kPa substrates was calculated, and no significant difference between the conditions was detected (Figure 5.15). Taken together, these data suggest that, while Calyculin A treatment on 30 kPa substrates may induce slight changes in force propagation to the nucleus, these changes to not appear significant enough to change the YAP localization, as seen on glass substrates.

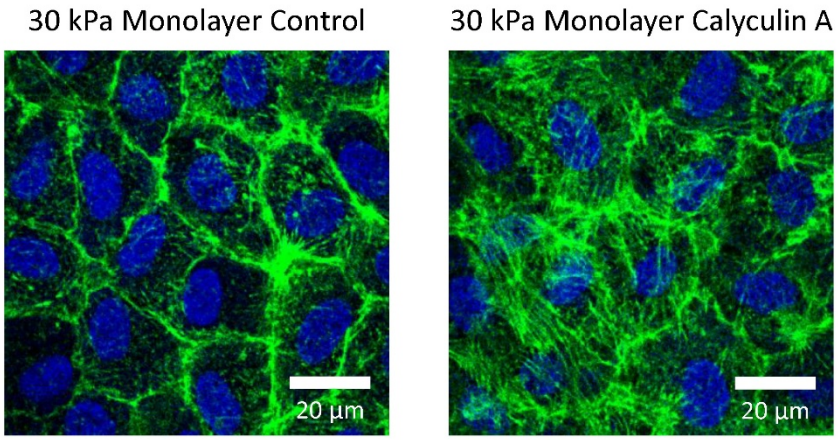

Figure 5.12: Actin stress fibers on 30 kPa substrates

Confocal images of actin stress fibers (green) and nuclei (blue) for each condition on 30 kPa elastic modulus substrates are shown. The z-slice which contained the most visible stress fibers for each condition is shown. Upon treatment with Calyculin A, an increase in stress fibers within the monolayer was noted.

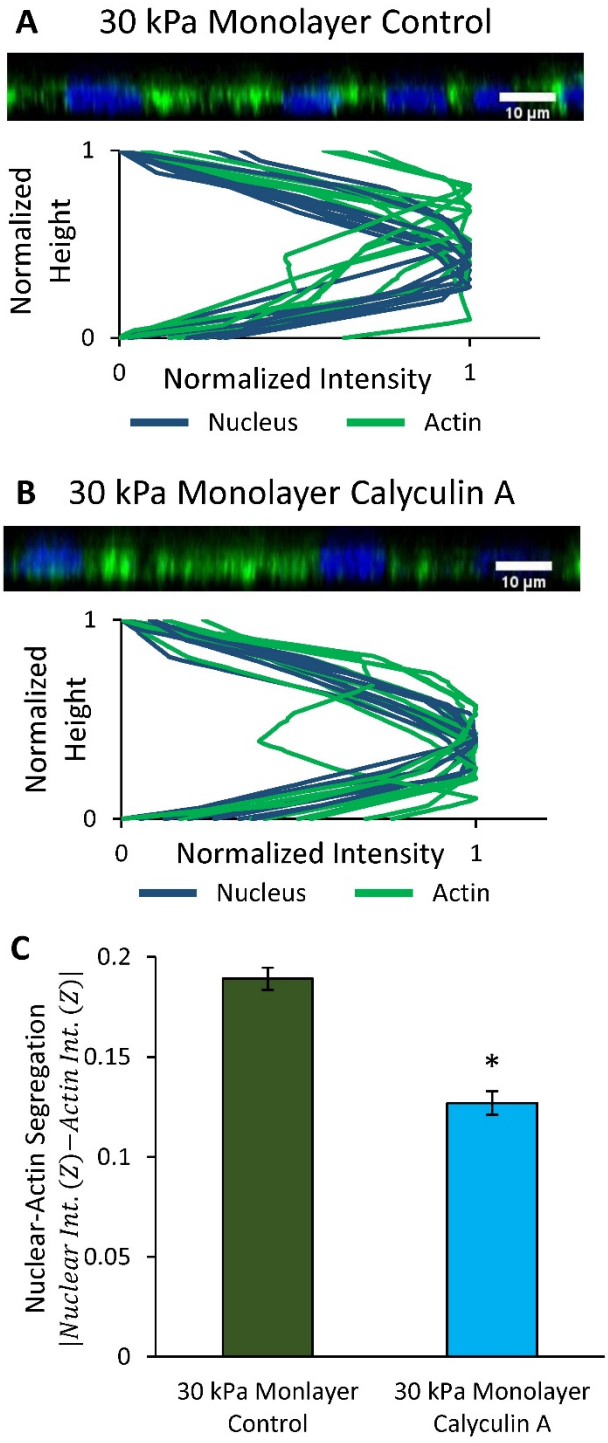

Figure 5.13: Actin distribution for cells on 30 kPa substrates

A representative orthogonal view of the actin (green) and nuclear (blue) channels are shown for ***(A)*** *30 kPa monolayer control and* ***(B)*** *30 kPa monolayer Calyculin A treated cells. The intensity*

*distribution of each channel along the height of the cell for nine fields of view is also shown. (**C**) A Nuclear-Actin Segregation parameter was calculated for each condition. An increase in actin cap compared to the monolayers on 2.5 kPa substrates was observed and is particularly evident in the actin distribution plot for the 30 kPa control monolayer cells. A decrease in the z-height of the peak intensity in the actin channel was observed after treatment with Calyculin A (similar to the monolayers on glass), however this decrease does not appear as segregated from the nuclear intensity as in the cells on glass. These data suggest that the cells are beginning to approach a subconfluent phenotype, but not to the extent of the cells on glass. Error bars represent standard error of the mean. Student's t-test was used to detect a significant difference. An * denotes detection of a significant difference ($p < 0.05$).*

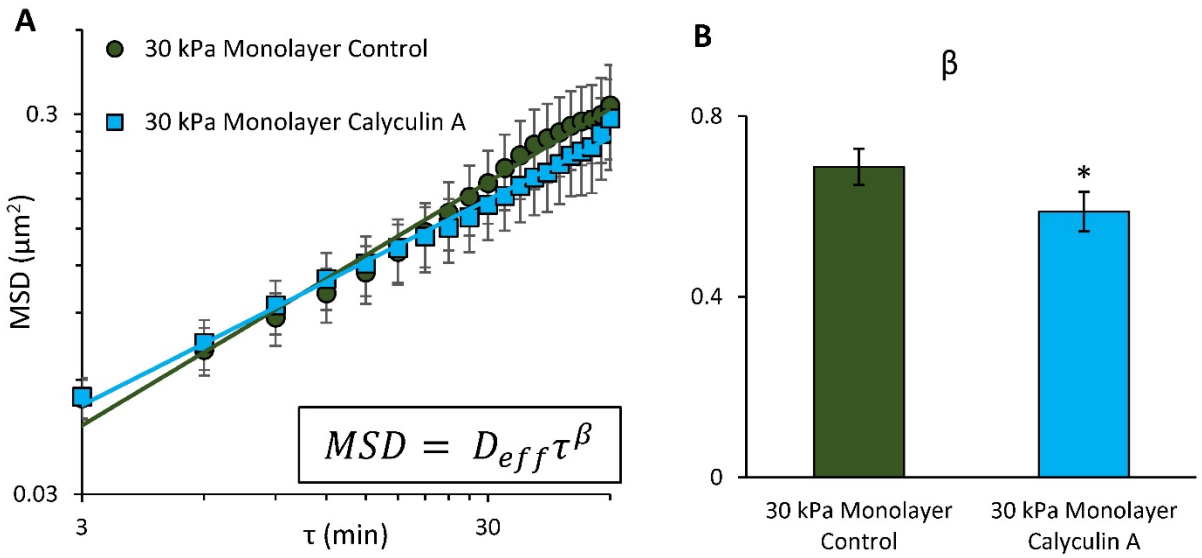

Figure 5.14: Quantification of chromatin dynamics for cells on 30 kPa substrates

*(**A**) The ensemble average mean squared displacement (MSD) versus lag-time (τ) plotted on log-log coordinates for each condition on 30 kPa substrates is shown. The monolayer cells treated with Calyculin A displayed a similar magnitude of MSD of intranuclear motion. The MSD data*

*were fit to the form of a power law equation, shown in the inset of (**A**). Error bars represent standard error of the mean. (**B**) The diffusive exponent (β) based on the power law fits for each condition is plotted. The monolayer Calyculin A treated cells appear to demonstrate a slight decrease in force propagation to the nucleus, however, the similarity in MSD makes this difference difficult to interpret. Both the actin cap, and co-planar actin are likely physically connected to the nucleus, thus both represent mechanisms for force propagation. These data suggest that the cells are beginning to approach a subconfluent phenotype, but not to the extent of cells on glass. Error bars represent the 95% confidence intervals of the power law fit. An * denotes a significant difference in β ($p < 0.05$).*

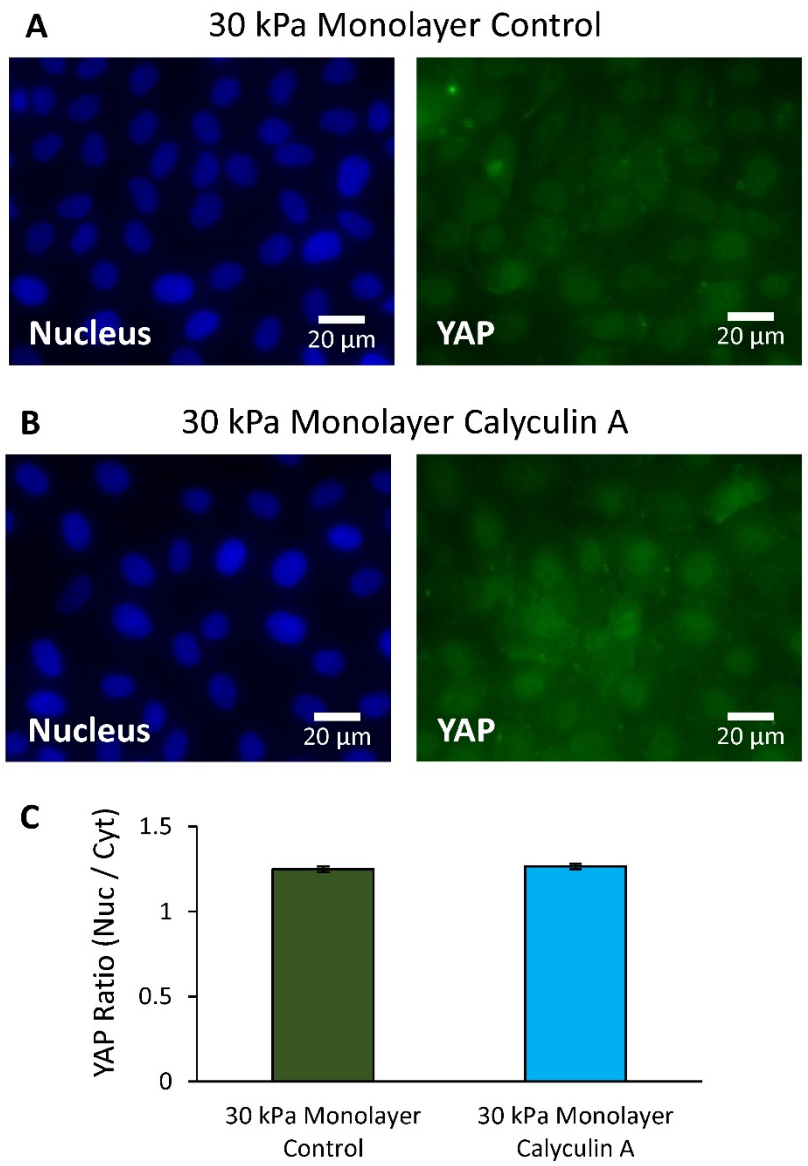

Figure 5.15: YAP nuclear localization for each condition on 30 kPa substrates

*(**A**) Representative images of the nuclear (blue) and YAP (green) channels for the 30 kPa monolayer control cells are shown. (**B**) Representative images of the nuclear (blue) and YAP (green) channels for the 30 kPa monolayer Calyculin A treated cells is shown. (**C**) The average ratio of the nuclear to cytoplasmic YAP intensity of 45 cells for each condition is shown. Error bars represent standard error of the mean. Student's t-test was used to detect a significant difference. No significant difference between the conditions was detected ($p > 0.05$). These data*

suggest that, while monolayers treated with Calyculin A on 30 kPa may be approaching a subconfluent phenotype, the differences are not significant enough to impact YAP localization, and cell-cell contacts are likely largely intact.

Discussion

In this work we have begun to demonstrate the complex, substrate-dependent, cellular response to increased contractility in epithelial monolayers. During tissue fibrosis, extracellular matrix proteins are often deposited at levels greater than in physiologically healthy tissue or rearranged, which increases tissue stiffness[21,52]. We demonstrate that epithelial monolayers are responsive to their substrate and, moreover, may respond to biochemical signals in a substrate-dependent manner. It has been hypothesized that this feedback loop between cells sensing their extracellular environment and further misregulating their behavior has implications in a range of diseases such as cardiovascular disease, cancer, and fibrotic scar formation[9,21,53–57]. In the case of epithelial cells, the extracellular matrix in conjunction with biochemical signaling molecules are key regulators of epithelial to mesenchymal transition (EMT)[54], which we begin to probe by characterizing actin distribution, chromatin dynamics, and YAP localization. Specifically, on glass substrates, the monolayer cells began to demonstrate a mesenchymal-like phenotype, along with increased YAP localization after Calyculin A treatment. This was in contrast to monolayers on soft gels, which showed little change in phenotype, but did demonstrate increased chromatin dynamics, likely due to increased actomyosin contractions reacting the nucleus. On intermediate stiffness (30 kPa) gels, we noted less dramatic changes in cell phenotype compared to monolayers on glass. Previous studies have demonstrated, using magnetic twisting cytometry, that endothelial cells respond differently to applied forces depending on the substrate stiffness[58]. Consistent with the data presented here, in which β has a more dramatic change on soft

substrates compared to stiff after treatment with Calyculin A, Andressen Eguiluz et al. demonstrate that on soft hydrogels, cell monolayers increase their stiffness to a greater extent than on stiff hydrogels after application of external forces transmitted through VE-cadherin[58].

In each of the cases presented here, a significant change in nuclear height after treatment with Calyculin A was not detected (Figure 5.16). Only in the subconfluent case was a significant increase in nuclear height detected, compared to the monolayer cells, as expected. It is important to note not only the differences in elastic moduli of the substrates, but also the surface coating. As the glass surfaces were not coated in collagen, the combination of a stiffer, potentially less adherent substrate may be a critical factor in the mechanosensing behavior of the monolayers, as our data suggest cells need to generate enough force and have reduced cell-cell connections for changes in YAP localization. While glass can be coated in collagen, it is difficult to interpret the results of glass coated with collagen versus polyacrylamide coated in collagen due to differences in surface chemistry between glass and polyacrylamide and thus changes in the available binding regions of the protein and adhesion of the protein to the surface.

We suggest that cells need to sufficiently disrupt cell-cell junctions and/or alter their actin distribution in order to cause changes in YAP localization. Consistent with this analysis, NRK52E cells appear to require both reduced cadherin junctions and cytokine treatment in order to express late stage markers of EMT[35]. Additionally, the actin cytoskeletal integrity appears necessary for nuclear YAP localization[59]. Likely, mechanosensitivity has multiple effectors such as actin distribution, cell-cell and cell-substrate interactions, substrate stiffness, apical and basal connectivity and contractility, and force propagation to the nucleus. A summary of the factors investigated in this study is presented in Figure 5.17. The presence of multiple pathways of EMT regulation may represent the necessary redundancy to properly control type 1 EMT (necessary

for organogenesis); however, when the chemical and physical environment favor type 2 or 3 EMT (which lead to tissue repair, or fibrosis and metastasis when misregulated[60]), a positive feedback loop type response likely leads to disease progression.

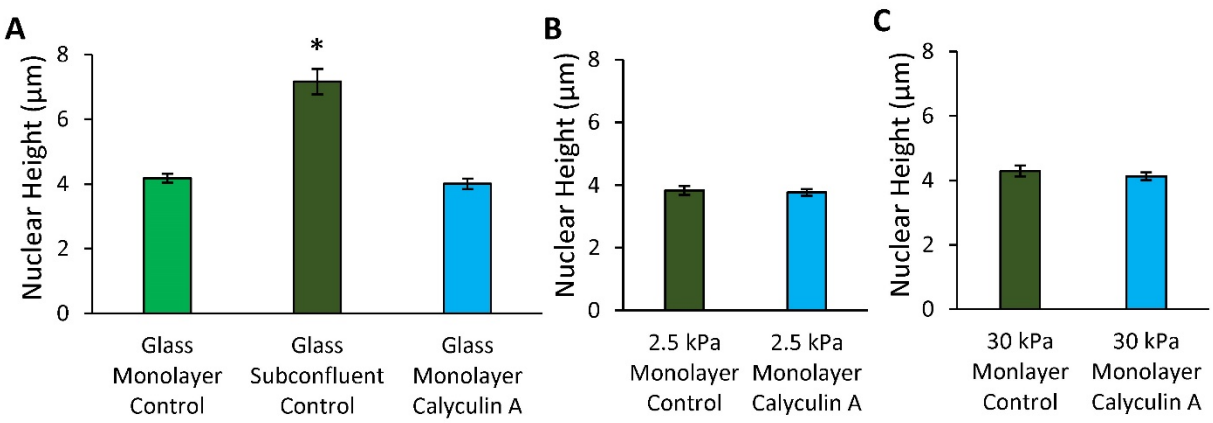

Figure 5.16: Comparison of nuclear height between all conditions

*Nuclear height for each condition was measured. Calyculin A treatment did not affect nuclear height. For all conditions, error bars represent standard error of the mean. The number of cells analyzed for each condition, going left to right was as follows N = 27, 11, 25, 31, 26, 34, 29. (**A**) On glass substrates, nuclear height was significantly increased ($p < 0.05$) compared to control cells. After Calyculin A treatment, no significant difference in nuclear height in monolayer cells was detected ($p < 0.05$). A 1-way ANOVA followed by Tukey's pairwise comparison was performed. (**B**) No significant difference in nuclear height was detected for monolayer cells on 2.5 kPa substrates following treatment with Calyculin A ($p > 0.05$). Student's T-test was performed. (**C**) No significant difference in nuclear height was detected for monolayer cells on 30 kPa substrates following treatment with Calyculin A ($p > 0.05$). Student's T-test was performed.*

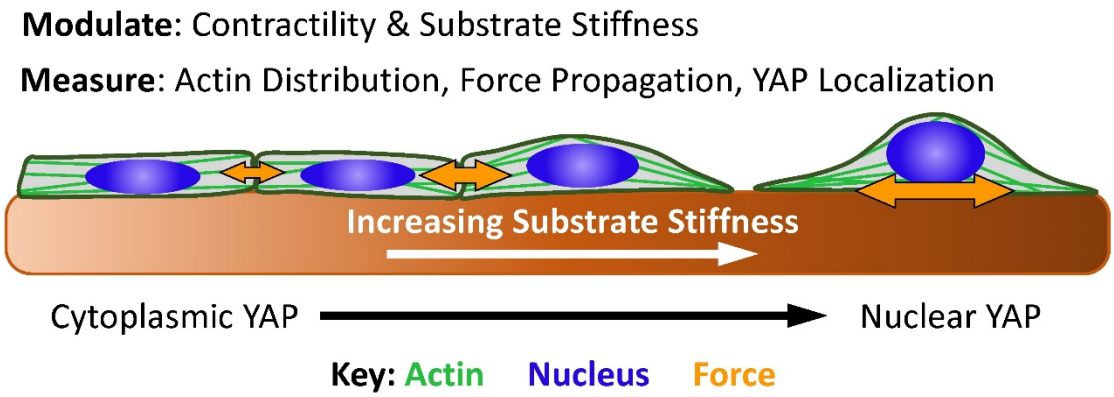

Figure 5.17: Factors influencing mechanosensitive response to cell contractility

In this work, we highlight various factors that impact the cellular response to contractions induced by Calyculin A treatment. We find that substrate stiffness (and likely surface coating) impact the cellular response, which may have implications in EMT, as cells on stiffer substrates may be primed for EMT. It appears that cell-cell contacts and actin distribution are also important factors for determining YAP nuclear localization.

In conclusion, this work has demonstrated that epithelial monolayers respond to increases in cell contractility in a substrate dependent manner. If enough force is generated to rupture cell-cell junctions, cells may begin to take on an isolated phenotype. We utilize three metrics (chromatin dynamics, actin distribution, and YAP localization) to quantify cell response to Calyculin A treatment. All three metrics are likely critical in mechanotransduction for regulating the extent that forces propagate to the nucleus and chromatin fibers, as well as the nuclear localization of YAP which can regulate transcription and proliferation. A similar analysis for cells on glass, treated with TGF-β is presented in Appendix B. On glass, cells approached a subconfluent phenotype by all three metrics. On soft gels, monolayer integrity was upheld, and YAP did not localize to the nucleus; however, chromatin dynamics increased likely due to increased force propagation to the nucleus. On stiff gels, chromatin dynamics were not as

severely impacted as on glass but may be approaching the subconfluent phenotype. Actin distribution and YAP localization were also minimally impacted, suggesting that on this substrate cell-cell junctions were largely intact after Calyculin A treatment. Collectively these data show the interplay between mechanosensing of the extracellular environment and the cellular response to chemical signals with implications in diseases such as fibrosis and cardiovascular disease.

Acknowledgements

We would like acknowledge G. Yang (Carnegie Mellon University) for providing the particle tracking software as well as A. W. Feinberg (Carnegie Mellon University), and R. Palchesko (Carnegie Mellon University) for the use of and training on the confocal microscope. This work was funded by NSF-CMMI-1634888 to K.N.D. and NIH-EB003392 to T.J.A.

References

1. Szczesny, S. E. & Mauck, R. L. The Nuclear Option: Evidence Implicating the Cell Nucleus in Mechanotransduction. *J. Biomech. Eng.* **139,** (2017).

2. Gilbert, P. M. *et al.* Substrate elasticity regulates skeletal muscle stem cell self-renewal in culture. *Science* **329,** 1078–81 (2010).

3. Gattazzo, F., Urciuolo, A. & Bonaldo, P. Extracellular matrix: A dynamic microenvironment for stem cell niche. *Biochim. Biophys. Acta - Gen. Subj.* **1840,** 2506–2519 (2014).

4. Yim, E. K. F. & Sheetz, M. P. Force-dependent cell signaling in stem cell differentiation. *Stem Cell Res. Ther.* **3,** 41 (2012).

5. Vining, K. H. & Mooney, D. J. Mechanical forces direct stem cell behaviour in development and regeneration. *Nat. Rev. Mol. Cell Biol.* **18,** 728–742 (2017).

6. Crowder, S. W., Leonardo, V., Whittaker, T., Papathanasiou, P. & Stevens, M. M.

Material Cues as Potent Regulators of Epigenetics and Stem Cell Function. *Cell Stem Cell* **18,** 39–52 (2016).

7. Engler, A. J., Sen, S., Sweeney, H. L. & Discher, D. E. Matrix elasticity directs stem cell lineage specification. *Cell* **126,** 677–89 (2006).

8. Choi, Y. S., Vincent, L. G., Lee, A. R., Dobke, M. K. & Engler, A. J. Mechanical derivation of functional myotubes from adipose-derived stem cells. *Biomaterials* **33,** 2482–2491 (2012).

9. Suresh, S. Biomechanics and biophysics of cancer cells. *Acta Biomater* **3,** 413–438 (2007).

10. Chin, L., Xia, Y., Discher, D. E. & Janmey, P. A. Mechanotransduction in cancer. *Curr. Opin. Chem. Eng.* **11,** 77–84 (2016).

11. Broders-Bondon, F., Nguyen Ho-Bouldoires, T. H., Fernandez-Sanchez, M.-E. & Farge, E. Mechanotransduction in tumor progression: The dark side of the force. *J. Cell Biol.* jcb.201701039 (2018). doi:10.1083/jcb.201701039

12. Wei, S. C. *et al.* Matrix stiffness drives epithelial–mesenchymal transition and tumour metastasis through a TWIST1–G3BP2 mechanotransduction pathway. *Nat. Cell Biol.* **17,** 678–688 (2015).

13. Baker, E. L., Lu, J., Yu, D., Bonnecaze, R. T. & Zaman, M. H. Cancer Cell Stiffness: Integrated Roles of Three-Dimensional Matrix Stiffness and Transforming Potential. *Biophys. J.* **99,** 2048–2057 (2010).

14. Discher, D. E., Janmey, P. & Wang, Y.-L. Tissue cells feel and respond to the stiffness of their substrate. *Science* **310,** 1139–43 (2005).

15. Engler, A. J. *et al.* Elasticity : Scar-Like Rigidity Inhibits Beating. *Cell* **121,** 3794–3802 (2009).

16. Califano, J. & Reinhart-King, C. Substrate Stiffness and Cell Area Predict Cellular Traction Stresses in Single Cells and Cells in Contact. *Cell Mol Bioeng* **3,** 68–75 (2011).

17. Huynh, J. *et al.* Age-Related Intimal Stiffening Enhances Endothelial Permeability and

Leukocyte Transmigration. *Sci Transl Med* **3,** (2011).

18. Buxboim, A. *et al.* Coordinated increase of nuclear tension and lamin-A with matrix stiffness outcompetes lamin-B receptor that favors soft tissue phenotypes. *Mol. Biol. Cell* **28,** 3333–3348 (2017).

19. Yeung, T. *et al.* Effects of substrate stiffness on cell morphology, cytoskeletal structure, and adhesion. *Cell Motil. Cytoskeleton* **60,** 24–34 (2005).

20. Ng, M. R., Besser, A., Danuser, G. & Brugge, J. S. Substrate stiffness regulates cadherin-dependent collective migration through myosin-II contractility. *J. Cell Biol.* **199,** 545–563 (2012).

21. Wells, R. G. Tissue mechanics and fibrosis. *Biochim. Biophys. Acta - Mol. Basis Dis.* **1832,** 884–890 (2013).

22. Samir, A. E. *et al.* Shear wave elastography in chronic kidney disease: a pilot experience in native kidneys. *BMC Nephrol.* **16,** 119 (2015).

23. Bensamoun, S. F., Robert, L., Leclerc, G. E., Debernard, L. & Charleux, F. Stiffness imaging of the kidney and adjacent abdominal tissues measured simultaneously using magnetic resonance elastography. (2011). doi:10.1016/j.clinimag.2010.07.009

24. Chang, W., Worman, H. J. & Gundersen, G. G. Accessorizing and anchoring the LINC complex for multifunctionality. *J. Cell Biol.* **208,** 11–22 (2015).

25. Thorpe, S. D. & Lee, D. A. Dynamic regulation of nuclear architecture and mechanics—a rheostatic role for the nucleus in tailoring cellular mechanosensitivity. *Nucleus* **8,** 287–300 (2017).

26. Maniotis, A. J., Chen, C. S. & Ingber, D. E. Demonstration of mechanical connections between integrins, cytoskeletal filaments, and nucleoplasm that stabilize nuclear structure. *Cell Biol.* **94,** 849–854 (1997).

27. Kim, D.-H., Chambliss, A. B. & Wirtz, D. The multi-faceted role of the actin cap in cellular mechanosensation and mechanotransduction. *Soft Matter* **9,** 5516–5523 (2013).

28. Tajik, A. *et al.* Transcription upregulation via force-induced direct stretching of

chromatin. *Nat. Mater.* **15,** 1–20 (2016).

29. Ling, H.-H., Kuo, C.-C., Lin, B.-X., Huang, Y.-H. & Lin, C.-W. Elevation of YAP promotes the epithelial-mesenchymal transition and tumor aggressiveness in colorectal cancer. *Exp. Cell Res.* **350,** 218–225 (2017).

30. Diepenbruck, M. *et al.* Tead2 expression levels control the subcellular distribution of Yap and Taz, zyxin expression and epithelial-mesenchymal transition. *J. Cell Sci.* **127,** 1523–1536 (2014).

31. Yuan, Y. *et al.* YAP overexpression promotes the epithelial-mesenchymal transition and chemoresistance in pancreatic cancer cells. *Mol. Med. Rep.* **13,** 237–242 (2016).

32. Yu, F.-X., Zhao, B. & Guan, K.-L. Hippo Pathway in Organ Size Control, Tissue Homeostasis, and Cancer. *Cell* **163,** 811–28 (2015).

33. Steinhardt, A. A. *et al.* Expression of Yes-associated protein in common solid tumors. *Hum. Pathol.* **39,** 1582–1589 (2008).

34. Zender, L. *et al.* Identification and Validation of Oncogenes in Liver Cancer Using an Integrative Oncogenomic Approach. *Cell* **125,** 1253–1267 (2006).

35. Zheng, G. *et al.* Disruption of E-Cadherin by Matrix Metalloproteinase Directly Mediates Epithelial-Mesenchymal Transition Downstream of Transforming Growth Factor-β1 in Renal Tubular Epithelial Cells. *Am. J. Pathol.* **175,** 580–591 (2009).

36. Masszi, A. *et al.* Integrity of Cell-Cell Contacts Is a Critical Regulator of TGF-β1-Induced Epithelial-to-Myofibroblast Transition: Role for β-Catenin. *Am. J. Pathol.* **165,** 1955–1967 (2004).

37. Yang, G., Cameron, L. a, Maddox, P. S., Salmon, E. D. & Danuser, G. Regional variation of microtubule flux reveals microtubule organization in the metaphase meiotic spindle. *J. Cell Biol.* **182,** 631–9 (2008).

38. Spagnol, S. T., Dahl, K. N. & Noel Dahl, K. Active cytoskeletal force and chromatin condensation independently modulate intranuclear network fluctuations. *Integr. Biol.* **6,** 523–31 (2014).

39. Kraning-Rush, C. M., Carey, S. P., Califano, J. P. & Reinhart-King, C. A. Quantifying Traction Stresses in Adherent Cells. in *Methods in Cell Biology* (eds. Asthagiri, A. R. & Arkin, A. P.) **110,** 139–178 (Elsevier Inc., 2012).

40. Lampi, M. C. *et al.* Simvastatin ameliorates matrix stiffness-mediated endothelial monolayer disruption. *PLoS One* **11,** 1–20 (2016).

41. Neelam, S., Hayes, P. R., Zhang, Q., Dickinson, R. B. & Lele, T. P. Vertical uniformity of cells and nuclei in epithelial monolayers. *Sci. Rep.* **6,** 19689 (2016).

42. Booth-Gauthier, E. a, Alcoser, T. a, Yang, G. & Dahl, K. N. Force-induced changes in subnuclear movement and rheology. *Biophys. J.* **103,** 2423–31 (2012).

43. Liu, Z. *et al.* Mechanical tugging force regulates the size of cell-cell junctions. *Proc. Natl. Acad. Sci. U. S. A.* **107,** 9944–9949 (2010).

44. Arsenovic, P. T. T. *et al.* Nesprin-2G, a Component of the Nuclear LINC Complex, Is Subject to Myosin-Dependent Tension. *Biophys. J.* **110,** 34–43 (2016).

45. Elosegui-Artola, A. *et al.* Force Triggers YAP Nuclear Entry by Regulating Transport across Nuclear Pores Molecular regulation of transport Force Triggers YAP Nuclear Entry by Regulating Transport across Nuclear Pores. *Cell* **171,** 1397–1410 (2017).

46. Heidary Arash, E., Song, K. M., Song, S., Shiban, A. & Attisano, L. Arhgef7 promotes activation of the Hippo pathway core kinase Lats. *EMBO J.* **33,** 2997–3011 (2014).

47. Hirate, Y. *et al.* Polarity-dependent distribution of angiomotin localizes Hippo signaling in preimplantation embryos. *Curr. Biol.* **23,** 1181–94 (2013).

48. Shiu, J.-Y., Aires, L., Lin, Z. & Vogel, V. Nanopillar force measurements reveal actin-cap-mediated YAP mechanotransduction. *Nat. Cell Biol.* **20,** 262–271 (2018).

49. Das, A., Fischer, R. S., Pan, D. & Waterman, C. M. YAP Nuclear Localization in the Absence of Cell-Cell Contact Is Mediated by a Filamentous Actin-dependent, Myosin II- and Phospho-YAP-independent Pathway during Extracellular Matrix Mechanosensing. *J. Biol. Chem.* **291,** 6096–6110 (2016).

50. Elosegui-Artola, A. *et al.* Mechanical regulation of a molecular clutch defines force

transmission and transduction in response to matrix rigidity. *Nat. Cell Biol.* **18,** 540–548 (2016).

51. Chiou, Y.-W., Lin, H.-K., Tang, M.-J., Lin, H.-H. & Yeh, M.-L. The Influence of Physical and Physiological Cues on Atomic Force Microscopy-Based Cell Stiffness Assessment. *PLoS One* **8,** e77384 (2013).

52. Wynn, T. A. Cellular and molecular mechanisms of fibrosis. *J. Pathol.* **214,** 199–210 (2008).

53. Jaalouk, D. E. & Lammerding, J. Mechanotransduction gone awry. *Nat. Rev. Mol. Cell Biol.* **10,** 63–73 (2009).

54. O'Connor, J. W. & Gomez, E. W. Biomechanics of TGFβ-induced epithelial-mesenchymal transition: implications for fibrosis and cancer. *Clin. Transl. Med.* **3,** 23 (2014).

55. Liu, F. *et al.* Feedback amplification of fibrosis through matrix stiffening and COX-2 suppression. *J. Cell Biol.* **190,** 693–706 (2010).

56. Liu, F. *et al.* Mechanosignaling through YAP and TAZ drives fibroblast activation and fibrosis. *Am. J. Physiol. - Lung Cell. Mol. Physiol.* **308,** (2015).

57. Takai, E., Tsukimoto, M. & Kojima, S. TGF-β1 downregulates COX-2 expression leading to decrease of PGE2 production in human lung cancer A549 cells, which is involved in fibrotic response to TGF-β1. *PLoS One* **8,** e76346 (2013).

58. Andresen Eguiluz, R. C., Kaylan, K. B., Underhill, G. H. & Leckband, D. E. Substrate stiffness and VE-cadherin mechano-transduction coordinate to regulate endothelial monolayer integrity. *Biomaterials* **140,** 45–57 (2017).

59. Dupont, S. *et al.* Role of YAP/TAZ in mechanotransduction. *Nature* **474,** 179–183 (2011).

60. Kalluri, R. & Weinberg, R. A. The basics of epithelial-mesenchymal transition. *J. Clin. Invest.* **119,** 1420–8 (2009).

Chapter VI: Conclusions

Summation and Conclusions

In this thesis, we have given an overview of cellular biomechanics with emphasis on cell function and cellular response to forces and the extracellular environment. We began with an overview of past monumental discoveries and innovations to contextualize the works presented. Examples of mechanical regulation of cells during healthy function, as well as cases in which mechanical misregulation can lead to disease or contribute to disease progression, were presented. We introduced the concept of mechanotransduction, which is a fundamental aspect of cellular environmental sensing and response made possible due to a complex network of structural proteins spanning from the extracellular space to the chromatin fibers within the nucleus. We highlighted these mechanical networks throughout cells while also noting the interplay between biochemical and biophysical regulation.

In Chapter II we studied the mechanical role of spectrin proteins in the nucleus, specifically αII-spectrin. This protein had previously been detected in the nucleus and shown to be involved in DNA damage repair[1]; however, while a mechanical role had been hypothesized, it had not been explicitly demonstrated. In order to investigate αII-spectrin, the levels of this protein were reduced in HeLa cells via RNA interference. We confirmed a reduction of αII-spectrin in the cell and the nucleus using Western Blot as well as immunofluorescence. For this study it was critical to identify which cells within a population had a reduction in αII-spectrin; therefore, we chose a short-hairpin RNA coding vector, which contained a GFP-reporter. We demonstrated that cells which express this GFP reporter had a reduction in αII-spectrin. Since αII-spectrin was shown previously to be involved in DNA damage repair, we hypothesized that chromatin dynamics may change once αII-spectrin levels were decreased. To test this hypothesis,

an RFP-tagged telomeric protein, TRF1, was expressed in HeLa cells and tracked over time. Wild type control cells were compared to cells which were clearly expressing the GFP, αII-spectrin knock-down reporter protein. No significant difference in mean squared displacement (MSD) of this protein was observed. Induction of DNA damage may be required in order to obtain a significant difference in chromatin dynamics. Additionally, a slight decrease in MSD (not found to be statistically significant) was observed, suggesting that αII-spectrin may be involved in force propagation to the nucleus; however, it does not appear to be as vital as other nucleoskeletal proteins such as lamins. It is also possible that αII-spectrin levels would need to be reduced further to observe differences in chromatin dynamics; however, further reduction in αII-spectrin appears lethal to cells. The main finding of Chapter II was that nuclear resilience was reduced with reduction of αII-spectrin. Compression assays followed by image analysis of nuclear size were performed to make this conclusion. For these experiments the GFP-reporter of αII-spectrin knock down was critical. This reporter allowed us to not only compare wild type, scramble control (i.e. a vector which does not knock-down any protein) and knock-down cells, but also perform a side-by-side comparison. The side-by-side control cells were untransfected (no GFP-reporter) but in the same field of view as the knock-down cells (GFP-reporter). Because the compression assay could not be calibrated for a guarantee of total reproducibility in terms of force distribution across the entire surface area, these side-by-side controls were invaluable. Through all of these studies, we found that αII-spectrin knock-down cell nuclei did not return to their initial area, whereas control nuclei were able to recover to their initial area. Additionally, we plotted the percent area increase during compression and after release, which demonstrated that, in nuclei which expanded in area to a similar amount, the αII-spectrin knock-down nuclei did not recover to the same extent as control cells. Several control cells reduced in area (relative

to initial area) after release of compression, indicating a nuclear prestressed state or tension generated to counteract the applied force. This was in contrast to αII-spectrin knock-down nuclei, which never reduced in area after removal of compression. Thus, αII-spectrin may also be critical for regulating nuclear prestress in a similar role to the proposed spring-like function. In terms of physiological function, these results collectively suggest that αII-spectrin may be vital for returning the nucleus to its initial shape and area after deformation, for example after cell migration through tight spaces. Further, αII-spectrin in the nucleus may be of particular importance in cells which undergo repeated stresses, such as cardiovascular and lung cells.

The experiments in Chapter III focused on studying the mutant lamin protein progerin, which is responsible for Hutchinson-Gilford progeria syndrome (HGPS). These works emphasized how a single protein defect can have dire outcomes in terms of disease and nuclear mechanics. It has long been established that progerin accumulation increases the stiffness of the nucleoskeleton and leads to nuclear deformations[2,3]. The studies in Chapter III suggested that the nuclear aberrations associated with HGPS are due to microaggregates of progerin which lead to a redistribution of forces through the nucleoskeleton. Of interest, in control nuclei, nuclear aberrations that appeared similar in shape did not show accumulation of healthy lamin A. In fact, a decrease in lamin A intensity, which suggests a dilation of the lamin network rather than accumulation, was seen in progerin expressing nuclei. Often the features of HGPS nuclei are described as “blebbs”; however, we suggest that a term such as “invaginations” be used to describe these features as they appear to result from the nucleoskeleton being pulled inward rather than pushed outward. The differences in force distribution between healthy and HGPS expressing cells was further examined through quantifying the degree that wrinkles in the nuclear lamina formed in the direction of cells patterned on lines in control and progerin-

expressing cells. In control cells, wrinkles largely correlated with the direction of the lines (i.e. the direction of force), while progerin-expressing cells showed less correlation, further implying a redistribution of forces in the nucleoskeleton. Finally, we utilized Comsol to demonstrate changes in stress in a two-dimensional sheet with a relatively small, stiff inclusion to begin to investigate the mechanism by which microaggregates may redistribute forces in the nucleoskeleton.

In Chapter IV we transitioned from focusing on specific proteins of the nucleoskeleton to focusing on epithelial monolayers as mechanically integrated systems. We aimed to determine the extracellular factors which lead to changes in force propagation through cells using our intranuclear particle tracking technique, termed Sensors from IntraNuclear Kinetics (SINK). Previously, this technique was demonstrated to be sensitive to force propagation to the nucleus[4], which we further confirmed through reducing cell contractility using the compound Y-27632 or through decoupling the linker of the nucleoskeleton and cytoskeleton (LINC) complex by transfecting cells with a dominant negative KASH construct (DN-KASH). In both cases a decrease in MSD of the GFP-tagged transcription factor UBF (GFP-UBF) was observed. Additionally, when data were fit to an exponential, the force generation exponent, β, was significantly decreased. These results were consistent with similar experiments performed previously[4]. Next, we explored the role of cell-cell contacts in force propagation to the nucleus by performing SINK on subconfluent (isolated) cells in comparison to cells in a fully enacted monolayer. We noted decreased β, potentially from changes in actin distribution between monolayer and isolated cells. Next, we modeled fibrosis of an epithelial basement membrane by growing monolayers on polyacrylamide gels of various stiffness. Increased β was observed as substrate stiffness was increased, suggesting that the increased forces generated on stiff

substrates are propagated to the nuclear interior in monolayer systems. These results demonstrate a possible means of mechanosensitive regulation and physical environment detection within monolayers. We concluded this chapter by demonstrating the use of SINK for investigating point defects in monolayer systems. We demonstrated that adjacent and distant (up to 40 μm away) cells from a nucleus with a disrupted LINC complex were affected, but to different extents. Together, these data highlight the inter-, intra-, and extra- cellular mechanical integration within monolayers. Long-range mechanical integrations may be crucial for governing collective cell behaviors with rapid responses to perturbation, as mechanical signaling can occur faster than diffusion-based paracrine signaling.

Finally, in Chapter V we aimed to elucidate the substrate dependent responses of monolayers to chemically-induced increased contractility, using Calyculin A drug treatment. We combined the SINK technique with analysis of the nuclear localization of the mechanosensitive protein, Yes Associated Protein (YAP) as well as basal to apical actin distribution. We analyzed the monolayer response to Calyculin A treatment for cells on glass, 2.5 kPa and 30 kPa acrylamide gels. The results indicated that on glass, the cells generated enough force to rupture cell-cell junctions and began to assume an isolated phenotype, with primarily basal plane actin and YAP nuclear localization. Additionally, the SINK analysis appeared similar to subconfluent cells which further suggested isolated-type behavior. On soft substrates YAP did not localize to the nucleus, and actin remained distributed through the height of the cell, similar to control monolayers. As the actin did not appear to redistribute, increased forces from Calyculin A treatment seemed to propagate to the nucleus as indicated by the particle tracking analysis (increased MSD and β). On stiff gels, between the stiffness of glass and the soft gel, the monolayers demonstrated intermediate behavior. Actin distribution and chromatin dynamics

changed slightly in the direction of an isolated phenotype but not to the extent seen on glass. No change in YAP localization was detected. Together these data indicated that the physical properties of the substrate can impact the monolayer response to chemical signaling, which has implications in regulating phenotypic shifts *in vivo,* such as epithelial to mesenchymal transition (EMT).

Future Outlook

In Chapter II, we probed primarily the elastic response of the cell nucleus to compression, as time scales of compression were on the order of seconds. The nucleus is known to be viscoelastic[5], and investigating nuclear strain over different time scales may lead to interesting results. Experiments could be performed in a controlled fashion in which cells are exposed to compression for an extended period of time and deformation is calculated. The difficulty in these experiments would be to assure cell viability throughout, as well as determining the proper time scales of compression application. Additionally, the role of αII-spectrin in cell invasion through tight spaces could be further investigated, with the hypothesis that nuclei with reduced αII-spectrin levels would fail to return to their control shape and size after migrating through areas of diameter smaller than that of their nucleus. We have previously attempted studies using micropillars with small (<10 μm) spacing; however, we could not image these with sufficient resolution to determine a difference in nuclear shape after migration. Custom microfluidic devices, along with a chemoattractant, may be required to obtain relevant data to investigate this hypothesis. Finally, our lab has demonstrated changes in chromatin dynamics in response to DNA damage (paper in review). It would be interesting to determine if these differences persisted longer in cells with reduced αII-spectrin (due to reduced DNA damage repair response). Finally, within all the studies performed on αII-spectrin, it was not possible to reduce

only the nuclear isoform of αII-spectrin (as it is currently not known). Once this isoform is determined, experiments could be performed to reinforce the conclusions of this work by testing the impact of only reducing the nuclear isoform, rather than reduction of nuclear and cytoskeletal αII-spectrin. Of note, cytoskeletal αII-spectrin is likely located primarily at the plasma membrane and is unlikely to have a direct impact on the nucleus. However, as we have demonstrated in this thesis, cells are mechanically integrated systems. As αII-spectrin is a relatively under investigated protein, many future experiments could be performed to truly reveal the nuclear function as novel techniques are continuing to be developed to probe cell mechanics.

In Chapter III, we again rely on physical manipulation of cells and image analysis to determine changes in nuclear architecture, in this case from progerin accumulation. As super-resolution microscopy and other high resolution imaging techniques have been used to investigate the nuclear lamina[6,7], the work performed in Chapter III could benefit from enhanced resolution. This could be used to further identify that progerin is accumulating at invaginations along the nucleoskeleton. Further, additional proteins such as actin could be labeled and, with increased resolution, their anchoring points along the nucleus could be determined. The contact areas between actin and the nucleus are likely regions of increased local forces, and the mapping of these with wrinkle and invagination location and angle could further develop the hypothesis that progerin leads to changes in force distribution across the nucleus. Finally, techniques such as atomic force microscopy or magnetic twisting cytometry could be employed to induce a local stress of a known magnitude to study the changes in lamin or progerin distribution. As cell mechanical properties (e.g. nuclear lamina thickness and stiffness) are continuing to be evaluated, more accurate models could also be produced to obtain greater insight into the mechanisms behind the changes in cell mechanics and function.

In Chapter IV the SINK technique was presented as a means to study mechanical features of monolayer systems. One benefit to this technique is the lack of external probe required for measurements, and thus it could be expanded to complex experimental set ups. Similar to the substrate stiffness experiments in Chapter IV, stiffness responses of cell systems could be probed in three-dimensional gel systems, in which cells would likely have increased contacts with the environment and may respond to extracellular rigidity in a different (e.g. more pronounced) fashion. We have begun to demonstrate the importance of cell-cell contacts in terms of force propagation to the nucleus; however, this could be investigated further by disruption of adherens junctions. Further, experiments such as knock-down or blocking of cadherin junctions could be performed to test the hypothesis that increased cell junctions leads to increased chromatin motion. Calcium depletion could also be used to disrupt cadherin junctions; however, calcium depletion likely has multiple other adverse effects on cell function. Additionally, experiments in which both focal adhesions and adherens junctions are labeled, while performing SINK, could be performed to determine a potential correlation between cell-cell or cell-surface contacts and β. Based on the data presented in this thesis, it is hypothesized that β would correlate weakly with focal adhesion number (due to increased forces in the basal plane) and strongly with adherens junction number (due to increased forces in the mid/apical plane). SINK could also be coupled with other force measurement techniques such as Förster resonance energy transfer (FRET) and traction force microscopy (TFM) to get a complete view of force propagation from outside the cell to within the nucleus. One of the most exciting findings within the thesis was the correlation between intranuclear movement and substrate stiffness within monolayers. This demonstrated a mechanosensitive feature of monolayers, but further experiments to investigate this mechanism would be of high importance. For example, mechanosensitive protein composition may change

in a substrate stiffness dependent manner. It is not clear if the increases in chromatin dynamics are due to direct force propagation, transcriptional changes (also active forces), through biochemical signaling cascades or a combination of these mechanisms. Knock-down studies of specific proteins within these systems could begin to shed light on the mechanism of mechanosensing. Additionally, a more precise calibration of the SINK method to determine a true force measurement would be groundbreaking in the field of biomechanics. One possible experiment to begin to investigate this would be to perform SINK in cells on micropatterned lines in which the actin is essentially oriented in a single direction. If the tracks in this system demonstrated increased persistence in the direction of patterning (compared to the random motion observed normally), this persistence could be quantified as an additional parameter. Based on the motion in the direction of force (i.e. actin) versus motion perpendicular to force, it may be possible to distinguish the extent that actomyosin forces are impacting probe motion. Additionally, we have only performed single point particle tracking which requires nuclear alignment. While two-point particle tracking requires many more particles to be tracked to obtain statistical significance compared to single point tracking, this analysis could be performed in nuclei expressing a large number of points. It may be necessary to develop a cell line that stably expresses a punctate marker of chromatin to obtain this data. A stable cell line would also be beneficial for any future experiments to obtain a larger sample size with increased efficiency. Finally, once the SINK technique is characterized further, it could be expanded to *in vivo* studies in model organisms to study mechanotransduction during development. Thus, we can envision utilizing the SINK technique to investigate mechanosensing of everything but the kitchen sink.

In Chapter V, the substrate dependent response of epithelial monolayers to increased contraction was observed. In these studies, Calyculin A was used as it has been well established

to increase cell contractility through actomyosin activity. Previous studies have indicated changes in chromatin dynamics after treatment of endothelial cells to vascular endothelial growth factor (VEGF)[4]. In the case of epithelial cells, EMT can be induced in subconfluent NRK52E cells through treatment with transforming growth factor β (TGF-β) and in monolayers through treatment with TGF-β in combination with cell-cell junction disruption through E-cadherin antibody blocking or calcium depletion[8]. Unfortunately, the blocking antibody used in this study is no longer available from Santa Cruz, and thus a new function blocking antibody would need to be determined and tested. However, monolayers treated with TGF-β did show a decrease in chromatin dynamics and increased YAP nuclear localization as shown in Appendix B. However, the actin distribution did not appear to shift towards an isolated phenotype, and β-catenin was not mislocalized indicating that these cells did not fully transition to a mesenchymal phenotype. Since TGF-β likely causes many changes within the cell, these results are difficult to properly interpret. Perhaps a combination of calcium depletion and TGF-β treatment would induce a greater phenotypic shift, leading to a dramatic change in actin distribution. Additionally, in these studies the presence of the actin cap may play a role in mechanotransduction; however, determining the role of the actin cap can be difficult and would require more precise image analysis. In this study TGF-β likely caused changes in chromatin condensation state due to changes in gene expression. Our lab has previously demonstrated the use of fluorescence lifetime imaging microscopy, FLIM, to investigate chromatin condensation state. In Appendix C, we demonstrate the use of FLIM for detecting changes in condensation state as during stem cell differentiation and show how FLIM could be used to determine spatial information regarding condensation state within the nucleus. Finally, the role of substrate coating in the experiments conducted in Chapter V was not fully examined. A library of data could be gathered by

performing SINK on monolayers of a single substrate stiffness, but with varying the concentration or type of extracellular matrix protein coating. These experiments may need to be combined with traction force and focal adhesion quantification in order to decipher how substrate coating leads to changes in chromatin dynamics in monolayer systems.

Collectively the works presented in this thesis reinforce the importance of mechanical integration through cells and multi-cell systems. Sensing the physical environment is a critical property for maintenance of cell function which is often coupled with biochemical regulation. Detecting surface rigidity is likely mediated through actomyosin contractions which correspond with the forces propagated through a cell. It remains a mystery precisely how cells, which contain the same DNA sequence, can navigate their environment and self-regulate to perform diverse biological functions within the human body; however, increasing studies of cellular biomechanics are beginning to shed light on these unknown areas.

References

1. McMahon, L. W., Zhang, P., Sridharan, D. M., Lefferts, J. A. & Lambert, M. W. Knockdown of alphaII spectrin in normal human cells by siRNA leads to chromosomal instability and decreased DNA interstrand cross-link repair. *Biochem. Biophys. Res. Commun.* **381,** 288–293 (2009).

2. Dahl, K. N. *et al.* Distinct structural and mechanical properties of the nuclear lamina in Hutchinson-Gilford progeria syndrome. *Proc. Natl. Acad. Sci. U. S. A.* **103,** 10271–6 (2006).

3. Booth, E. A., Spagnol, S. T., Alcoser, T. A., Dahl, K. N. & Matter, S. Nuclear stiffening and chromatin softening with progerin expression leads to an attenuated nuclear response to force. *Soft Matter* **11,** 6412–6418 (2015).

4. Spagnol, S. T., Dahl, K. N. & Noel Dahl, K. Active cytoskeletal force and chromatin condensation independently modulate intranuclear network fluctuations. *Integr. Biol.* **6,**

523–31 (2014).

5. Dahl, K. N., Engler, A. J., Pajerowski, J. D. & Discher, D. E. Power-law rheology of isolated nuclei with deformation mapping of nuclear substructures. *Biophys. J.* **89,** 2855–64 (2005).

6. Shimi, T., Kittisopikul, M., Tran, J., Goldman, A. E. & Adam, S. A. Structural Organization of Nuclear Lamins A , C , B1 and B2 Revealed by Super-Resolution Microscopy. *Mol. Biol. Cell* **26,** 4075–4068 (2015).

7. Turgay, Y. *et al.* The molecular architecture of lamins in somatic cells. *Nature* **543,** 261–264 (2017).

8. Zheng, G. *et al.* Disruption of E-Cadherin by Matrix Metalloproteinase Directly Mediates Epithelial-Mesenchymal Transition Downstream of Transforming Growth Factor-β1 in Renal Tubular Epithelial Cells. *Am. J. Pathol.* **175,** 580–591 (2009).

Appendix A: Nuclear Compression and Intranuclear Movement Appear Unchanged After Emerin Knock-Down

Methods

These studies were performed using HeLa cells, cultured in accordance with the methods presented in Chapter II. Compression and particle tracking were performed according to the methods in Chapter II. RFP-TRF1 was used for the particle tracking studies. For emerin knock-down, cells were transfected with an emerin knock-down plasmid coding for shRNA against emerin RNA (ThermoFisher, RHS4430-200179682) using lipofectamine 3000 according to manufacturer's protocol. Similar to the spectrin knock-down plasmid in Chapter II, the emerin knock-down plasmid contained a GFP-reporter protein to determine which cells in a given field of view had been transfected. For particle tracking and compression studies, only cells which were strongly expressing GFP were used for analysis. All analysis was performed 2 days after transfection. Knock-down was confirmed after this time period using immunofluorescence. For immunofluorescent labeling, the same methods in Chapter II were utilized. The primary emerin antibody was a mouse anti-emerin monoclonal antibody (Santa Cruz Biotechnology sc-25284) at 1:100 dilution in a 0.2% BSA solution, and the secondary antibody was a donkey anti-mouse conjugated to Alexa fluorophore 647 (Thermo Fisher, A31571) at a 1:200 dilution in a 0.2% BSA solution. For compression studies, 35 wild type control (WT) and 15 emerin knock-down (KDEm) nuclei were examined for analysis.

Results

Emerin knock-down was confirmed using immunofluorescence, as seen in Figure A.1. Cells which are expressing the GFP reporter showed a decrease in emerin. Once knock-down

was confirmed, particle tracking experiments to determine changes in chromatin dynamics were performed (Figure A.2). No significant difference in the mean squared displacement (MSD) of the intranuclear motion between wild type control (WT) and emerin knock-down (KDEm) cells was detected at any lag time ($P > 0.05$). Therefore, it does not appear that emerin knock-down has a significant impact on chromatin dynamics. It was hypothesized that emerin may be involved in regulating the elastic properties of the nucleus (similar to spectrin, presented in Chapter II) since emerin is a nucleoskeletal protein which can bind nesprins, lamins, and actin. In the compression studies emerin knock-down nuclei expanded slightly less than the wild type cells as shown in Figure A.3 ($0.05 > p > 0.01$). However, this extent of variability in compression may be within the variability expected from these studies and does not seem unreasonable when comparing the data to the other controls in Chapter II. Additional control studies would need to be performed to determine if this slight decrease is truly meaningful, which seems unlikely. Perhaps emerin reduction caused an upregulation in another nucleoskeletal protein such as lamin. Again, multiple additional experiments would need to be performed to determine if this finding was meaningful. Upon release of compression, no significant difference in change in nuclear area was detected between control and emerin knock-down cells ($p > 0.05$). Additionally, these data were plotted with individual nuclei as unique points to determine the extent that a given nucleus returned to its initial shaped based on the amount it expanded (Figure A.3 B). From these data, it appears that nuclei which expanded to a similar extent also retracted to a similar extent regardless of emerin knock-down. This is in contrast to the spectrin knock-down data presented in Chapter II. Together these data suggest that emerin does not appear to alter nuclear mechanics in terms of nuclear resilience or intranuclear motion.

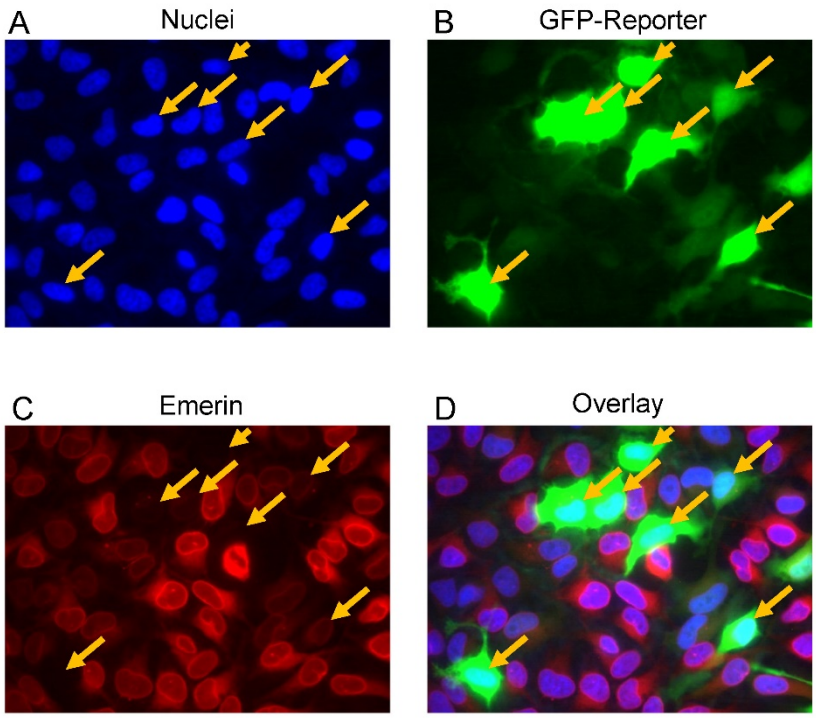

Figure A.1: Immunofluorescence for confirmation of emerin knockdown

*Fluorescent images showing (**A**) nuclei stained with Hoechst, (**B**) the GFP reporter present when cells take up the emerin knock-down vector, (**C**) immunofluorescent labeling of emerin, and (**D**) the overlay of each channel. Yellow arrows point to cells expressing the GFP-reporter and show decreased emerin fluorescence.*

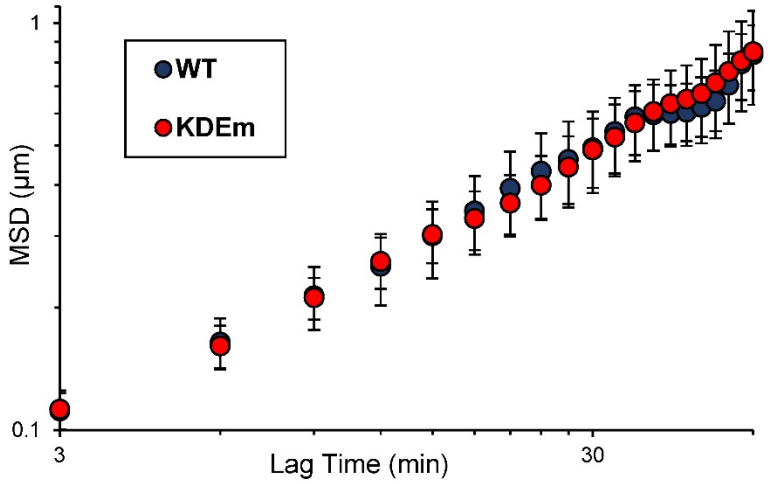

Figure A.2: Comparison of chromatin dynamics

No change in intranuclear movement was detected through tracking RFP-TRF1 in wild type (WT) and emerin knock-down (KDEm) nuclei. Student's T-test was performed at each lag time with no significant difference detected ($p > 0.05$).

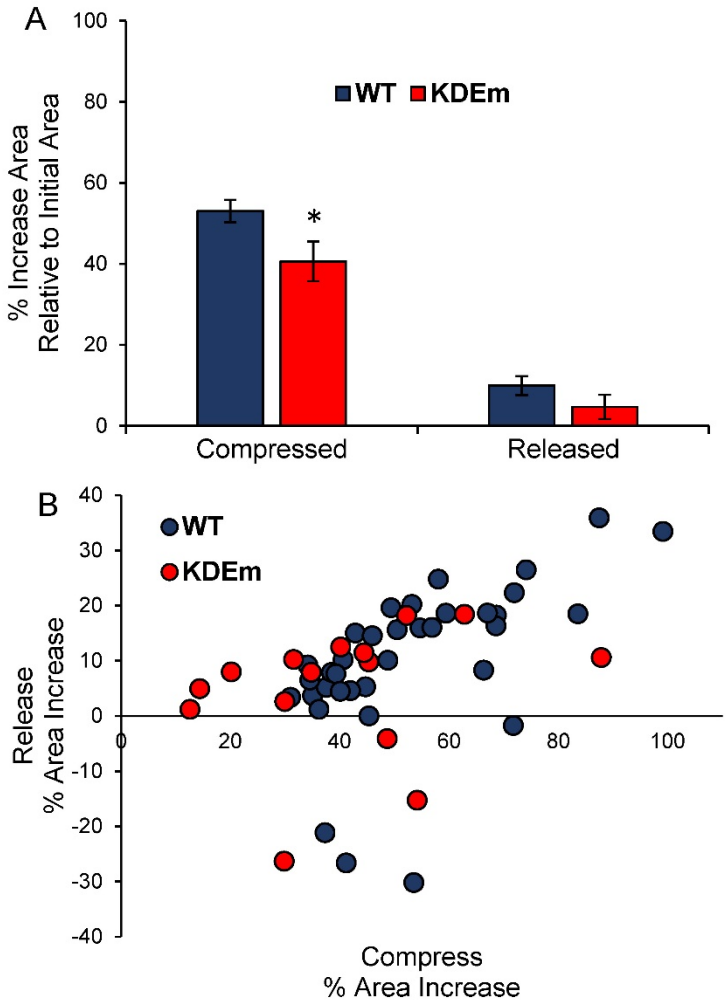

Figure A.3: Compression assay for WT and KDEm cells

*(**A**) Percent increase in nuclear area was measured during compression and after the release of compression for WT and KDEm cells. KDEm cells appeared to compress less than WT cells ($0.01 < p < 0.05$ using Student's T-test); however, this difference may be due to variability within the compression assay. No significant difference in percent area increase after removal of the weight was detected. (**B**) The percent area increase upon release of compression plotted versus the percent area increase during compression is shown. It is important to note that many nuclei which were compressed to the same decrease also returned to a similar relative area upon release of compression.*

Appendix B: Effects of TGF-β Treatment on Epithelial Monolayers

Methods

NRK52E cells were cultured on uncoated glass, as described in the methods of Chapter V. Immunofluorescent staining was performed using the same methods described in Chapter V; however, the primary antibodies used were a mouse anti β-catenin antibody conjugated to Alexa fluorophore 488 (Santa Cruz Biotechnology, sc-7963 AF488) and a mouse anti-, α-smooth muscle actin conjugated to an Alexa fluorophore 647 (Santa Cruz Biotechnology, sc-32251 AF647) both at 1:100 dilution in a 0.2% BSA solution. Actin distribution, chromatin dynamics, and YAP localization analyses were performed according to the methods described in Chapter V. Once cells were grown to a monolayer, recombinant human transforming growth factor-β1 (TGF-β, 10ng/mL) was added to dishes and cells were incubated for 72 hours before analysis. In addition to treatment with only TGF-β (the data discussed in Results below), E-cadherin blocking treatment aimed to induce epithelial to mesenchymal transition (EMT) was performed in an attempt to replicate the data in reference[1]. The antibody used in this study was no longer available; however, an antibody listed as comparable was purchased (Santa Cruz Biotechnology, sc-8426). After treatment with this antibody for 72 hours, no markers of EMT such as shape change, β-catenin mislocalization, or α-smooth muscle actin expression were observed (data not shown). Thus, it was concluded that this antibody did not successfully induce EMT. This antibody was also used in combination with TGF-β, but no EMT was detected by the same metrics. The TGF-β only treatment experiments were performed and analyzed as in Chapter V, as TGF-β likely causes multiple downstream effects prior to full EMT. We aimed to investigate these changes here.

Results

TGF-β treatment did not induce full epithelial to mesenchymal transition in monolayer cells, as it appears cell-cell junctions need to be disrupted prior to treatment for EMT markers, such as α-smooth muscle actin expression and β-catenin mislocalization, to be seen in NRK52E cells[1]. α-smooth muscle actin was not expressed and β-catenin mislocalization was not seen after 72 hours of treatment as confirmed via immunofluorescence (Figure B.1 TGF-β did not cause redistribution of β-catenin, α-smooth muscle actin data not shown as there was no α-smooth muscle actin fluorescence). While nuclear intensity appeared slightly above the actin peak intensity, no significant difference was detected in the actin segregation parameter (Figure B.2 Actin distribution appears unchanged after TGF-β treatment). Even without full transition to a mesenchymal phenotype, chromatin dynamics decreased compared to control monolayers and YAP nuclear localization increased (Figure B.3 and Figure B.4). TGF-β likely causes a wider range of changes in cells than Calyculin A, and, therefore, the results are more difficult to interpret after TGF-β treatment than after Calyculin A. These results suggest that changes in transcription and force propagation (or generation) are possible, even without the drastic actin rearrangement seen after Calyculin A treatment, observed in Chapter V.

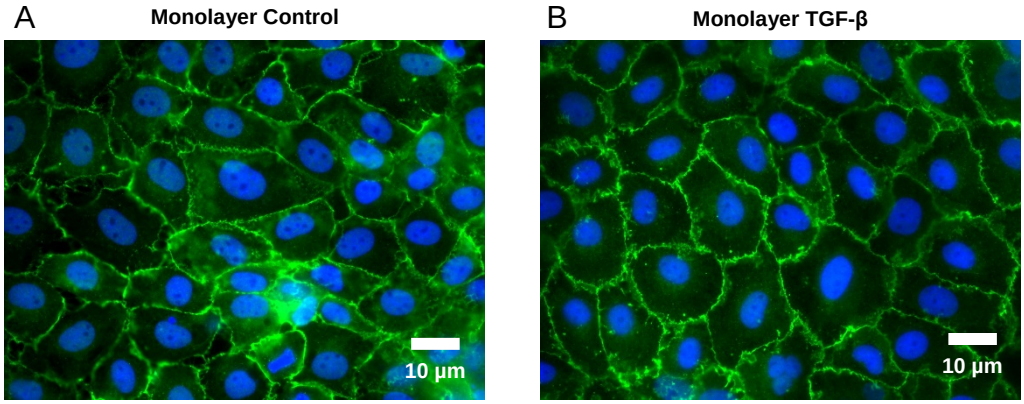

Figure B.1 TGF-β did not cause redistribution of β-catenin

*Immunofluorescent images of (**A**) monolayer control and (**B**) monolayer cells treated with TGF-β. After TGF-β treatment, β-catenin (green) remained localized at cell-cell junctions, suggesting intact adherens junctions. Nuclei are stained with Hoechst (blue).*

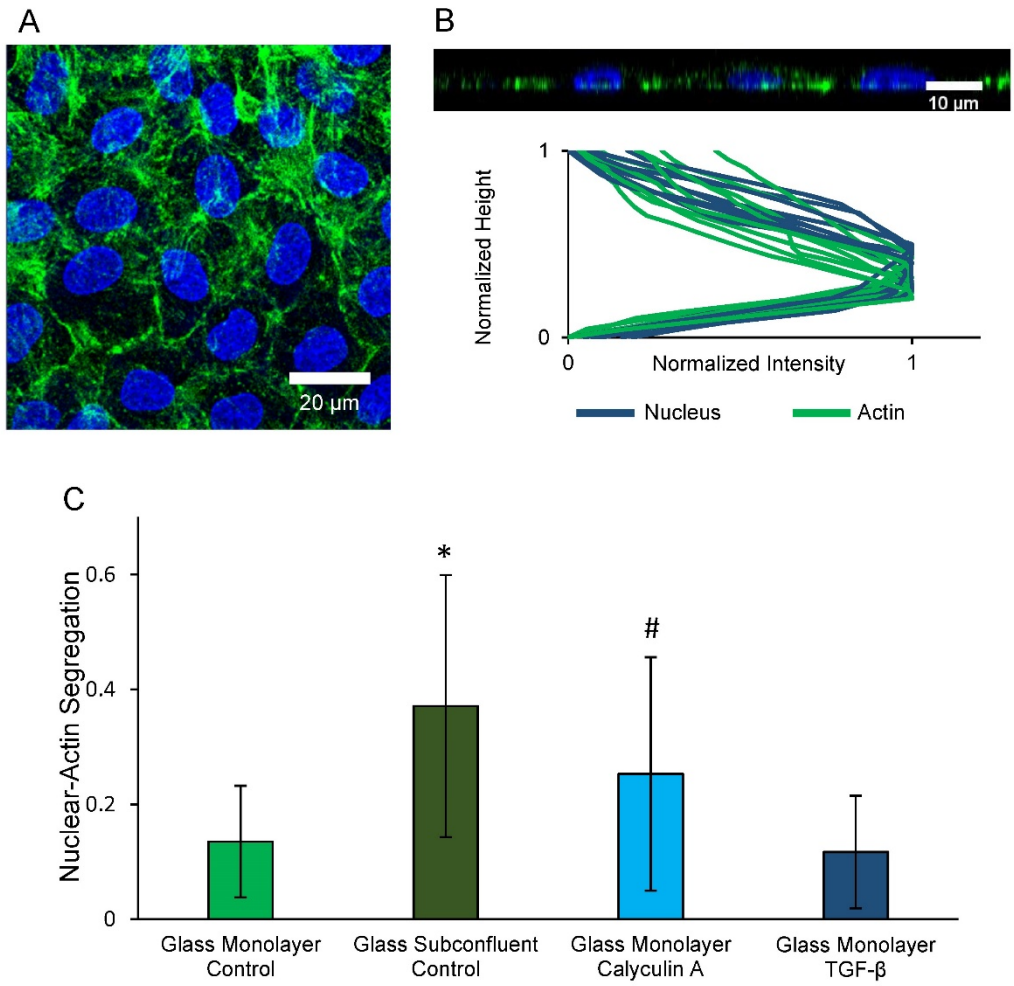

Figure B.2 Actin distribution appears unchanged after TGF-β treatment

*(**A**) A fluorescent image of actin (green) and nuclei (blue) of monolayer cells treated with TGF-β is shown. (**B**) Confocal imaging was utilized to analyze apical to basal actin distribution. Nine fields of view were analyzed. (**C**)The Nuclear-Actin segregation parameter was calculated and compared to the experimental conditions in Chapter V. The TGF-β treated monolayer cells on glass did not appear statistically different than the glass control monolayer condition, as detected by a 1-way ANOVA followed by Tukey's pairwise comparison ($p > 0.05$). Imaging and analysis were conducted according to the methods in Chapter V. Error bars represent standard deviation.*

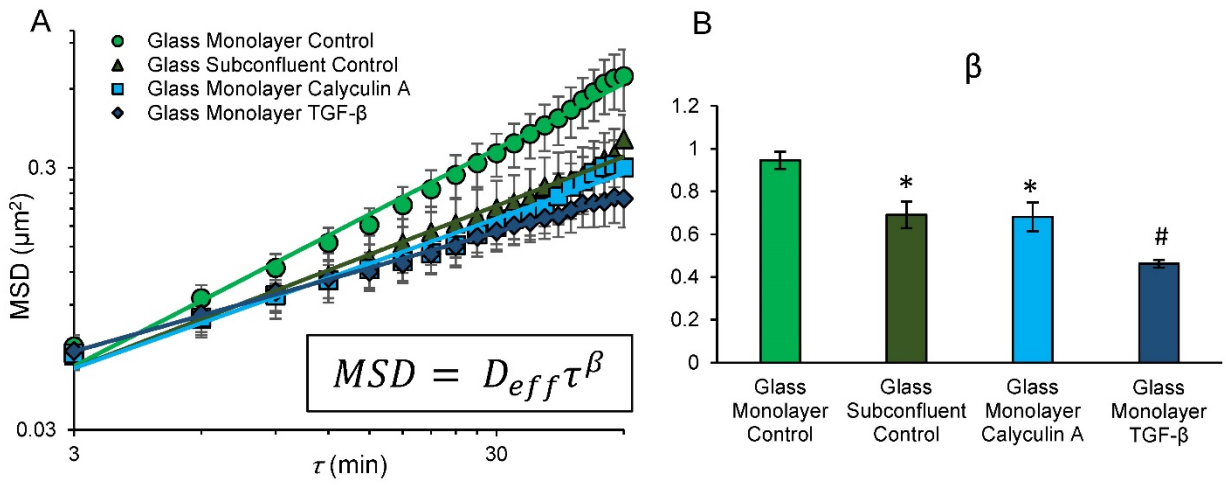

Figure B.3: Chromatin dynamics of TGF-β treated monolayers on glass

*(**A**) Mean squared displacement (MSD) of GFP-UBF of TGF-β treated monolayers (dark blue) compared with the other conditions presented in Chapter V are shown. TGF-β treated cells had the lowest MSD compared to other conditions shown. 13 cells were analyzed for the TGF-β treated condition. Error bars represent standard error of the mean (**B**) The force generation exponent, β, was plotted for these conditions. For TGF-β treated monolayer cells on glass a significant decrease in β was detected compared to the other conditions. Data which do not share a common symbol were found to be significantly different by a 1-way ANOVA followed by Tukey's pairwise comparison ($p < 0.05$). Error bars represent 95% confidence intervals based on the fitting of β. These data suggest that TGF-β causes a decrease in propagation of force to the nucleus, and/or a decrease in overall force generation.*

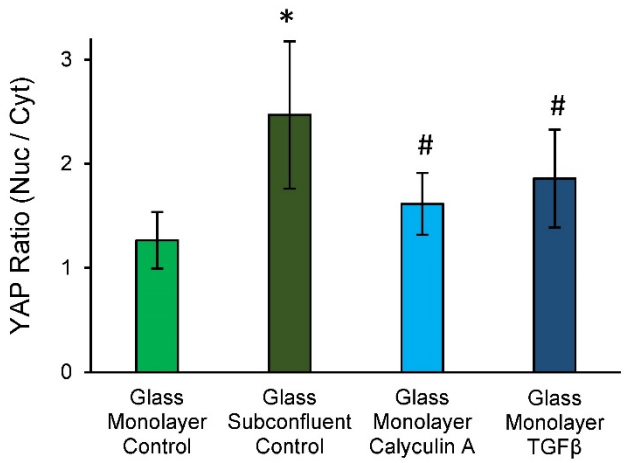

Figure B.4: YAP nuclear localization increases after TGF-β treatment

Glass monolayers treated with TGF-β were analyzed to determine the YAP nuclear to cytoplasmic ratio. A significant increase in this ratio over monolayer control cells was detected by a 1-way ANOVA followed by Tukey's pairwise comparison ($p < 0.05$). Data which do not share a common symbol were found to be significantly different. Analysis was performed according to the methods presented in Chapter V. Error bars represent standard deviation. 45 cells were analyzed for each condition.

References

1. Zheng, G. *et al.* Disruption of E-Cadherin by Matrix Metalloproteinase Directly Mediates Epithelial-Mesenchymal Transition Downstream of Transforming Growth Factor-β1 in Renal Tubular Epithelial Cells. *Am. J. Pathol.* **175,** 580–591 (2009).

Appendix C: Fluorescent Lifetime Imaging of Stem Cell Nuclei to Assess Differentiation State via Chromatin Condensation State

Methods

The aim of this section is to highlight the use of fluorescence lifetime imaging microscopy (FLIM) for chromatin condensation detection and to further demonstrate the analysis that can be performed on the data collected. Stem cell differentiation is used as an example in this appendix; however, the methods for stem cell osteogenic differentiation as well as electrospinning are the expertise of the Brown lab at Penn State University. Thus, the cell culture and electrospinning methods are not presented in detail here.

Cell Culture, Fixation, Labeling, and Nanofiber Electrospinning

All cells were cultured, fixed and stained for imaging and analysis by the lab of Dr. Justin Brown (Penn State University). All mMSCs were cultured in growth media, with the exception of the 10 Day Osteo group, which was cultured in osteogenic media for 10 days as a positive control for differentiated cells. Cells were grown on either electrospun poly(methyl methacrylate) (PMMA) fibers of diameters of approximately 300 nm or on flat PMMA. Cell fixation and labeling procedures were performed according the those presented in references[1,2]. DNA was stained with Hoechst33342 at a concentration of 5 μg/mL.

Fluorescence Lifetime Imaging Microscopy and Analysis

Fluorescence lifetime imaging microscopy (FLIM) was performed according to the methods presented in references[1,2]. Images were collected using a Leica TCS SP5 inverted laser scanning microscope with a 100x (1.4 NA) oil immersion objective. A Ti:sapphire mode-locked,

pulsed infrared laser system (Chameleon, Coherent) with a multiphoton laser excitation was used. The multiphoton laser was tuned to 750nm for excitation. The photomultiplier tube for collection was set to 404-536 nm. Scans were taken at 256 pixels by 256 pixels at a speed of 400 Hz. For mean lifetime calculation at a given pixel, the mean lifetime of the surrounding pixels was averaged (i.e. a binning of 2). Visually, the images in Figure C.1 have a resolution of .58μm/pixel; however, within an apparent pixel, there may be multiple pixels for lifetime analysis, as zoom was adjusted for a given field of view in order to increase photon counts for lifetime analysis. Scans were collected for a minimum of 100 s, with the photon counts per second between 1E4 and 1E5 for the length of acquisition. The filter wheel was set to 6%, with an offset of 73%, and gain set to 70%. For cells on fibers, only cells which were spread on an individual fiber, and thus the nuclei were elongated in one direction, were used for analysis. Lifetime data was acquired using Becker & Hickel SPC-830 software, with 10 ps resolution. The fitting for the lifetime of the photon decay was set to a double exponential, of the form:

$$I(t) = I_0 + a_1 e^{-t/\tau 1} + a_2 e^{-t/\tau 2}$$

Where the mean fluorescence lifetime is calculated as:

$$\tau_m = \frac{\Sigma a_i \tau_i}{\Sigma a_i}$$

In these equations, τ_m is the mean fluorescence lifetime, $I(t)$ is the number of photons collected in a time t, I_0 is the offset, a_i is the amplitude, and τ_i is the lifetime of the i^{th} exponential decay. Once lifetime data was acquired for each pixel in a field of view, further analysis was performed using MATLAB to generate heat maps and for spatial analysis. Masks for thresholding the nuclei were generated in ImageJ and used in conjunction with the MATLAB code to determine the mean lifetimes within a given nucleus.

Results

Mouse mesenchymal stem cell (mMSC) nuclei stained with Hoechst were imaged using fluorescence lifetime imaging microscopy (FLIM). The aims of these experiments were to confirm that FLIM could be used to detect changes in chromatin condensation as stem cells differentiate, determine if mMSCs were able to differentiate on fibers without osteogenic media, and observe the spatial distribution of chromatin condensation based on fluorescence lifetime maps within mMSC nuclei. Fixed mMSC cells for 5 experimental conditions were analyzed. These conditions were cells grown on flat surfaces in growth media for 3 and 10 days (3 Day Flat and 10 Day Flat respectively), cells grown on a flat surface in oestogenic differentiation media for 10 days (10 Day Oesteo), and cells grown on electrospun nanofibers in growth media for 3 and 10 days (3 Day Fibers and 10 Day Fibers respectively). The 3 and 10 day Flat cells represent a negative control for undifferentiated stem cells. The 10 Day Osteo Cells represent a positive control for osteogenic differentiated cells. Representative images of the mean fluorescent lifetime heat maps are show in Figure C.1. Previously, our lab has demonstrated that a lower fluorescence lifetime corresponds with more condensed chromatin, while a longer fluorescence lifetime corresponds with less condensed chromatin[1,2]. Typically, undifferentiated stems cells contain less condensed chromatin relative to differentiated cells and thus lifetime of the DNA-bound fluorophore may be used as a metric of differentiation. This was confirmed using FLIM, as the 10 Day Osteo nuclei demonstrated a lower mean fluorescence lifetime compared to undifferentiated cells (3 and 10 Day Flat). Additionally, it appears that after 10 days of growth on fibers, cells begin to differentiate, as the mean fluorescence lifetime was similar between the 10 Day Fibers and 10 Day Osteo cells. After only 3 days of grown on fibers, the

mean lifetime appears similar to the undifferentiated cells (Figure C.1, Figure C.2, and Figure C.3).

Two approaches were taken to further analyze this data. The data were analyzed using a sample size based on number pixels per condition or a sample sized based on number of nuclei per condition (Figure C.2 and Figure C.3). Additionally, the trend in standard deviation within a nucleus based on mean lifetime within that nucleus was analyzed (Figure C.4). The values of the data presented in the figures is shown in Table C.1 and Table C.2. Regardless of the method of analysis, the 10 Day Osteo and 10 Day Fibers conditions had similar mean lifetimes, less than those of the other three conditions. This suggests that after 10 days, the cells grown on fibers are differentiated, while after 3 days the cells have not yet differentiated. When data were analyzed based on the total number of pixels, N was large enough (thousands) that all data were significantly different from each other. When data were analyzed using number of nuclei as a sample size (with the average lifetime within a nucleus being one data point), the 10 Day Flat Osteo condition was found to be significantly less than the 3 Day Flat and 3 Day Fiber conditions ($P < 0.05$). It is expected that with increased N, a significant difference between other groups may be detectable. It should be noted that the detector used for imaging has ~10 picosecond sensitivity. While the data appears to split into two groups (undifferentiated (blue): 3 Day Flat, 10 Day Flat, 3 Day Fibers, and differentiated (red): 10 Day Osteo, 10 Day Fibers), further trends are observed based on the range (standard deviation) of lifetimes within a given nucleus for a given condition (Figure C.4). As the average lifetime within a nucleus decreases, the standard deviation of lifetimes within the nucleus apparently increases. Since a decrease in lifetime is associated with increased chromatin condensation (and differentiation), it is logical that as chromatin condenses, the range of condensation states increases. In other words, in

undifferentiated cells, chromatin is more uniformly decondensed compared with differentiated cells with a more heterogeneous distribution of condensation states.

Finally, we wanted to highlight how FLIM could be used to distinguish spatial features within nuclei. It is hypothesized that differentiated nuclei have a shell of heterochromatin towards the periphery of the nucleus. Thus, we wrote custom MATLAB code such that the outer shell and nuclear interior fluorescent lifetime data could be compared, for which an example is shown in Figure C.5. Unfortunately using this data, no difference between lifetime at the interior or outer shell of the nucleus was found for any condition (data not shown). Multiple sizes of the outer shell were investigated, with no difference detected. Perhaps the shell of heterochromatin is too thin for detection using this method. While this method was unsuccessful here, it demonstrates the type of analysis that may be performed using these heat maps of FLIM data. Collectively we demonstrated FLIM as a metric to detect stem cell differentiation and investigated the heterogeneities associated with chromatin condensation state as cells undergo osteogenic differentiation.

Acknowledgements

We would like to thank J. Brown (Penn State University) for providing the slides of fixed cells for analysis. We would also like to thank M. Islam (Carnegie Mellon University) for the use of the FLIM system. Finally, we would like to thank B. Holt and S. Spagnol for their training on use of the FLIM systems as well as insight on the analysis and skeleton MATLAB code for further editing.

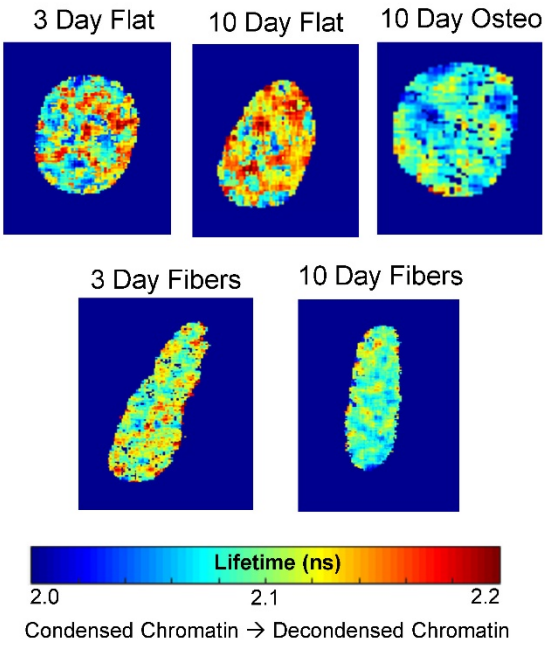

Figure C.1: Representative Fluorescence lifetime heat maps for each condition

Heat maps of the fluorescence lifetime for each condition analyzed are shown. The 10 Day Osteo and 10 Day Fibers had the lowest lifetime, suggesting condensed chromatin compared to the other conditions. This change was likely due to osteogenic differentiation.

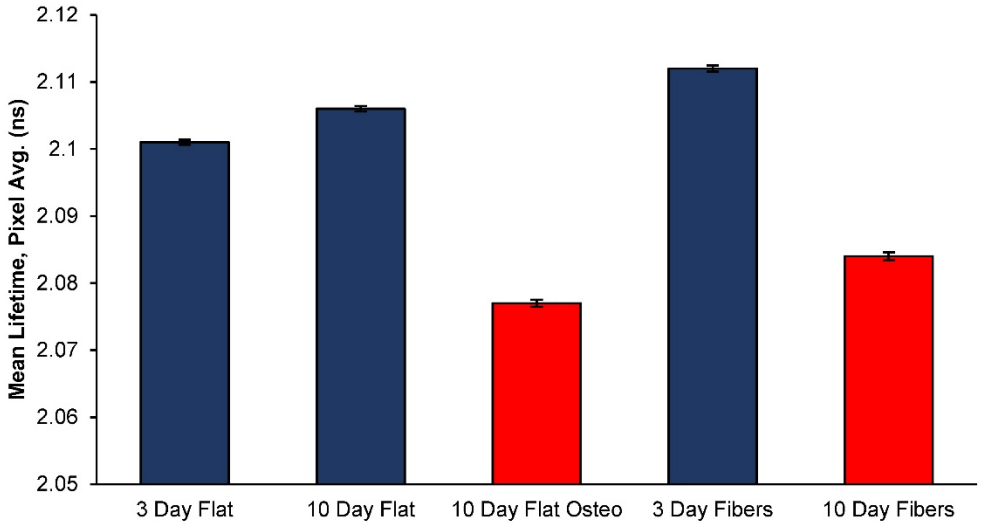

Figure C.2: Mean lifetimes for each condition based on pixel averages

The average mean fluorescence lifetime of each condition based on the pixel average is shown. Error bars represent standard error of the mean. Values were all found to be statistically significantly different (1-way ANOVA, followed by Tukey's pairwise comparison, $p > 0.05$), likely due to the high N (thousands) for each condition. The data appear to separate into two categories assumed to be undifferentiated (dark blue) and differentiated (red). The values plotted are given in Table C.1 below.

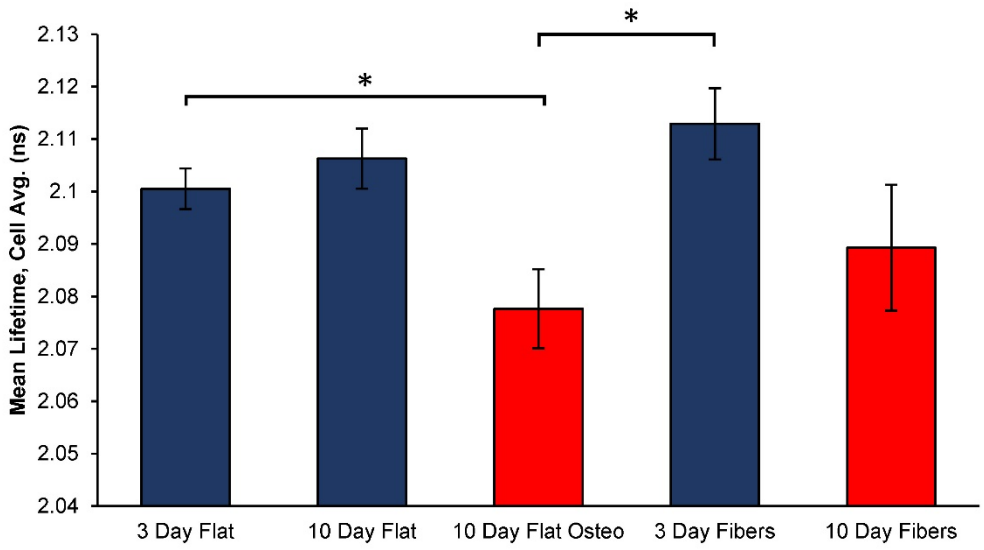

Figure C.3: Mean lifetimes for each condition based on nuclei averages

*The average mean fluorescence lifetime of each condition using the average lifetime within a single nucleus as 1 data point. Error bars represent standard error of the mean. An * denotes statistical significant via a 1-way ANOVA, followed by Tukey's pairwise comparison ($p < 0.05$), The data appear to separate into two categories thought to be undifferentiated (dark blue) and differentiated (red). The values plotted are given in Table C.2 below.*

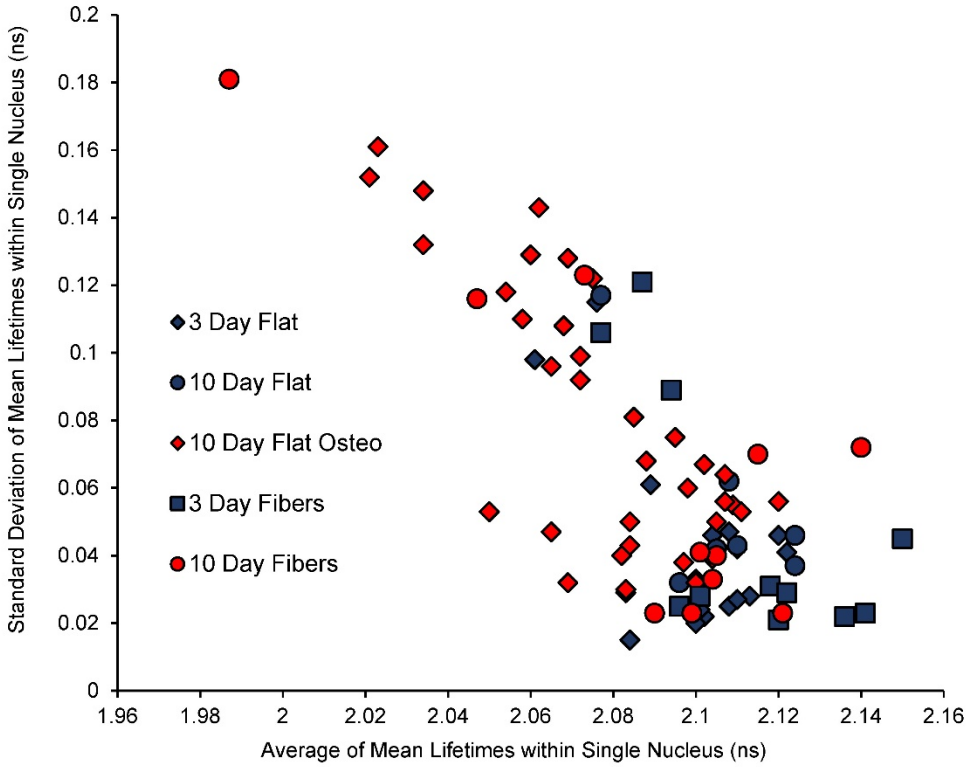

Figure C.4: Analysis of range of lifetimes within individual nuclei

The standard deviation of mean lifetimes within a given nucleus versus the average mean lifetime within a nucleus is plotted. A trend is observed in which nuclei with a lower average mean lifetime demonstrate a higher standard deviation of mean lifetimes within that nucleus. This is consistent with differentiated cells containing more condensed, heterogeneous chromatin compared to undifferentiated cells.

Table C.1: Mean lifetime averages, standard deviations, and standard error of the mean, with sample size based on pixels

	3 Day Flat	10 Day Flat	10 Day Flat Osteo	3 Day Fibers	10 Day Fibers
Mean Lifetime (ns)	2.101	2.106	2.077	2.108	2.075
Std. Dev. (ns)	0.0494	0.0590	0.0956	0.0630	0.1016
SEM (ns)	0.00037	0.00041	0.00053	0.00055	0.00091
N (pixels)	17,826	20,708	32,536	21,511	23,528

Table C.2: Mean lifetime averages, standard deviations, and standard error of the mean, with sample size based on nuclei

	3 Day Flat	10 Day Flat	10 Day Flat Osteo	3 Day Fibers	10 Day Fibers
Mean Lifetime (ns)	2.101	2.106	2.078	2.122	2.089
Std. Dev. (ns)	0.043	0.015	0.025	0.023	0.040
SEM (ns)	0.012	0.022	0.016	0.020	0.027
N (nuclei)	16	7	36	11	11

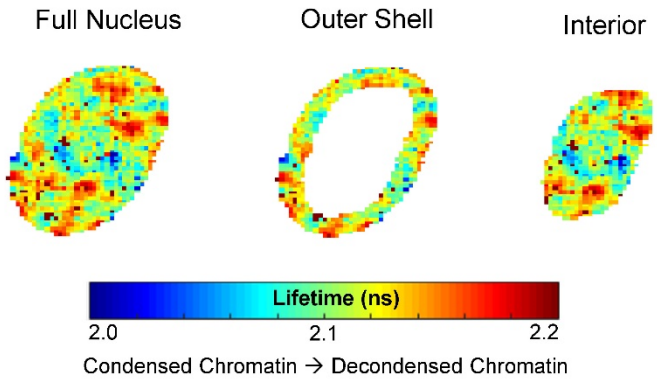

Figure C.5: Example of spatial analysis from FLIM heatmap

MATLAB code was generated such that spatial analysis of mean fluorescence lifetimes within a nucleus could be performed. Here, the outer shell and nuclear interior regions are separated for comparison. Shell width can be varied based on desired analysis.

References

1. Spagnol, S. T. & Dahl, K. N. Spatially Resolved Quantification of Chromatin Condensation through Differential Local Rheology in Cell Nuclei Fluorescence Lifetime Imaging. *PLoS One* **11,** e0146244 (2016).

2. Spagnol, S. T., Dahl, K. N. & Noel Dahl, K. Active cytoskeletal force and chromatin condensation independently modulate intranuclear network fluctuations. *Integr. Biol.* **6,** 523–31 (2014).

Appendix D: Publications and Conference Proceeding Resulting from Thesis

Publications

D. Whitefield*, S. Spagnol*, **T. Armiger**, L. Lan, K. Dahl, "Quantifying site-specific chromatin mechanics and DNA damage response" (2018) Manuscript in Review. *These authors contributed equally

V. Narayanan, C. Mayer, P. Arsenovic, A. Mohan, A. Duke, **T. Armiger**, S. Dumbali, V. Maruthamuthu, K. Dahl, D. Conway, "Mechanical force across E-cadherin regulates epithelial acini homeostasis" (2018) Manuscript in Review.

T. Armiger, M. Lampi, C. Reinhart-King, K. Dahl, "Probing epithelial monolayers with subnuclear sensors of cellular forces" (2018) Manuscript in Review.

T. Armiger*, K. Bathula*****, P. Vellala*****, R. Taylor, D. Conway, K. Dahl, "Progerin expression in cells under confinement and force reveal the physical mechanism of lamina defects" (2018) Manuscript in Review. *****These authors contributed equally

T. Armiger, S. Spagnol, K. Dahl, "Nuclear mechanical resilience but not stiffness is modulated by α-II spectrin". Journal of Biomechanics, 49 (2016), pp 3982-3989.

S. Spagnol, **T. Armiger**, K. Dahl, "Mechanobiology of Chromatin and the Nuclear Interior". Cellular and Molecular Bioengineering, 9 (2016), pp 268-276.

Podium Presentations

T. Armiger, M. Lampi, C. Reinhart-King, K. Dahl, "Cellular force propagation through monolayers investigated by tracking sub-nuclear sensors". The American Society for Cell Biology and European Molecular Biology Organization Meeting, Philadelphia PA, December 2017

T. Armiger, M. Lampi, C. Reinhart-King, K. Dahl, "Investigating changes in cellular based forces in monolayers by tracking sub-nuclear sensors". American Institute of Chemical Engineers Annual Meeting, Minneapolis MN, October 2017

S. Spagnol, **T. Armiger**, K. Dahl, "Quantification of chromatin condensation by nuclear particle-tracking microrheology and fluorescence lifetime imaging". American Chemical Society Colloid Surface Science Symposium. Carnegie Mellon University, June 2015

Poster Presentations

T. Armiger, M. Lampi, C. Reinhart-King, K. Dahl. “Probing Epithelial Monolayers with Subnuclear Sensors of Cellular Forces”. Cellular and Molecular Bioengineering Conference, Key Largo, Florida, January 2018

D. Whitefield, S. Spagnol, **T. Armiger**, L. Lan, K. Dahl. “Quantifying DNA Damage Response in Transcriptionally Active vs Repressed Chromatin”. Cellular and Molecular Bioengineering Conference, Key Largo, Florida, January 2018

T. Armiger, K. Dahl, “Investigation of a Nucleoskeletal Spectrin Network in Live Cells Using Particle Tracking Microrheology and Cellular Compression Assays”. GEM4 Summer Institute: Mechanobiology of the Brain. Carnegie Mellon University, July 2015

T. Armiger, K. Dahl, “The Role of α-II spectrin on Chromatin and Nucleoskeletal Rheology in Live Cells”. ACS Colloid Surface Science Symposium. Carnegie Mellon University, June 2015

T. Armiger, K. Dahl, “The Role of alpha II-Spectrin in Mechanics and Compressive Resilience of the Cell Nucleus”. Northeast Bioengineering Conference. Rensselaer Polytechnic Institute, April 2015